Unconventional Superconductivity near Inhomogeneities

Zur Erlangung des akademischen Grades eines

DOKTORS DER NATURWISSENSCHAFTEN

der Fakultät für Physik der Universität
Karlsruhe (TH)

genehmigte

DISSERTATION

von

Dipl.-Phys. Andreas Frank Poenicke
aus Karlsruhe

Tag der mündlichen Prüfung: 25.01.2008
Referent: Prof. Dr. Gerd Schön
Korreferent: Prof. Dr. Wolfgang Belzig

Acknowledgments

First of all, I would like to thank Professor Gerd Schön for giving me the great opportunity to be part of his group and his support in all the years. His group provides a wonderful and inspiring environment. The possibility to present my work at conferences and to visit workshops and summer schools is highly appreciated.

I thank Professor Wolfgang Belzig for kindly agreeing to co-referee this thesis and all the helpful discussions when I entered the world of quasiclassics.

I appreciate the fruitful collaborations and discussions with Professor Christoph Bruder, Carlos Cuevas, Yuri Barash, Matthias Eschrig, Micke Fogelström, and Jim Sauls.

During my work on the cuprates, I enjoyed stimulating discussions with the members of the experimental group of Professor Rudolf Gross: Lambert Alff, Stephan Kleefisch, Achim Marx, and Bettina Walter.

Many thanks are due to Achim Mildenberger, Daniel Hermann, and Tobias Ulbricht for sharing the duty of setting up and administrating the computer environment of our institutes.

Deep thanks to Oliver D. Mücke for proofreading large parts of this thesis, and many useful hints.

Patrick Mack for all his support in planning and organizing the lecture "Einführung in das computergestützte Arbeiten".

I thank all the members of the TFP and TKM for not only creating a perfect atmosphere at the institute, but also many activities beyond physics.

My parents gave me invaluable support throughout all the years.

Contents

1 Introduction

Writing about unconventional superconductivity, one is obliged to review the long and successful history of research on this topic. Ironically though, the first and best understood unconventional "superconductor"is neither a (solid state) superconductor nor was called unconventional.

The discovery of the superfluid phases in the rare isotope ^{3}He in 1972 by David M. Lee, Douglas D. Osheroff and Robert C. Richardson [1] was starting point of remarkable theoretical and experimental investigations [2–7]. The research on the superfluid state of ^{3}He is still ongoing with progress even relevant beyond condensed matter physics [8].

The fermionic nature of ^{3}He atoms, and thus the formation of Cooper pairs, provides a system similar to the conventional solid state superconductors. On the other hand important differences where observed. The order parameter shows a momentum dependence with p-wave symmetry and the neutral atoms condense in a spin triplet state.

With superconductivity in the heavy fermion compounds $CeCu_2Si_2$and UPt_3 a new class of superconducting materials was found. [9,10]. Soon it became obvious that these alloys where the first candidates for unconventional pairing in a solid state systems, even with a triplet order parameter [10]. In this context also the term "unconventional"superconductivity was introduced, defined as breaking in addition to the local gauge invariance at least one additional symmetry of the system.

But of probably the utmost significance was another family of superconductors. Bednorz and Müller [11] reported 1986 that the doped antiferromagnet $La_{2-x}Ba_xCuO_4$ was superconducting up to the unusual high temperature of 35K. Subsequent research on related systems yield a whole group of cuprate superconductors. With $YBa_2Cu_3O_{7-x}$ and $Bi_2Sr_2Ca_nCu_{n+1}O_{2n+6+\delta}$ providing technological important members, because their critical temperature T_c is high enough to access superconductivity with liquid nitrogen. The theoretical understanding of the pairing mechanism of the high-temperature superconductors (HTSC) is still incomplete, thus the symmetry of the order parameter gives important insights. For the hole-doped cuprates mentioned above d-wave symmetry seems to be well established by now, while in the case of the electron-doped compounds like $Nd_{2-x}Ce_xCuO_{4-\delta}$ or $Pr_{2-x}Ce_xCuO_{4-\delta}$ contradictory experimental findings are not yet completely resolved.

In recent years Sr_2RuO_4 attracted a lot of attention [12]. Strontium ruthenate is isostructural to the HTSC but without copper. In contrast to the cuprates it shows triplet pairing and a p-wave order parameter like in ^{3}He was proposed [13].

In this thesis we will address different systems and superconductors, but always inhomogeneities will play a crucial role. As will be explained, in unconventional superconductors Anderson's theorem is not valid any more and also non-magnetic scattering sites are pair breaking, and can give rise to bound states and low energy quasiparticle states. In these systems also scattering on boundaries can locally suppress superconductivity, making fully selfconsistent calculations and spatially resolved calculation necessary even to get correct qualitative results.

While this sensitivity makes the numerical description more burdensome, it also provides new possibilities. The exact behavior of superconductors at inhomogeneities is strongly connected to the symmetry of the order parameter. This enables to test the order parameter, and thus microscopic theories which propose different symmetries, by studying, e.g., the surface properties. As will become obvious later, this way one can not only gain information about the absolute value of the order parameter like in angle-resolved photo emission spectroscopy (ARPES) but also extract information about the momentum dependence of the phase.

Vice versa in case of known order parameters, information and understanding of technological relevant interfaces like grain boundary junctions can be obtained.

In the first chapter we briefly introduce the basic theoretically concepts used throughout this thesis. The quasiclassical theory of superconductivity is an excellent tool to describe inhomogeneous superconducting systems. It can be interpreted as a generalization of Landau's Fermi liquid theory to the superconducting state, allowing the self-consistent determination of the order parameter including impurities and other pair-breaking mechanism. The transport equations for the quasiclassical Green's functions are well suited for numerical evaluations of static and dynamical properties at arbitrary temperature. In case of weak perturbations varying on large scales, systems far from equilibrium are well described. And also strong perturbations like interfaces, which are beyond the quasiclassical approximation, can be included by using proper boundary conditions.

Having introduced the basic tools, we apply them to the simple case of homogeneous systems in equilibrium. Basic thermodynamic properties like the order parameter and specific heat are calculated and differences between conventional s-wave and unconventional superconductors discussed.

With chapter 3 we will turn to the first specific system, Sr_2RuO_4. Still bulk properties are on the focus. For two different proposed models the influence of impurities on the specific heat and spin susceptibility will be studied. Zhitomirsky and Rice [14] discussed multiband superconductivity with an active band and induced pairing on a passive band, which gives rise to an order parameter with line nodes as possible mechanism. We will adopt this model taking into account also impurities and compare our results with experimental data.

Point contact measurements in the group of Von Löhneysen [15] investigated the superconducting gap function of Sr_2RuO_4. The obtained conductance spectra strongly

support a p-wave order parameter. But the observed enhancement current reveals an unusual temperature dependence. To account for this dependence, a different model was introduced by Laube et al. [16]. The authors showed that a low lying boson mode, which effectively can be described as impurities with a temperature dependent scattering rate, would consistently fit the experimental findings. Also for this model, with a p-wave order parameter, the specific heat will be investigated. Within the calculations the method is extended to Eliashberg strong coupling theory to consistently describe the low temperature limit.

The following two chapters are devoted to the high-temperature superconductors. In these compounds the underlying pairing mechanism giving rise to the unexpected high critical temperature is still under debate. Fundamental to verify the different theories is the knowledge of symmetry of the order parameter. Many different experiments have been performed to extract this information but unfortunately most observables are phase insensitive. A direct and elegant way to access information about the phase are systems involving Josephson junctions. Since the Josephson current through a weak link is dependent on the phase difference across the interface, elaborate geometries with several junctions allow phase sensitive tests of the order parameter [17]. With the pioneering corner junction experiment by Wollman et al. [18] and tricrystal ring by Tsuei et al. [19, 20] demonstrated d-wave symmetry in the hole-doped cuprates. Many experiments based on the same idea where performed and the so called "π-junctions"have interesting applications on their own. But also the conductance of weak links like point-contacts and tunneling junctions is sensitive to the momentum dependence of the phase. At first glance only observing the local density of states (LDOS), these experiments are measuring a quantity which at inhomogeneities is strongly affected by a momentum dependent phase of the order parameter.

Scanning-tunneling microscopy and spectroscopy (STM/STS) measurements on (110) interfaces and measurements on misaligned grain boundary junctions exhibit a striking zero bias conduction peak (ZBCP). It has been shown [21] that an interface, for which the sign of the order parameter changes along a given trajectory, will always support a bound state at the Fermi energy. This zero energy bound state (ZEBS) is a consequence of intrinsic Andreev reflection at the interface. A d-wave order parameter with sign changes is in accordance with this observation and can also explain the absence of the ZBCP in STM measurements on (100) surfaces. While in clean systems the bound state should be strictly at zero energy, in experiments a broad conduction peak was observed. We will study the broadening of the bound state at an interface by bulk impurity scattering. The broadening of bound states due to unitary scattering will be shown to be substantially weaker than in the Born limit. We study various model geometries and calculate the temperature dependence of the Josephson critical current in the presence of these impurity-broadened bound states.

While impurity scattering can well account the broadening of the bound state, bulk impurities will also lead to significant suppression of superconductivity and a reduced

critical temperature. The experimentally observed strongly broadened ZBCP is better accounted for by a disordered interface. We will introduce a model of an layer with enhanced impurity scattering at the surface which is capable to explain the strong broadening without a reduction of the critical temperature.

Magnetic field experiments are an essential way to distinguish a ZBCP due to Andreev bound states from other mechanisms. In a magnetic field, applied along the crystal $\hat{c}$-axis, induced Meissner screening currents shift the bound states to finite energy, leading to a splitting of the ZBCP. This splitting has been reproducible seen in some experiments, while others cannot reproduce it. We will show that in an applied field, magnetic and potential scatterer will affect the ZEBS differently and the conflicting experimental observations are compatible with d-wave origin of the ZBCP taking into account different surface disorder.

The d-wave symmetry of the order parameter for hole-doped cuprate superconductors is well established by now. In case of electron-doped compounds the situation is still unclear. In the early days, s-wave seemed to be well founded. Based on s-wave symmetry in the electron-doped compounds, the diffing findings in STM measurements on and hole-doped HTSC could be used to support the d-wave and Andreev bound state picture in the latter. Later experiments supported d-wave pairing also in the electron-doped compounds posing the question why no ZBCP has been observed. The argumentation that impurity scattering is responsible will be tested by explicit calculation of the differential conductance for different pairing symmetries, including magnetic as well as potential impurities. We will demonstrate that d-wave symmetry and impurities are incompatible with the experiments. Calculations with s-wave and anisotropic s-wave, on the other hand, can fit the data even quantitatively.

In chapter 5 we will drop the restriction to the tunneling limit. In contacts with high transparency Andreev reflection and multiple Andreev reflection (MAR) dominate the transport characteristics. We present a self-consistent theory of current-voltage characteristics of d-wave/d-wave contacts at *arbitrary* transparency and in particular address the problem of the observation of subharmonic gap structure (SGS) in cuprate junctions. Our analysis shows that the SGS is possible also in d-wave superconductors and the existence of bound states within the gap results in an even-odd effect in the SGS. Elastic scattering mechanisms like impurities or surface roughness may suppress the SGS. In the presence of a magnetic field the Doppler shift of the Andreev bound states leads to a splitting of the SGS, which is an unambiguous fingerprint of d-wave superconductivity.

The final chapter 6 will not deal with unconventional superconductors. But also in systems with conventional BCS superconductors, unconventional pairing correlations can become crucial. Despite the fact, that ferromagnetism destroys singlet pair correlations on a short length scale, for superconductor-ferromagnet heterostructures the possibility of Josephson currents has been proposed and experimentally verified [22]. In this case, the coupling through the ferromagnetic layer is mediated by a long range proximity

effect of triplet correlations. To render this possible, the singlet pair amplitudes in the BCS superconductor must be transformed to triplet correlations when entering the ferromagnet. This transformation involves spin rotation and spin flip processes. While spin rotation is automatically present when these two systems are coupled, the physical origin of the spin flip processes is unclear. We will investigate a microscopic model of magnetic impurities close to the boundary and calculate the S-matrix describing the coupling. As will be shown, magnetic impurities in combination with a broken rotational spin symmetry will result in the necessary processes.

Parts of this thesis have been published:

- Section 4.1.1
  Poenicke A, Barash YS, Bruder C, Istyukov V
  Broadening of Andreev bound states in d(x(2)-y(2)) superconductors
  Physical Review B 57, 7102–7107 (1999)

- Section 4.1.2
  Poenicke A., Fogelström M.
  Tunneling into high-T_c superconductors: Influence of surface disorder
  Preprint for the LT99, Helsinki

- Chapter 5
  Poenicke A, Cuevas JC, Fogelström M,
  Subharmonic gap structure in d-wave superconductors
  Physical Review B 65, 220510 (2002)

2 Quasiclassical theory in a nutshell

Before turning to unconventional superconductivity and the specific systems advertised in the introduction, a general introduction in the methods and concepts used within this thesis should be provided. Standard quantum field theory methods are a powerful tool to address superconducting systems [23, 24], but the computational effort especially in inhomogeneous and out-of-equilibrium systems is a critical drawback. A Fermi liquid description, the quasiclassical theory of superconductivity, proved to be perfectly suited not only for these tasks. The quasiclassical transport equations derived independently by Eilenberger [25] and Larkin and Ovchinnikov [26] for equilibrium systems have been generalized to nonequilibrium situations by Eliashberg [27] and Larkin and Ovchinnikov [28] [29], making the quasiclassical theory one of the most successful tools to describe superconducting systems.

In the following pages only a very condensed overview of basic ideas, notations and equations is given, adverting that derivations and exhaustive treatments are available in excellent reviews [30–32] and of course the cited original papers.

2.1 Quasiclassical Green's functions

With the description of strongly interacting fermionic systems by a distribution of quasiparticles, Landau formulated a non-perturbative theory of strongly interacting fermions. However, the validity is determined by the smallness of key parameters. The relevant energy scales like temperature, Debye energy and frequencies of external perturbations have to be much smaller than the Fermi energy. The dynamic and spatial evolution of the quasiparticle distribution function is given by the quasiclassical Landau-Boltzmann equation under the assumption, that intrinsic length scales like the mean free path and thermal coherence length are large and external perturbations smooth on the scale of the Fermi wavelength. If the scales characterizing the superconducting state, i.e. order parameter and superconducting coherence length, also fulfill this requirement, a generalization including the BCS pairing interaction can be formulated:

The central object of the quasiclassical theory of superconductivity is the quasiclassical

or ξ-integrated [1] Green's function [2]

$$\check{g}(\boldsymbol{p}_F, \boldsymbol{R}; \varepsilon, t) = \frac{1}{a} \int \mathrm{d}\xi_{\boldsymbol{p}} \hat{\tau}_3 \check{G}(\boldsymbol{p}, \boldsymbol{R}; \varepsilon, t) \tag{2.1}$$

a is the quasiparticle weight and $\xi_{\boldsymbol{p}} = \boldsymbol{v}_F(\boldsymbol{p} - \boldsymbol{p}_F)$. The 2x2 Keldysh matrix $\check{g}$ has the form

$$\check{g}(\boldsymbol{p}_F, \boldsymbol{R}; \varepsilon, t) = \begin{pmatrix} \hat{g}^R & \hat{g}^K \\ 0 & \hat{g}^A \end{pmatrix} \tag{2.2}$$

with the retarded $\hat{g}^R(\boldsymbol{p}_F, \boldsymbol{R}; \varepsilon, t)$, the advanced $\hat{g}^A(\boldsymbol{p}_F, \boldsymbol{R}; \varepsilon, t)$ and the Keldysh Green's functions $\hat{g}^K(\boldsymbol{p}_F, \boldsymbol{R}; \varepsilon, t)$ being in general 4x4-Nambu matrices in spin and particle hole space [3]. In the following $\hat{\tau}_i$ will always denote Pauli matrices in particle-hole space and $\hat{\sigma}_i$ in spin space.

The evolution of the propagator $\check{g}(\boldsymbol{p}_F, \boldsymbol{R}; \varepsilon, t)$ is given by the transport-like Eilenberger equation

$$[\check{\varepsilon} - \hat{\sigma}_{mf} - \check{\sigma}_i - \hat{v}_{ext}, \check{g}]_{\otimes} + i\hbar \boldsymbol{v}_F \boldsymbol{\nabla} \check{g} = 0, \tag{2.3}$$

which, to determine the quasiclassical propagator $\check{g}$ uniquely, has to be accompanied with a normalization condition

$$\check{g} \otimes \check{g} = -\pi^2 \check{1} \,. \tag{2.4}$$

For the sake of readability not all definitions and notations like the non-commutative product $\otimes$ will be given here, but are addressed in the appendices A and B.

The energy $\check{\varepsilon}$, mean field self-energy $\check{\sigma}_{mf}$, impurity and phonon scattering self-energy $\check{\sigma}_i = \check{\sigma}_{imp} + \check{\sigma}_{ph}$ and the external potential $\check{v}_{ext}$ have the Keldysh structure

$$\check{\varepsilon} = \begin{pmatrix} \varepsilon\hat{\tau}_3 & 0 \\ 0 & \varepsilon\hat{\tau}_3 \end{pmatrix} \quad \check{\sigma}_{mf} = \begin{pmatrix} \hat{\sigma}_{mf} & 0 \\ 0 & \hat{\sigma}_{mf} \end{pmatrix} \quad \check{\sigma}_i = \begin{pmatrix} \hat{\sigma}_i^R & \hat{\sigma}_i^K \\ 0 & \hat{\sigma}_i^A \end{pmatrix} \quad \check{v}_{ext} = \begin{pmatrix} \hat{v}_{ext} & 0 \\ 0 & \hat{v}_{ext} \end{pmatrix} \tag{2.5}$$

The external potential $\hat{v}_{ext}$ contains the vector potential $\boldsymbol{A}$ and the scalar potential ϕ in the form ($e = -|e|$)[4].

$$\hat{v}_{ext} = -\frac{e}{c} \boldsymbol{v}_F \boldsymbol{A} \hat{\tau}_3 + e\phi\hat{1}. \tag{2.6}$$

[1] The ξ-integration is in fact non-trivial, the caveats are addressed, e.g., in [30] and [33]

[2] In the literature sometimes the full propagator $\check{G}$ is defined with an additional factor $\hat{\tau}_3$, and the definition of the quasiclassical propagator changes accordingly.

[3] In case of spin-singlet superconductivity, the formulation can be reduced to 2x2 Nambu matrices. The connection to the formulation given here is explained in appendix B

[4] This convention (sadly often not mentioned explicitly) is chosen in most of the cited publications, therfore we adopt it to avoid unnecessary confusion. While we try to be consistent in notation, nevertheless eV will be the standard energy unit defined with e = $|e|$

In some cases it is convenient to decompose the matrices in spin space explicitly in terms of Pauli matrices. This way, e.g., the mean field self-energy can be written as

$$\hat{\sigma}_{mf} = \begin{pmatrix} \nu + \boldsymbol{\nu}\boldsymbol{\sigma} & (\Delta + \boldsymbol{\Delta}\boldsymbol{\sigma})i\hat{\sigma}_2 \\ (\tilde{\Delta} + \tilde{\boldsymbol{\Delta}}\boldsymbol{\sigma}^*)i\hat{\sigma}_2 & \tilde{\nu} + \tilde{\boldsymbol{\nu}}\boldsymbol{\sigma}^* \end{pmatrix} \tag{2.7}$$

where the parameters with and without twiddle are connected by symmetries as explained below.

In addition to the self-energies given by the Landau parameters A^s and A^a

$$\nu_{mf}(\boldsymbol{p}_F, \boldsymbol{R}; t) = \int \frac{\mathrm{d}\varepsilon}{4\pi i} \left\langle A^s(\boldsymbol{p}_F, \boldsymbol{p}_F{}') g^K(\boldsymbol{p}_F, \boldsymbol{R}; \varepsilon, t) \right\rangle_{\boldsymbol{p}_F{}'} \tag{2.8}$$

$$\boldsymbol{\nu}_{mf}(\boldsymbol{p}_F, \boldsymbol{R}; t) = \int \frac{\mathrm{d}\varepsilon}{4\pi i} \left\langle A^a(\boldsymbol{p}_F, \boldsymbol{p}_F{}') \boldsymbol{g}^K(\boldsymbol{p}_F, \boldsymbol{R}; \varepsilon, t) \right\rangle_{\boldsymbol{p}_F{}'} , \tag{2.9}$$

in the superconducting state singlet V^s and triplet V^t pairing interactions are giving rise to the offdiagonal terms

$$\Delta(\boldsymbol{p}_F, \boldsymbol{R}; t) = \int \frac{\mathrm{d}\varepsilon}{4\pi i} \left\langle V^s(\boldsymbol{p}_F, \boldsymbol{p}_F{}') f^K(\boldsymbol{p}_F{}', \boldsymbol{R}; \varepsilon, t) \right\rangle_{\boldsymbol{p}_F{}'} \tag{2.10}$$

$$\boldsymbol{\Delta}(\boldsymbol{p}_F, \boldsymbol{R}; t) = \int \frac{\mathrm{d}\varepsilon}{4\pi i} \left\langle V^t(\boldsymbol{p}_F, \boldsymbol{p}_F{}') \boldsymbol{f}^K(\boldsymbol{p}_F{}', \boldsymbol{R}; \varepsilon, t) \right\rangle_{\boldsymbol{p}_F{}'} . \tag{2.11}$$

Scattering on dilute impurity potentials enters the theory by a impurity self-energy which can be calculated in t-matrix approximation

$$\check{\sigma}_{imp}(\boldsymbol{p}_F, \boldsymbol{R}; \varepsilon, t) = n_{imp} \check{t}(\boldsymbol{p}_F, \boldsymbol{p}_F; \boldsymbol{R}; \varepsilon, t) \tag{2.12}$$

$$\check{t}(\boldsymbol{p}_F, \boldsymbol{p}_F{}') = \check{u}(\boldsymbol{p}_F, \boldsymbol{p}_F{}') + N_F \left\langle \check{u}(\boldsymbol{p}_F, \boldsymbol{p}_F{}'') \otimes \check{g}(\boldsymbol{p}_F{}'') \otimes \check{t}(\boldsymbol{p}_F{}'', \boldsymbol{p}_F{}') \right\rangle_{\boldsymbol{p}_F{}''} . \tag{2.13}$$

The impurities are characterized by their concentration n_{imp} and the potential $\hat{u} = u_p + \boldsymbol{u}_s\hat{\boldsymbol{\sigma}}$ with the Coulomb potential u_p) and spin exchange scattering $\boldsymbol{u}_s$ on randomly oriented classical moments.

Redundancy in the Nambu notation gives rise to symmetries (Appendix B) making the parametrization

$$\hat{g}^{R,A} = \begin{pmatrix} g^{R,A} & f^{R,A} \\ \tilde{f}^{R,A} & \tilde{g}^{R,A} \end{pmatrix} \qquad \hat{g}^K = \begin{pmatrix} g^K & f^K \\ -\tilde{f}^K & -\tilde{g}^K \end{pmatrix} \tag{2.14}$$

convenient, where the twiddle ($\tilde{}$) denotes conjugation defined as

$$\widetilde{X}(\boldsymbol{p}_F, \boldsymbol{R}; \varepsilon, t) = X(-\boldsymbol{p}_F, \boldsymbol{R}; -\varepsilon, t)^* . \tag{2.15}$$

Knowing the quasiclassical propagator, important properties like the momentum resolved local density of states

$$N(\boldsymbol{p}_F, \boldsymbol{R}; \varepsilon) = -\frac{1}{4\pi} \operatorname{tr}_4 \left[\hat{\tau}_3 \mathrm{Im}\left[\hat{g}^R(\boldsymbol{p}_F, \boldsymbol{R}; \varepsilon)\right]\right] \tag{2.16}$$

and the current density

$$\boldsymbol{j}(\boldsymbol{R}, t) = eN_F \int \frac{\mathrm{d}\varepsilon}{8\pi i} \left\langle \boldsymbol{v}_F \operatorname{tr}_4 \left[\hat{\tau}_3 \hat{g}^K(\boldsymbol{p}_F, \boldsymbol{R}; \varepsilon, t)\right]\right\rangle_{\boldsymbol{p}_F} \tag{2.17}$$

are directly available.

2.1.1 Boundary conditions

While it seems that all the low energy physics can be well described within the quasiclassical theory, a mayor complicacy should not be concealed. As noted in the beginning, the validity of the method requires that everything is smooth on the atomic scale. Boundaries and interfaces, which are crucial in heterostructures and systems like tunnel junctions and point contacts, are usually strong inhomogeneities on a short length scale and thus beyond the quasiclassical approach. Pretending to be perfectly suited for inhomogeneous systems but not addressing central inhomogeneities sounds like an antagonism. But as in WKB in quantum mechanics, the solution are boundary conditions. The Eilenberger equation (2.3) describes propagation on classical trajectories parametrized by spatial coordinates $\boldsymbol{R}$ and the momentum on the Fermi surface $\boldsymbol{p}_F$. By laborious work on a microscopic level it is possible to determine conditions which relate propagators on "incoming" to propagators on "outgoing" trajectories at the inhomogeneity [34–40]. Applying these boundary conditions in addition to the Eilenberger equation allows also a selfcontained quasiclassical treatment of these problems.

2.2 Equilibrium

In thermal equilibrium the formulation simplifies significantly. The Keldysh propagator is given by the retarded and advanced Green's function by

$$\hat{g}^K = (\hat{g}^R - \hat{g}^A) \tanh\left(\frac{\varepsilon}{2\mathrm{k_B}T}\right) \tag{2.18}$$

and since the quantities are time independent, the product $\otimes$ is reducing to a simple matrix product.

Furthermore it is possible to formulate the theory in terms of Matsubara Green's functions. These propagators are defined on the imaginary energy axis for discrete Matsubara energies ε_n (fermions) or ω_n (bosons) given by

$$\varepsilon_n = (2n+1)\pi \mathrm{k_B}T \qquad \omega_n = 2n\pi \mathrm{k_B}T, \qquad n \in \mathbb{Z}\,. \tag{2.19}$$

The retarded and advanced Green's functions are connected with the Matsubara Green's functions by analytical continuation

$$\hat{g}^{R,A}(\boldsymbol{p}_F, \boldsymbol{R}; \varepsilon) = \hat{g}^M(\boldsymbol{p}_F, \boldsymbol{R}; \varepsilon_n)\big|_{i\varepsilon_n \to \varepsilon \pm i0^+} \tag{2.20}$$

As the full Keldysh propagator the Matsubara propagator fulfills the Eilenberger equation which now reads

$$\left[i\varepsilon_n \hat{\tau}_3 - \hat{\sigma}(\boldsymbol{p}_F, \boldsymbol{R}; \varepsilon_n) - \hat{v}(\boldsymbol{p}_F, \boldsymbol{R}), \hat{g}^M(\boldsymbol{p}_F, \boldsymbol{R}; \varepsilon_n)\right]_\otimes + i\boldsymbol{v}_F \nabla \hat{g}^M(\boldsymbol{p}_F, \boldsymbol{R}; \varepsilon_n) = 0\ . \tag{2.21}$$

For compact notation, here $\hat{\sigma}$ contains all self-energies.

The observables can then be calculated by replcaing $\hat{g}^K \to \hat{g}^M$ and $\int \frac{\mathrm{d}\varepsilon}{4\pi i} \to \mathrm{k_B}T \sum_{\varepsilon_n}$ in the original Keldysh formulas.

This way the order parameter is expressed as

$$\Delta(\boldsymbol{p}_F, \boldsymbol{R}) = \mathrm{k_B}T \sum_{\varepsilon_n} \left\langle V(\boldsymbol{p}_F, \boldsymbol{p}_F{}') f^M(\boldsymbol{p}_F{}', \boldsymbol{R}, \varepsilon_n) \right\rangle_{\boldsymbol{p}_F{}'} \tag{2.22}$$

and the current density can be calculated by

$$\boldsymbol{j}(\boldsymbol{R}) = 2eN_F \mathrm{k_B}T \sum_{\varepsilon_n} \left\langle \boldsymbol{v}_F(\boldsymbol{p}_F) g^M(\boldsymbol{p}_F, \boldsymbol{R}; \varepsilon_n) \right\rangle_{\boldsymbol{p}_F}) \ . \tag{2.23}$$

2.3 Order parameter

Characterizing the central quantity of the superconducting state, the order parameter Δ, at first the pairing interaction is expanded in orthogonal basis functions

$$V(\boldsymbol{p}_F, \boldsymbol{p}_F{}') = \sum_\Gamma V_\Gamma \sum_\nu^{d_\Gamma} \mathcal{Y}_{\Gamma\nu}(\boldsymbol{p}_F) \mathcal{Y}^*_{\Gamma\nu}(\boldsymbol{p}_F{}'). \tag{2.24}$$

In a crystal $\mathcal{Y}_{\Gamma\nu}$ are the basis functions from irreduzible representations of the point group of the crystal lattice symmetry. The largest attractive interaction $V_\Gamma > 0$ will determine the transition temperature T_c and the corresponding symmetry of the dominant order parameter $\Delta(\boldsymbol{p}_F)$.

Expanding the Eilenberger equation in orders of Δ, one notes that the equation for the offdiagonal self-energy is logarithmic divergent. But fortunately the dependence on a cut-off energy ω_c and the unknown coupling parameter V_Γ can be removed in favour of an experimental observable, the critical bulk temperature T_c:

Using the solution of the homogeneous Eilenberger equation

$$f^M(\boldsymbol{p}_F; \varepsilon_n) = \frac{\pi \Delta(\boldsymbol{p}_F)}{\sqrt{|\Delta(\boldsymbol{p}_F)|^2 + {\varepsilon_n}^2}} \tag{2.25}$$

Eq.(2.22) is a self-consistency equation for the order parameter which close to the transition temperature T_c can be linearized giving the BCS relation

$$\frac{1}{\langle|\mathcal{Y}_\Gamma|^2\rangle V_\Gamma} = 2\pi T_c \sum_{\varepsilon_n>0}^{\omega_c} \frac{1}{|\varepsilon_n|} = \Psi\left(\frac{1}{2}+\frac{\omega_c}{2\pi T_c}\right) - \Psi\left(\frac{1}{2}\right) \approx \ln\left(\frac{2\gamma\omega_c}{\pi T_c}\right). \tag{2.26}$$

The divergency is then addressed by using a standard trick of subtracting and adding the divergent term

$$2\pi T \sum_{\varepsilon_n>0}^{\omega_c} \frac{1}{|\varepsilon_n|} = \Psi\left(\frac{1}{2}+\frac{\omega_c}{2\pi T}\right) - \Psi\left(\frac{1}{2}\right) \approx \ln\left(\frac{2\gamma\omega_c}{\pi T}\right), \tag{2.27}$$

which combined with Eq. (2.26) leads to the self-consistency equation ($\Delta(\boldsymbol{p}_F) = \Delta_\Gamma \mathcal{Y}_\Gamma(\boldsymbol{p}_F)$)

$$\Delta_\Gamma \log\left(\frac{T}{T_c}\right)\langle|\mathcal{Y}_\Gamma|^2\rangle = \pi T \sum_{\varepsilon_n}^{\omega_c} \left\langle \mathcal{Y}_\Gamma^*(\boldsymbol{p}_F{}') \left[\frac{\Delta(\boldsymbol{p}_F{}')}{\sqrt{|\Delta(\boldsymbol{p}_F{}')|^2+{\varepsilon_n}^2}} - \frac{\Delta(\boldsymbol{p}_F{}')}{|\varepsilon_n|}\right]\right\rangle_{\boldsymbol{p}_F{}'} \tag{2.28}$$

for the bulk order parameter, and the general self-energy

$$\Delta_\Gamma(\boldsymbol{R}) = \frac{\mathrm{k_B}T\sum_{\varepsilon_n}\left\langle \mathcal{Y}_\Gamma^*(\boldsymbol{p}_F{}') f^M(\boldsymbol{p}_F{}', \boldsymbol{R}; \varepsilon_n)\right\rangle_{\boldsymbol{p}_F{}'}}{\langle|\mathcal{Y}_\Gamma|^2\rangle\left(\ln\frac{T}{T_c} + \sum_{n>0}\frac{1}{n-0.5}\right)}. \tag{2.29}$$

For the sake of completeness, the Keldysh expression

$$\Delta_\Gamma(\boldsymbol{R}) = \frac{\int_{-E_c}^{E_c}\frac{\mathrm{d}\varepsilon}{4\pi i}\left\langle \mathcal{Y}_\Gamma^*(\boldsymbol{p}_F{}') f^K(\boldsymbol{p}_F{}'; \varepsilon)\right\rangle_{\boldsymbol{p}_F{}'}}{\langle|\mathcal{Y}_\Gamma|^2\rangle\left(\ln\frac{T}{T_c} + \int_{-E_c}^{E_c}\frac{\mathrm{d}\varepsilon}{2\varepsilon}\tanh\frac{\varepsilon}{2T}\right)} \tag{2.30}$$

can be obtained along the same lines.

2.4 Bulk properties and thermodynamics

While in general the Eilenberger equation can only be solved numerically, in the clean homogeneous (bulk) case it is possible to obtain analytical solutions in a straightforward manner. To provide a basis for the later discussion, an overview of the basic thermodynamic bulk properties of conventional and unconventional superconductors should be at hand. Assuming a cylindrical Fermi surface (as the case in the HTSC), the *s*-wave ($\Delta(\boldsymbol{p}_F) = \Delta$) case and *d*-wave ($\Delta(\boldsymbol{p}_F) = \Delta\cos(2\phi)$) as examples of an unconventional order parameter with nodes on the Fermi surface will be compared.

2.4.1 Density of states

Carrying out the Fermi surface average of equation (2.16)

$$N(\varepsilon) = -\frac{1}{\pi} \left\langle \mathrm{Im}\left[g^R(\varepsilon, \boldsymbol{p}_F)\right] \right\rangle_{\boldsymbol{p}_F} \tag{2.31}$$

the total density of states is gained.

In the s-wave case due to the isotropic order parameter quasiparticle states are gapped

$$N^s(\varepsilon) = \frac{\varepsilon}{\sqrt{\varepsilon^2 - |\Delta|^2}} \theta(\varepsilon - |\Delta|) \tag{2.32}$$

with a square root divergency at the gap edge.

The nodes in the spectral gap of a d-wave order parameter allow states at all energies, the corresponding DOS can be expressed as [41]

$$N^d(\varepsilon) = \begin{cases} \frac{2}{\pi} \frac{\varepsilon}{\Delta} K\left(\frac{\varepsilon}{\Delta}\right) & \varepsilon \leq \Delta \\ \\ \frac{2}{\pi} K\left(\frac{\Delta}{\varepsilon}\right) & \varepsilon > \Delta \end{cases} \tag{2.33}$$

$K(x)$ are complete elliptic integrals of the first kind [42].

It is important to note, that for low energies $\varepsilon \ll \Delta$ the density increases linearly $N(\varepsilon) \approx \frac{\varepsilon}{\Delta}$ as expected for a gap with line-nodes (point-nodes) in 3D (2D). This linear dependence will govern many of the low temperature properties, as the discussion in the next paragraphs will show.

2.4.2 Specific heat

The general calculation of the specific heat within the quasi-classical formalism turns out to be in many cases specifically difficult. To express the specific heat in terms of quasiclassical propagators might pose problems not found in the other observables mentioned before. To study this property and get aware of the obstacles one has to go back to the full (non-quasiclassical) propagators.

The starting point to calculate the specific heat

$$C = -T \frac{\partial^2 \Omega}{\partial T^2} = T \frac{\partial S}{\partial T} \tag{2.34}$$

in a self-consistent quantum field formulation is the Luttinger-Ward functional [43] for the free energy, first generalized to superfluid systems by De Dominicis and Martin [44,45]

$$\Omega(\hat{\Sigma}, \hat{G}; \hat{V}) = -\,\mathrm{Tr}\left[\hat{\Sigma}\hat{G} + \ln\left(\hat{\tau}_3(-\hat{G}_0^{-1} + \hat{\Sigma} + \hat{V})\right)\right] + \Phi\left[\hat{G}\right] \tag{2.35}$$

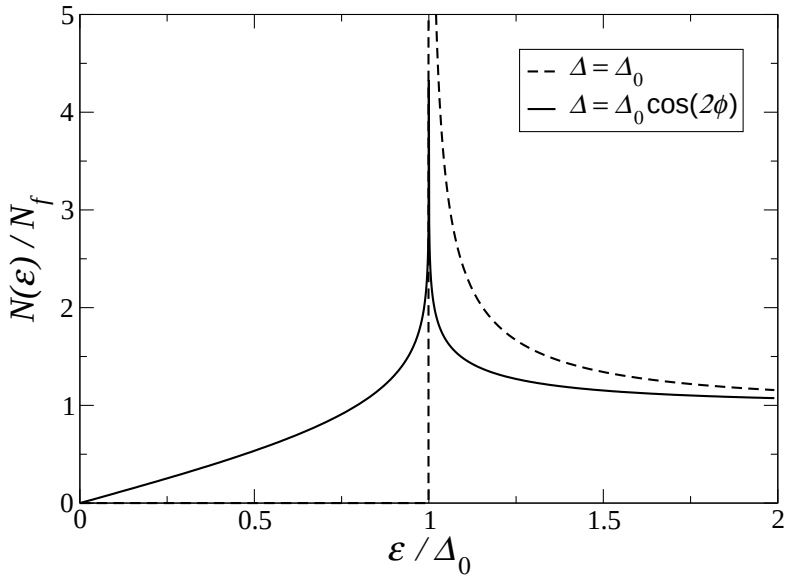

Figure 2.1: Bulk density of states for s-wave and d-wave superconductors

with

$$\hat{G}_0^{-1} = i\varepsilon_n - \xi\hat{\tau}_3$$

$\hat{G}_0$ is the free electron Green's function, $\hat{V}$ are external potentials like impurities, and $\hat{\Sigma}$ is the self-energy. The functional $\Phi\left[\hat{G}\right]$ is generating all skeleton self-energy diagrams as given below. In this short notation, indices and variables are omitted, products are Nambu matrix products together with folding in internal variables, and $\mathrm{Tr}[\dots]$ is defined as

$$\mathrm{Tr}[\dots] = T\sum_{\varepsilon_n}\int\frac{\mathrm{d}^3\boldsymbol{p}}{(2\pi)^3}\int\mathrm{d}^3\boldsymbol{R}\,\frac{1}{2}\,\mathrm{tr}_4[\dots] \tag{2.36}$$

The functional is stationary with respect to variations of $\hat{\Sigma}$ and $\hat{G}$ giving

$$\frac{\delta\Omega}{\delta\hat{G}} = 0 \quad \longrightarrow \quad \hat{\Sigma} = \frac{\delta\Phi}{\delta\hat{G}} \qquad \text{the self-energy} \tag{2.37}$$

$$\frac{\delta\Omega}{\delta\hat{\Sigma}} = 0 \quad \longrightarrow \quad \hat{G} = \left(\hat{G}_0^{-1} - \hat{\Sigma} - \hat{V}\right)^{-1} \qquad \text{and Dyson equation.} \tag{2.38}$$

Doing the ξ-integration to obtain an expression in terms of quasiclassical quantities turns out to be non-trivial. In general ξ is an operator, and the operator logarithm cannot be integrated by simple means and technical tricks are needed [5]. In the simple

[5] These tricks like diffentiating and reintegrating are dangerous and have to be applied carefully, e.g., not to cross branch-cuts or miss boundary terms.

homogeneous case discussed now, these complications are absent and the only problems are divergencies which are cured by subtracting the normal state $\Omega_N(T)$ and absorbing infinite constants in $\Omega_N(T=0)$. The free energy is then given by

$$\Omega_S(T) - \Omega_N(T) = N_F \frac{|\Delta_\Gamma|^2}{V_\Gamma} - 2\pi N_F \mathrm{k_B} T \sum_{\varepsilon_n} \left(\left\langle \sqrt{{\varepsilon_n}^2 + |\Delta(\boldsymbol{p}_F)|^2} \right\rangle - |\varepsilon_n| \right) \tag{2.39}$$

and, using the above mentioned methods to cure the divergencies, it can be written as

$$\begin{aligned} \Omega_S(T) - \Omega_N(T) =& N_F \log\left(\frac{T}{T_c}\right) \langle |\Delta(\boldsymbol{p}_F|^2 \rangle \\ & - 2\pi N_F \mathrm{k_B} T \sum_{\varepsilon_n} \left(\left\langle \sqrt{{\varepsilon_n}^2 + |\Delta(\boldsymbol{p}_F)|^2} \right\rangle - |\varepsilon_n| - \frac{\langle |\Delta(\boldsymbol{p}_F)|^2 \rangle}{2|\varepsilon_n|} \right). \end{aligned} \tag{2.40}$$

In the low temperature limit, $T \ll T_c$, it is posssible to derive an equation for the specific heat particularly suited for analytic treatment. The entropy of independent fermions

$$S = -2\mathrm{k_B} \sum_{\boldsymbol{k}} [1 - f(E_{\boldsymbol{k}})] \ln[1 - f(E_{\boldsymbol{k}})] + f(E_{\boldsymbol{k}}) \ln f(E_{\boldsymbol{k}}) \tag{2.41}$$

can also be derived for the superconducting state using the partition function. With the approximation of a constant order parameter at low temperatures and consequently a temperature independent density of states, the specific heat

$$C = 2\mathrm{k_B} \int \mathrm{d}\varepsilon N(\varepsilon) (\beta\varepsilon)^2 \left(-\frac{\mathrm{d}f(\varepsilon)}{\mathrm{d}\varepsilon} \right) \qquad (T \ll T_c) \tag{2.42}$$

is determined by the low energy density of states. With the Fermi distribution function $f(\varepsilon) = (1 + \exp(\varepsilon/\mathrm{k_B}T))^{-1}$.

The normal state specific heat can be instantaneously read off to be

$$\frac{C_N}{T} = \frac{2}{3}\pi^2 N_F {\mathrm{k_B}}^2 \equiv \gamma_S. \tag{2.43}$$

In the *s*-wave superconducting state, the density of states are fully gapped, as expected the specific heat shows activated behaviour

$$\frac{C_S^s(T)}{\gamma_S T} = \frac{3\sqrt{2}}{\pi^{3/2}} \left(\frac{\Delta}{\mathrm{k_B}T} \right)^{5/2} \exp\left[-\frac{\Delta}{\mathrm{k_B}T} \right] \tag{2.44}$$

while the linear low energy DOS in the *d*-wave case manifests in

$$\frac{C_S^d(T)}{\gamma_S T} = \frac{3}{\pi^2} 9\, \zeta(3) \frac{\mathrm{k_B}T}{\Delta}. \tag{2.45}$$

Equation (2.42) shows apparently, that if the low energy DOS grows potentially as $N(\varepsilon) \propto \varepsilon^n$, the specific heat over temperature $C/T \propto T^n$ follows the same power law. In Figure 2.2 the specific heat is plotted over the whole temperature range.

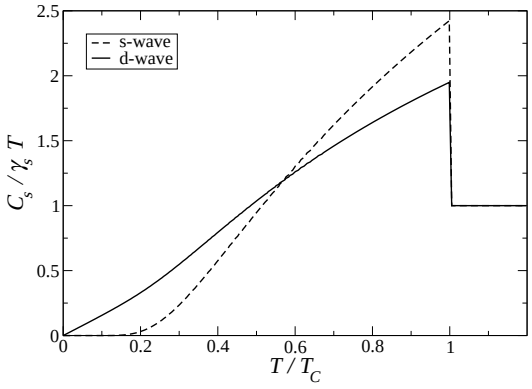

Figure 2.2: Specific heat for s-wave and d-wave superconductors as function of reduced temperature

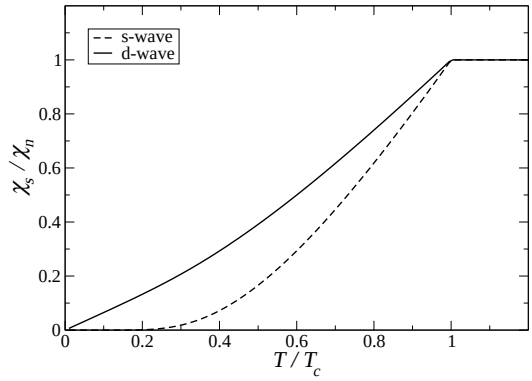

Figure 2.3: Electron spin susceptibility for s-wave and d-wave superconductors as function of reduced temperature

2.4.3 Spin susceptibility

Investigation of the electron spin susceptibility is a powerful way to distinguish singlet and triplet superconductivity.

In singlet superconductors the total spin of a Cooper pair is zero, thus quasiparticles of the condensate cannot contribute to the magnetic moment. As effect below T_c the spin susceptibility of the electrons is reduced

$$\frac{\chi_S}{\chi_N} = 1 - \pi \mathrm{k_B} T \sum_{\varepsilon_n} \left\langle \frac{|\Delta(\boldsymbol{p}_F)|^2}{\left({\varepsilon_n}^2 + |\Delta(\boldsymbol{p}_F)|^2\right)^{3/2}} \right\rangle \tag{2.46}$$

$$= \frac{1}{\mathrm{k_B} T} \int_{-\infty}^{\infty} \mathrm{d}\varepsilon N(\varepsilon) \Big(-\frac{\mathrm{d}f(\varepsilon)}{\mathrm{d}\varepsilon} \Big) \tag{2.47}$$

vanishing at zero temperature ($\chi_N = 2\mu_e^2 N_F$), while in triplet superconductors it will not change for $T < T_c$. Like the specific heat, the spin suszeptibility drops exponentially as $T \to 0$

$$\frac{\chi_S^s(T)}{\chi_N} = \sqrt{\frac{2\pi\Delta}{\mathrm{k_B} T}} \exp\Big[-\frac{\Delta}{\mathrm{k_B} T} \Big] \qquad T \ll T_c \tag{2.48}$$

for s-wave and shows power-law dependence

$$\frac{\chi_S^d(T)}{\chi_N} = 2 \log 2 \, \frac{\mathrm{k_B} T_c}{\Delta} \frac{T}{T_c} \qquad T \ll T_c \tag{2.49}$$

for d-wave superconductors as shown in Figure 2.3.

2.4.4 Nuclear spin relaxation

In the end the relaxation rate of nuclear spins defined as $R = (T_1 T)^{-1}$ is connected to the density of states in a similar way

$$\frac{R_S}{R_N} = \frac{1}{\mathrm{k_B} T} \int_{-\infty}^{\infty} \mathrm{d}\varepsilon N(\varepsilon)^2 \left(1 + \frac{\langle\Delta\rangle^2}{\varepsilon^2}\right) \left(-\frac{\mathrm{d}f(\varepsilon)}{\mathrm{d}\varepsilon}\right). \tag{2.50}$$

2.4.5 Impurity scattering

In this subsection we will study the influence of impurities on the superconducting properties of conventional s-wave and unconventional d-wave superconductors. For simplicity the scattering potentials will be assumed to be momentum independent but can nevertheless be of arbitrary strength. As explained before the self-energy is obtained via the the solution of the t-matrix equation (2.13). In equilibrium and s-wave scattering, it reduces to a simple matrix equation,

$$\hat{t}(\varepsilon_n) = \hat{u} + \hat{u} \left\langle \hat{g}(\boldsymbol{p}_F, \varepsilon_n) \right\rangle_{\boldsymbol{p}_F} \hat{t}(\varepsilon_n) \qquad \hat{u} = u_p + \hat{u}_s \hat{\sigma} \tag{2.51}$$

omitting obvious arguments from now on.

The self-energies will be characterized by the elastic scattering time τ, entering the mean free path $l = \boldsymbol{v}_F \tau$, and the potential strength σ as

$$\frac{1}{2\tau_{p/s}} = n_{imp} \frac{\pi N_F u_{p/s}^2}{1 + (\pi N_F u_{p/s})^2} \qquad \sigma_{p/s} = \frac{(\pi N_F u_{p/s})^2}{1 + (\pi N_F u_{p/s})^2} \,. \tag{2.52}$$

In terms of the scattering phase shift δ the potential u is given by $\pi N_F u = \tan\delta$ and all expressions can be changed to this parametrization by the simple replacement $\sigma = \sin^2\delta$. Often only the two limiting cases, the weak scattering Born limit ($\pi N_F u \ll 1, \sigma \to 0, \delta \to 0$) or strong unitary scattering ($\pi N_F u \to \infty, \sigma \to 1, \delta \to \pi/2$), are examined, to obtain these limits from the general equations given here is straightforward.

Potential scatterer

At first let us address pure potential impurities without any spin flip $\hat{u} = u_p$. By inverting the t-matrix equation the impurity self-energy is given as

$$\hat{\sigma}_{imp} = \frac{1}{2\tau} \frac{c\hat{\tau}_0 + \langle\hat{g}\rangle / \pi}{1 - \sigma_p - \sigma_p \langle\hat{g}\rangle^2 / \pi^2} \qquad c = \sqrt{\frac{1 - \sigma_p}{\sigma_p}} \tag{2.53}$$

The diagonal term $c\hat{\tau}_0$ is shifting the chemical potential and will not enter in the characteristic superconducting properties. It is thus ignored in the further discussion.

The limiting values are found to be

$$\hat{\sigma}_{imp} = \frac{1}{2\tau}\frac{\langle\hat{g}\rangle}{\pi} \quad \text{in Born,} \qquad \text{and} \qquad \hat{\sigma}_{imp} = \frac{-1}{2\tau}\frac{\langle\hat{g}\rangle\,\pi}{\langle\hat{g}\rangle^2} \qquad \text{in unitary limit.} \tag{2.54}$$

It is important to note, that for an s-wave order parameter the self-energies renormalize energy ε_n and order parameter Δ the same way, effectively dropping out, a fact known as Anderson theorem.

Analyzing the effect of impurities on the transition temperature T_c, again the propagator now including the self-energies is linearized in the order parameter, and the attained equation for the impurity self-energy can be explicitly solved. The linearized Green's function

$$\hat{g}^M \approx -i\pi\,\mathrm{sign}(\varepsilon_n)\hat{\tau}_3 + \frac{\pi\hat{\Delta}}{|\varepsilon_n| + \frac{1}{2\tau}} + \frac{1}{2\tau}\frac{\pi\langle\hat{\Delta}\rangle}{|\varepsilon_n|\left(|\varepsilon_n| + \frac{1}{2\tau}\right)} \tag{2.55}$$

is now entering the selfconsistency equation (2.22) and the critical temperature is given by

$$\log\left(\frac{T_{c,0}}{T_c}\right) = \psi\left(\frac{1}{2} + \frac{1}{4\tau\pi\mathrm{k_B}T_c}\right) - \psi\left(\frac{1}{2}\right) + \frac{|\langle\mathcal{Y}\rangle|^2}{\langle|\mathcal{Y}|^2\rangle}\left[\psi\left(\frac{1}{2} + \frac{1}{4\tau\pi\mathrm{k_B}T_c}\right) - \psi\left(\frac{1}{2}\right)\right] \tag{2.56}$$

with $T_{c,0}$ being the critical temperature for clean systems. In contrast to the s-wave case ($\mathcal{Y} = 1$), where as expected the transition temperature is unaffected by potential scattering, in d-wave superconductors $\langle\mathcal{Y}\rangle = 0$ the impurities are pair breaking (indepenend of scattering strength), reducing the crititical temperature. A fact which is true not only for d-wave but all order parameters with vanishing Fermi surface average $\langle\hat{\Delta}\rangle = 0$.

Paramagnetic scatterer

Analzing the effect of spin-flip scattering we will use a model of classical spins introduced by Shiba [46]. In the time reversal symmetry breaking potential

$$\hat{u} = \frac{1}{2}J\boldsymbol{S}\hat{\boldsymbol{\alpha}} = \boldsymbol{u_s}\boldsymbol{\alpha} \qquad \hat{\boldsymbol{\alpha}} = \begin{pmatrix}\hat{\sigma} & 0\\ 0 & \hat{\sigma}^*\end{pmatrix} \tag{2.57}$$

$\boldsymbol{S}$ denotes the spin operator of the localized moment and $\boldsymbol{\alpha}$ is the electron spin operator in 4x4 Nambu representation. The limit of classical impurity spins is takeb by sending $J \to 0$ and $|\boldsymbol{S}| \to \infty$, keeping $J|S|$ finite. Again inverting the t-matrix equation and assuming no net magnetization ($\langle\boldsymbol{S}\rangle = 0$) one finds the impurity self-energy

$$\hat{\sigma}_{imp} = \frac{1}{2\tau_s}\frac{-\left(1 - \sigma + \sigma\left\langle\hat{g}\right\rangle^2/\pi^2\right)\left\langle\hat{g}\right\rangle/\pi + (2 - 2\sigma)\left\langle\hat{g}_3\right\rangle/\pi}{\left(1 - \sigma + \sigma\left\langle\hat{g}\right\rangle^2/\pi^2\right)^2 - 4\sigma(1-\sigma)\left\langle\hat{g}_3\right\rangle^2/\pi^2} \tag{2.58}$$

with the limits

$$\hat{\sigma}_{imp} = \frac{1}{2\tau}\frac{2\langle\hat{g}_3\rangle - \langle\hat{g}\rangle}{\pi} \quad \text{(Born)} \qquad \text{and} \qquad \hat{\sigma}_{imp} = \frac{-1}{2\tau}\frac{\langle\hat{g}\rangle\pi}{\langle\hat{g}\rangle^2} \quad \text{(unitary limit)}. \tag{2.59}$$

This result exhibits some interesting properties. At first, if the Fermi surface average of the offdiagonal elements is vanishing, like for a d-wave order parameter, the self-energy is

$$\hat{\sigma}_{imp} = \frac{1}{2\tau}\frac{\langle\hat{g}_3\rangle/\pi}{1-\sigma-\sigma\langle\hat{g}_3\rangle^2/\pi^2} \tag{2.60}$$

as for potential scatterers. The two different scattering mechanisms are indistinguishable in this case. Secondly due to the broken time reversal symmetry, impurities become also relevant in the conventional s-wave case. But this situation weakens with growing impurity strength, vanishing in the unitary limit where the potential result is regained.

Turning to the ramifacation on the transition temperature the solution for the linearized propagator is now

$$\hat{g}^M \approx -i\pi\,\mathrm{sign}(\varepsilon_n)\hat{\tau}_3 + \frac{\pi\hat{\Delta}}{|\varepsilon_n| + \frac{1}{2\tau}} - \frac{1-2\sigma}{2\tau}\frac{\pi\langle\hat{\Delta}\rangle}{\left(|\varepsilon_n| + \frac{1}{2\tau}\right)\left(|\varepsilon_n| + \frac{2-2\sigma}{2\tau}\right)} \tag{2.61}$$

leading to the dependence of the critical temperature

$$\begin{aligned}\log\left(\frac{T_{c,0}}{T_c}\right) = {} & \psi\left(\frac{1}{2} + \frac{1}{4\tau\pi\mathrm{k_B}T_c}\right) - \psi\left(\frac{1}{2}\right) \\ & - \frac{|\langle\mathcal{Y}\rangle|^2}{\langle|\mathcal{Y}|^2\rangle}\left[\psi\left(\frac{1}{2} + \frac{1}{4\tau\pi\mathrm{k_B}T_c}\right) - \psi\left(\frac{1}{2} + \frac{1-\sigma}{2\tau\pi\mathrm{k_B}T_c}\right)\right].\end{aligned} \tag{2.62}$$

In conclusion the transition temperature is given by a universal dependence [47]

$$\log\left(\frac{T_c}{T_{c,0}}\right) = \psi\left(\frac{1}{2}\right) - \psi\left(\frac{1}{2} + \frac{\alpha}{2\pi\mathrm{k_B}T_c}\right) \tag{2.63}$$

depicted in Figure 2.4 with a pair breaking parameter α which depends on impurity type and order parameter.

Scattering on impurities does not only reduce the transition temperature, also the density of states are affected. Weak scatterer induce states below the band edge, in high concentration leading to gapless superconductivity [47]. In unconventional superconductors bound states on strong impurity sites can be found, giving rise to impurity bands and the possibility of a finite residual density of states at zero energy [48–51].

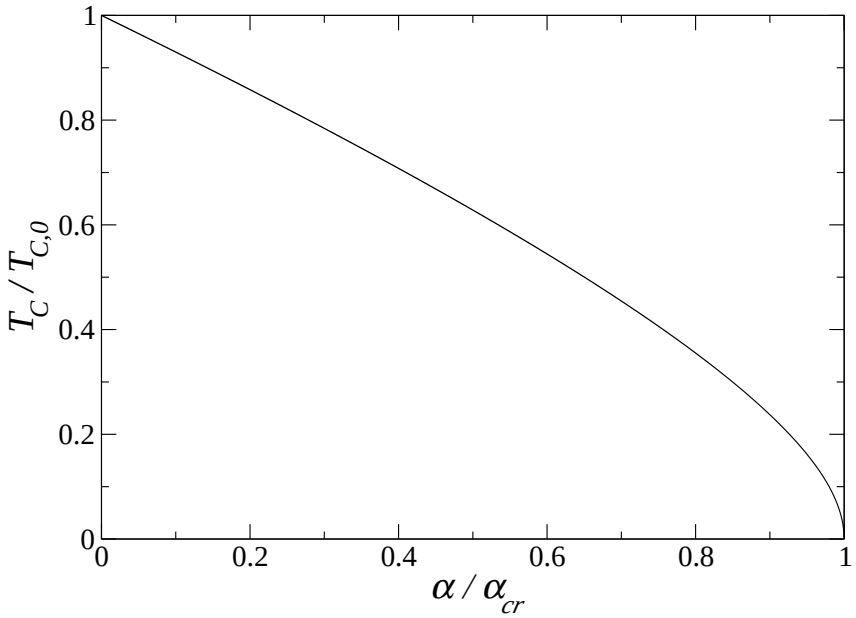

Figure 2.4: Universal dependence of the critical temperature as function of the pair breaking parameter α.

3 Specific heat of Sr_2RuO_4

3.1 Unconventional superconductivity

In the discussion of the superconducting state of novel superconducting materials, the order parameter is usually analyzed according to symmetry considerations. In this considerations the term "unconventional", as used within this thesis, was introduced in literature. A order parameter is defined to be unconventional if it breaks in addition to the gauge invariance at least one additional symmetry of the system. These possibly broken symmetries include time reversal, spin rotational and the crystal symmetry. As sketched in Fig. 3.1 an anisotropic order parameter, even with nodes, is not necessary unconventional. Furthermore an unconventional order parameter might nevertheless give rise to an isotropic spectral gap. A p-wave order parameter like, $k_x + ik_y$ in two dimensions, is unconventional, breaking gauge, lattice and time reversal symmetry but the gap is isotropic. In a solid, due to the crystal field, the angular momentum is not

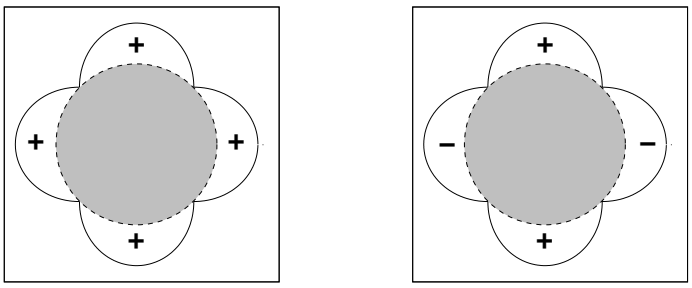

Figure 3.1: Anisotropic vs. unconventional order parameter. The anisotropic s-wave parameter in the left panels the symmetry of the 2d square lattice. I the panel unconventional d-wave order parameter is breaking the rotational symmetry of the crystal lattice.

a good quantum number anymore. Instead of spherical harmonics, the order parameter is given in terms of basis functions obeying the crystal symmetry. Nonetheless the naming scheme s-wave, p-wave, d-wave is still common, classifying the order parameter according to it's rotational symmetry. The basis functions can be interpreted as linear combinations of spherical harmonics with the according angular momentum L.

In this context the name "s-wave" is special. It is frequently used for any conventional order parameters, only breaking the gauge symmetry. In these cases terms like "extended

s-wave" or "anisotropic s-wave" are used to indicate anisotropy.

3.1.1 Triplet superconductivity

The Pauli principle requires the pair amplitude

$$F_{\alpha\beta}(\boldsymbol{r},t;\boldsymbol{r}',t') = \left\langle \psi_\alpha(\boldsymbol{r},t)\psi_\beta(\boldsymbol{r}',t')\right\rangle \tag{3.1}$$

to be odd under the exchange $\alpha \leftrightarrow \beta$, $\boldsymbol{r} \leftrightarrow \boldsymbol{r}'$ in the equal time limit ($t = t'$). If, like in conventional superconductors, the condensate forms a singlet state, the pair amplitude is an even function in momentum. In terms of spherical harmonics these even pairity states correspond to even angular momentum quantum numbers $L = 0, 2, \ldots$.

Like in ^{3}He triplet pairing is also possible. In this case the pair amplitude is even in spin and odd in momentum ($L = 1, 3 \ldots$).

A third possibility is realized in superconductor-ferromagnet heterostructures as discussed in chapter 6. If the equal time limit of the pair amplitude is vanishing, the Pauli principle is also fulfilled. This is the case if the correlation function is odd in frequency. A triplet state with even orbital symmetry might form, which in case of s-wave symmetry is unaffected by non-magnetic disorder.

Working on ^{3}He Balian and Werthammer [52] introduced a convenient notation characterising the order parameter.

In Nambu notation the order parameter is a matrix in spin space of the form

$$\Delta = \begin{pmatrix} \Delta_{\uparrow\uparrow} & \Delta_{\uparrow\downarrow} \\ \Delta_{\downarrow\uparrow} & \Delta_{\downarrow\downarrow} \end{pmatrix} . \tag{3.2}$$

This matrix can alway be written in terms of Pauli matrices as

$$\Delta(\boldsymbol{k}) = (d_0(\boldsymbol{k}) + \boldsymbol{d}(\boldsymbol{k})\boldsymbol{\sigma})i\hat{\sigma}_2 = \begin{pmatrix} -d_x + id_y & d_z + d_0 \\ d_z - d_0 & d_x + id_y \end{pmatrix} . \tag{3.3}$$

Using this parametrization, a singlet order parameter $\Delta_{\uparrow\uparrow} = \Delta_{\downarrow\downarrow} = 0$ and $\Delta\uparrow\downarrow = -\Delta_{\downarrow\uparrow} = \Delta^s$,is characterized by a scalar $d_0(\boldsymbol{k})$ which is odd in momentum. Triplet superconductors are described by a "$\boldsymbol{d}$-vector". A name which is unfortunate and shouldn't be confused with d-wave superconductivity. The energy spectrum is determined by the $\boldsymbol{d}$-vector in the form

$$E_k = \sqrt{\varepsilon_k^2 + \boldsymbol{d}\boldsymbol{d}^* \pm |\boldsymbol{d} \times \boldsymbol{d}^*|} \tag{3.4}$$

and states for which $|\boldsymbol{d} \times \boldsymbol{d}^*| = 0$ are called "unitary". In this case $\hat{\Delta}\hat{\Delta}^\dagger$ is proportional to the unit matrix and the magnitude is given by $\boldsymbol{d}\boldsymbol{d}^* = |\Delta(\boldsymbol{k})|^2$. In the non-unitary case two different energy gaps emerge, by which one can even be equal to zero. Throughout this thesis only unitary order parameter will be discussed. For these the $\boldsymbol{d}$-vector has a direct physical meaning: The direction of $\boldsymbol{d}$ in spin space defines the normal to the

plane in which the electrons are equally spin paired with respect to all quantization axis in the plane, it's magnitude is proportional to the order parameter.

To set some examples for this parametrization the B-phase (or BW-state named after Balian and Werthammer) of ^{3}He has an order parameter

$$\hat{\Delta} = \Delta_0 \begin{pmatrix} -\hat{k}_x + i * \hat{k}_y & \hat{k}_z \\ \hat{k}_z & \hat{k}_x + i\hat{k}_y \end{pmatrix} \tag{3.5}$$

which in terms of the $\boldsymbol{d}$-vector is given by $\boldsymbol{d}(\boldsymbol{k}) = e^{i\phi}\Delta\hat{k}$. In the A-phase, the ABM-state (Anderson Brinkman Morel)

$$\hat{\Delta} = \Delta_0 \begin{pmatrix} \hat{k}_x + i\hat{k}_y & 0 \\ 0 & \hat{k}_x + i\hat{k}_y \end{pmatrix} \tag{3.6}$$

is given by $\boldsymbol{d}(\boldsymbol{k}) = \Delta_0\hat{\boldsymbol{d}}(\hat{\boldsymbol{k}} \cdot \hat{\boldsymbol{m}} + i\hat{\boldsymbol{k}} \cdot \hat{\boldsymbol{n}})$, where $\hat{m}$ and $\hat{n}$ are orthogonal vectors in real space.

3.2 Sr_2RuO_4

Superconductivity in the compound Sr_2RuO_4 was discovered in 1994 by Maeno et al. [53]. A discovery particularly interesting because Sr_2RuO_4 is a layered perovskite oxide and thus isostructural to the high-T_c materials. There the CuO_2 planes are believed to be crucial in the mechanism of high-temperature superconductivity. In Sr_2RuO_4 the copper is replaced by ruthenate, therefore a comparison of this ruthenium oxide with the cuprates could give additional insight in understanding the high temperature superconductors. And the low T_c of 1.5K in Sr_2RuO_4 is a first indication of important differences. But the compound is also interesting by itself, because soon after discovery an unconventional order parameter with triplet pairing was proposed [13]. This time reversal symmetry (TRS) breaking order parameter would be similar to the A phase of superfluid ^{3}He but realized in a solid state system.

Comprehensive reviews of the Fermi liquid and superconducting properties of Sr_2RuO_4 are given by Bergemann et al. [54] and Mackenzie and Maeno [12]. In the following section we will give a very brief summary of the properties relevant for the further discussions.

3.2.1 Basic properties

Early experimental works based on the de-Haas-van-Alphen effect [55] find three Fermi surfaces denoted by α, β and γ-bands, as predicted by band structure calculations [56–58] based on the local-density approximation (LDA).

These three Fermi surfaces are weekly corrugated cylindrical sheets and as also shown by newer ARPES measurements [59] one is hole-like (α) and two are electron-like (β and

γ). In Figure 3.2 the Fermi surfaces as given by the tight binding parametrization of Ref. 60 are shown.

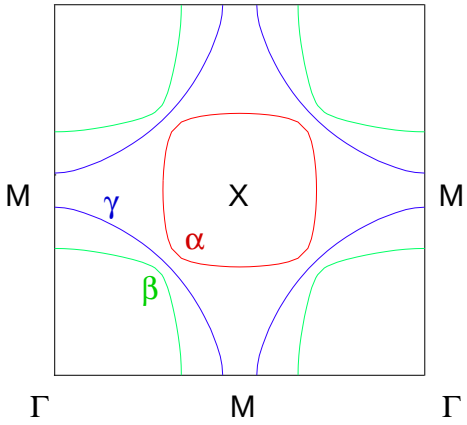

Figure 3.2: Fermi surface of Sr_2RuO_4 as obtained from tight binding parameterization

In contrast to the cuprates (which in the undoped state are Mott insulators), stoichiometric Sr_2RuO_4 is a conductor and can be well described within the Landau Fermi liquid theory [54]. E.g., the normal state specific heat [61] shows the expected $C_V/T \propto \gamma_{el} + \beta_{ph}T^2$ temperature dependence.

As in the HTSC the resistivity of Sr_2RuO_4 single crystals exhibit a strong anisotropy with a ratio of interplane (ρ_c) to intraplane (ρ_{ab}) resistivity of the order 1000 [53,62–65]. But again it obeys the T^2 power-law dependence as expected for a Fermi liquid.

The effective quasiparticle masses are significantly enhanced pointing to strong electron-electron interactions. Due to the similarities of these enhancements to the values found in ^{3}He and other evidence like the ferromagnetism of the three dimensional analogue $SrRuO_3$, Rice and Sigrist [13] early proposed triplet pairing. Knight shift measurements [66] as well as measurements of the magnetic susceptibility [67] support this prediction. Furthermore muon spin relaxation (μSR) experiments [68] suggest a time-reversal symmetry breaking superconducting state.

Finally the strong dependence of superconductivity on non-magnetic disorder [69, 70] is a further indication of unconventional pairing.

3.3 Specific heat in the multiband model

While all the cited experiments allow the conclusion of unconventional triplet pairing in Sr_2RuO_4 the exact symmetry is still an open question. Mostly discussed is an p-wave order parameter $\Delta = \hat{\boldsymbol{z}}(k_x \pm ik_y)$ an two-dimensional anlogue of the ABM-state in ^{3}He. This order parameter would result in an isotropic spectral gap without nodes and thus in

thermally activated (exponential) low-temperature dependence of the specific heat like in conventional s-wave superconductors.

Early measurements [71] on samples with a reduced T_c of $0.8 - 1.14K$ exhibit a high residual specific heat, and an unusual small specific heat jump at T_c. The high density of states at the Fermi level was attributed to non-magnetic impurities in the unitary limit or passive non-superconducting bands. The poor quality of the samples and the measurement only down to $0.3K$ prevented a conclusive interpretation.

Later measurements by the same authors [72] on high quality samples and temperatures down to $0.1K$ show a linear low temperature dependence of C/T and extrapolate to a low γ_0, which suggests that it vanishes in the clean limit. With $\Delta C/\gamma_N T_{c,0} = 0.74 \pm 0.01$ neither the specific heat jump at T_c nor the linear dependence are in accordance with an isotropic spectral gap where a value of $\Delta C = 1.43\gamma_N T_{c,0}$ would be expected. Furthermore the low residual specific heat observed rules out non-superconducting bands.

Further evidence for an order parameter with line nodes are the power-law dependences observed in nuclear spin-lattice relaxation experiments [73], thermal conductivity measurements [74, 75], in measurements of the penetration depth [74] and of the electronic ultrasound attenuation [76].

Since vertical gap nodes are not supported by experiments [75,77,78] and energetically not favorable, Zhitomirsky and Rice proposed a model giving rise to horizontal line nodes of the order parameter [14]: Different pair coupling strength (which is probable looking at the different mass enhancements) on the bands result in varying transition temperatures. A dominant active band becoming superconducting can then by interband scattering (or interband proximity effect) induce superconductivity on the passive bands. Additional to in-plane scattering the authors are taking into account interlayer contributions to the coupling. Their analysis showed that a p-wave order parameter $(k_x + ik_y)$ can induce a gap on the passive bands with horizontal nodes of the form $(k_x + ik_y)\cos(k_z + ik_y)$. In a weak coupling analysis of the specific heat they show that for a range of coupling parameters the experimental curve for the clean data [72] is reproduced.

In the following we will adopt this model and study the influence of impurities on the specific heat. As in Ref. 14 we assume, that the interband coupling of α and β bands are very strong and an effective two-band model can be applied. The total density of states is accordingly assumed to be distributed on the two bands as $N_{F,0} : N_{F,1} = N_{F,\gamma} : (N_{F,\alpha} + N_{F,\beta}) = 0.57 : 043$. In our analysis we will not vary the coupling parameters independently, but as explained below, construct the coupling in such a way, that always only one phase transition occurs, as the experiments suggest.

3.3.1 n-band model

The quasiclassical weak-coupling self-consistency equation can be generalized to a Fermi surface with several sheets, with n conduction bands denoted in the following by index α and β. The gap equation with inter- and intraband coupling can be formulated in

matrix form as

$$\Delta_\alpha(\boldsymbol{p}_F) = \sum_\beta \int_{-\varepsilon_c}^{\varepsilon_c} \frac{\mathrm{d}\varepsilon}{4\pi i}\, N_{F,\beta} \left\langle V_{\alpha\beta}(\boldsymbol{p}_F, \boldsymbol{p}_F{}') f_\beta^K(\varepsilon, \boldsymbol{p}_F{}') \right\rangle_{\boldsymbol{p}_F{}'} \tag{3.7}$$

where the matrix $\hat{V}$ is the generalized coupling parameter. The diagonal elements of $\hat{V}$ are intraband, off-diagonal interband coupling. $N_{F,\alpha}$ is the Fermi-surface density of states on band α and we assume an isotropic DOS on all bands.

The total density of states is distributed on the different bands α as partial density of states $n_\alpha = \frac{N_{F,\alpha}}{N_F}$ and the total density of states is given by $N_F = \sum_\alpha N_{F,\alpha}$.

To solve Eq.(3.7) the coupling parameter and cutoff energies have again to be expressed in terms of the critical temperature. As a first step the interaction is decomposed and diagonalized as

$$N_F \sum_\beta \sqrt{n_\alpha} \left\langle V_{\alpha\beta}(\boldsymbol{p}_F, \boldsymbol{p}_F{}') \sqrt{n_\beta}\, \mathcal{Y}_\beta^{(i)}(\boldsymbol{p}_F{}') \right\rangle_{\boldsymbol{p}_F{}'} = \lambda^{(i)} \mathcal{Y}_\alpha^{(i)}(\boldsymbol{p}_F) \tag{3.8}$$

with eigenvalues $\lambda^{(i)}$and orthonormal eigenvectors $\mathcal{Y}^{(i)}$

$$\sum_\beta \left\langle \mathcal{Y}_\beta^{(i)}(\boldsymbol{p}_F) \mathcal{Y}_\beta^{(j)}(\boldsymbol{p}_F)^* \right\rangle_{\boldsymbol{p}_F} = \delta_{ij}\ . \tag{3.9}$$

In terms of the eigenvectors $\mathcal{Y}^{(i)}$ the order parameter is now given by

$$\sqrt{n_\alpha}\Delta_\alpha(\boldsymbol{p}_F) = \sum_i \lambda^{(i)} \mathcal{Y}_\alpha^{(i)}(\boldsymbol{p}_F) \sum_\beta \int \frac{\mathrm{d}\varepsilon}{4\pi i} \left\langle \mathcal{Y}_\beta^{(i)}(\boldsymbol{p}_F{}')^* \sqrt{n_\beta}\, f_\beta^K(\boldsymbol{p}_F{}'; \varepsilon) \right\rangle_{\boldsymbol{p}_F{}'}\ . \tag{3.10}$$

To proceed we define

$$\Delta^{(i)} = \sum_\alpha \sqrt{n_\alpha} \left\langle \mathcal{Y}_\alpha^{(i)}(\boldsymbol{p}_F)^* \Delta_\alpha(\boldsymbol{p}_F) \right\rangle_{\boldsymbol{p}_F} \tag{3.11}$$

$$f^{(i)}(\varepsilon) = \sum_\alpha \sqrt{n_\alpha} \left\langle \mathcal{Y}_\alpha^{(i)}(\boldsymbol{p}_F)^* f_\alpha^K(\boldsymbol{p}_F; \varepsilon) \right\rangle_{\boldsymbol{p}_F} \tag{3.12}$$

and gap equation for the new order parameters $\Delta^{(i)}$ is then given by

$$\Delta^{(i)} = \lambda^{(i)} \int_{-\varepsilon_c}^{\varepsilon_c} \frac{\mathrm{d}\varepsilon}{4\pi i} f^{(i)}(\varepsilon)\ . \tag{3.13}$$

The largest eigenvalue (chosen to be $\lambda^{(0)}$) and the cutoff energy ε_c can now be eliminated in favor of the superconducting transition temperature T_c.

The original anisotropic order parameters on the bands can be obtained by

$$\sqrt{n_\alpha}\Delta_\alpha(\boldsymbol{p}_F) = \sum_i \mathcal{Y}_\alpha^{(i)}(\boldsymbol{p}_F)\Delta^{(i)} \ . \tag{3.14}$$

We use a model system with two bands and assume that no subdominant coupling is present ($\lambda^{(1)} = 0$). Accordingly the subdominant order parameter is vanishing $\Delta^{(0)}$. In this case, the gaps on the two Fermi sheets are simply given by

$$\Delta_0(\boldsymbol{p}_F) = \frac{\mathcal{Y}_0^{(0)}(\boldsymbol{p}_F)}{\sqrt{n_0}}\Delta^{(0)} \qquad \Delta_1(\boldsymbol{p}_F) = \frac{\mathcal{Y}_1^{(0)}(\boldsymbol{p}_F)}{\sqrt{n_1}}\Delta^{(0)} \ . \tag{3.15}$$

The active band is assumed to obey p-wave symmetry while while the interband coupling has horizontal line nodes.

The interband coupling strength is parameterized by the ratio of the maximum gaps on both bands near T_c

$$\frac{\Delta_1}{\Delta_0} = \alpha(\boldsymbol{p}_F)\sqrt{\frac{n_0}{n_1}} \tag{3.16}$$

and assuming line nodes, the coupling parameter α has the form

$$\alpha(\boldsymbol{p}_F) = \alpha_0\sqrt{2}\cos\left(\frac{p_z}{2}\right) \ . \tag{3.17}$$

At full length the eigenvectors characterizing the interactions are chosen as

$$\begin{pmatrix}\mathcal{Y}_0^{(0)}\\ \mathcal{Y}_1^{(0)}\end{pmatrix} = \frac{(p_x + ip_y)}{\sqrt{1+|\alpha_0|^2}}\begin{pmatrix}1\\ \alpha_0\sqrt{2}\cos(k_z/2)\end{pmatrix} \tag{3.18}$$

$$\tag{3.19}$$

$$\begin{pmatrix}\mathcal{Y}_0^{(1)}\\ \mathcal{Y}_1^{(1)}\end{pmatrix} = \frac{(p_x + ip_y)}{\sqrt{1+|\alpha_0|^2}}\begin{pmatrix}\alpha_0^*\sqrt{2}\cos(p_z/2)\\ -1\end{pmatrix} \ . \tag{3.20}$$

The coupling $V_{\alpha,\beta}$ obtained this way almost reproduces the one of Zhithomirsky and Rice [14], just in our case the diagonal and off-diagonal elements are not independent.

Having obtained the order parameters on the bands, the specific heat of the is calculated by

$$\tag{3.21}$$

3.3.2 Thermodynamic properties

To study the thermodynamic properties of Sr_2RuO_4 the model described above is used. In addition intraband scattering on impurities is included in t-matrix approximation. At first the density of states is investigated.

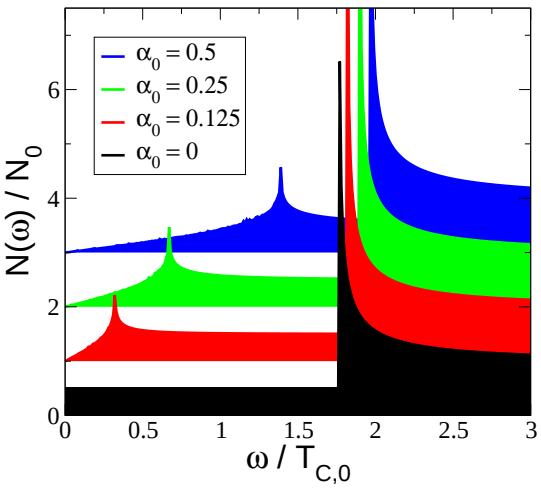

Figure 3.3: Density of states in the clean case for different interband coupling strength α_0

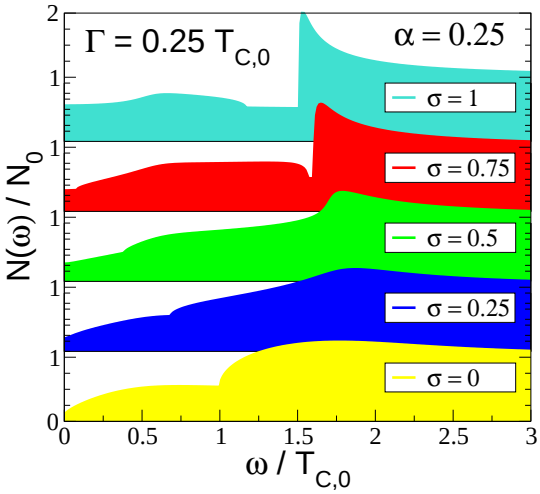

Figure 3.4: Density of states with impurities of different scattering strength

In Fig. 3.3 the DOS for a clean case is shown, and the coupling strength α_0 is varied. Without coupling $\alpha_0 = 0$ the passive band is normal resulting in a finite density of states at all energies. On the active band the DOS is gapped with $\Delta_0 = 1.76T_{c,0}$ as expected. Turning on the coupling, superconductivity is induced also in the normal band. Due to the symmetry of the coupling the order parameter on the passive band has line nodes which result in a linear increasing of the DOS at low energies. The position of the logarithmic divergence due to the induced order parameter is given by the interaction parameter α_0. In the active band the additional coupling increases the size of the gap.

The influence of impurities on the DOS is given in the next Figure. In Fig. 3.4 for fixed $\alpha_0 = 0.25$ and scattering rate $\Gamma = 0.25T_{c,0}$ the impurity strength is varied. For weak scattering, $\sigma = 0$, the gap-like structures are strongly washed out, but the residual DOS at zero energy is low. With increasing impurity strength the influence on the gap divergence is reduced, on the other hand low energy states are induced as impurity band.

To extract the relevant parameters the residual density of states (RDOS) is analyzed. In the experiment of Ishida et al. [73] a RDOS of $N_{res} = 0.6N_0$ was observed in samples with a transition temperature of $T_c = 0.7K$. In Fig. 3.5 the residual density of states for different coupling parameters and impurity strength are displayed as function of the scattering rate. The experimental value and the according scattering rate given by T_c are indicated by dashed lines. The values obtained in Born limit are much lower, the ones in unitary limit considerably higher than the experimental value independent of the coupling strength. The comparison indicates an intermediate scattering strength of $\sigma \approx 0.5$ and a coupling parameter of $\alpha_0 \approx 0.3$.

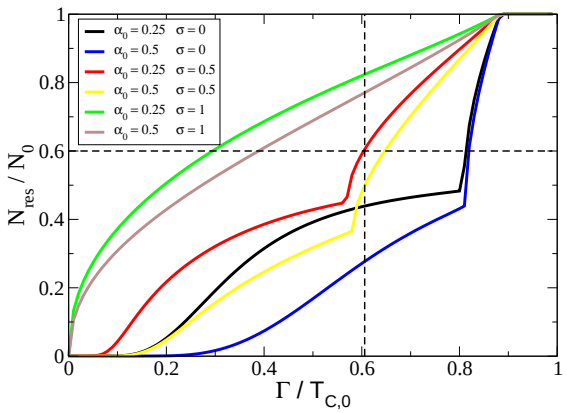

Figure 3.5: Residual density of states for different couplings and impurity strength

Turning to the specific heat in the clean case (Fig. 3.6) the dependence on the coupling

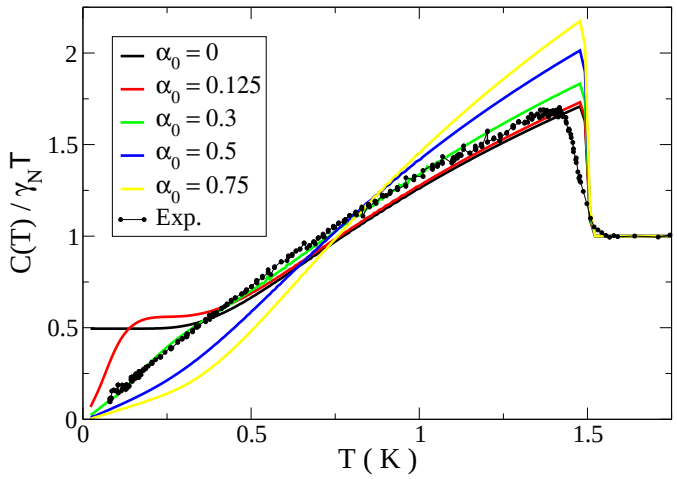

Figure 3.6: Specific heat of the clean system. The experimental values of NishiZaki et al. [79] are included.

parameter is examined. Without coupling the specific heat saturates at a finite value at low temperature as a consequence of the normal passive band. With interband coupling the passive band is superconducting, but due to the line nodes C/T is increasing linearly at low temperatures. The precise temperature dependence is coupling dependent. The best agreement with experiment is found for $\alpha_0 = 0.3$ consistent with the value extracted before.

With the same parameters also the nuclear spin relaxation rate can be calculated. In Fig. 3.7 we show the spin relaxation rate as obtained for two different scattering rates.

The scattering rates correspond to the critical temperatures T_c of the two samples in the

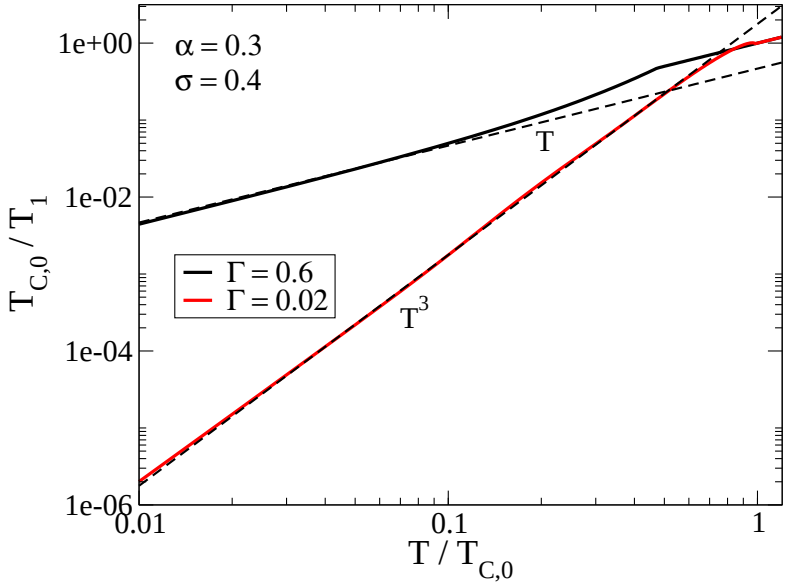

Figure 3.7: Nuclear spin relaxation rate for fixed interband coupling and two different impurity scattering rates as extracted from experiment.

nuclear spin relaxation experiment of Ishida et al. [73]. Having fixed the coupling α and impurity scattering strength σ before, the calculations are without any free parameter. The experimental observed crossover from a cubic temperature dependence $1/T_1 \propto T^3$ in the clean sample, to a linear behaviour in low T_c samples is reproduced.

3.4 p-wave model with boson mode

Point contact measurements in the group of von Löhneysen [15] investigated the superconducting gap function and conductance spectra of Sr_2RuO_4. In the paper, the conductance spectra could be well fitted by calculations assuming a p-wave order parameter $k_x + ik_y$. But the observed enhancement current reveals an unusual temperature dependence. A p-wave scenario alone does not account for the experimental findings. Using a model including a low-energy boson mode,Laube et al. [16] could obtain an excellent agreement with the experimental data.

In a unconventional superconductor, a Millis et al. [80] showed, an Einstein mode characterized by a spectral weight

$$A_B(\omega) = \frac{\pi}{2} J \omega_B \delta(\omega - \omega_B) \tag{3.22}$$

in good approximation can be ed by a temperature dependend pair breaking parameter

$$\Gamma_{in}(T) = \pi J_B \omega_B \coth(\frac{\omega_B}{2T}) \ . \tag{3.23}$$

The pair breaking is increasing with temperature, changing the usual temperature dependence of the order parameter. Since with this model the temperature dependence of the enhancement current could be consistently explained, an investigation of the specific heat for the same model is crucial.

Like the authors of [16], we assume a single band with p-wave pairing $k_x + ik_y$. Pair breaking due to the boson mode is included as self-energy calculated in self-consistent Born approximation,i.e., $\hat{\sigma}_{in} = \Gamma_i n(T) \langle \hat{g}(\varepsilon, \boldsymbol{p}) \rangle_{\boldsymbol{p}_F}$. In the calculation it is assumed, that the boson spectrum does not change with the superconducting transition.

The result for the specific heat are shown in Fig. 3.8. The boson mode does not change

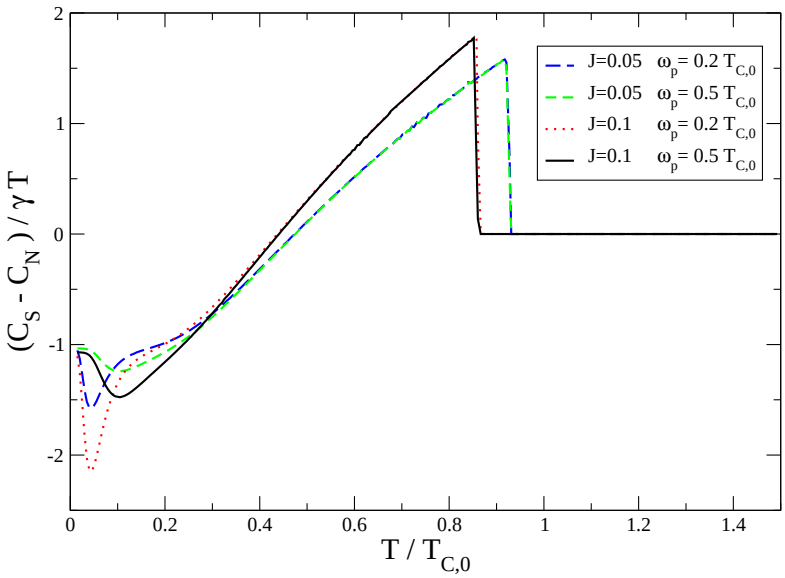

Figure 3.8: Specific heat including a pair breaking boson mode. The coupling strength is given by J, the energy of the mode by ω_p.

the activated behavior in the superconducting state, however a clear dip given by the boson energy is observable. In the calculation only the difference of superconducting free energy to the free energy in the normal state can be obtained. The low temperature structure is attributed to an enhanced specific heat in the normal state, coupling to the boson mode. An important quantity is the jump of the specific heat at the superconducting transition. Due to the temperature dependence of the pairbreaking parameter the zero temperature order parameter given in units of the critical temperature $\Delta(T = 0)/T_c$ is increasing. As consequence, the jump at the transition is increasing with increasing

coupling to the boson mode. In experiment a jump of $\Delta C/\gamma_N T_{c,0} = 0.74 \pm 0.01$ was observed, while $\Delta C = 1.43\gamma_N T_{c,0}$ would be expected for a fully gapped p-wave order parameter. Including the boson mode the size of the jump is even increasing, clearly deviating from the experimental result.

3.4.1 Boson mode in strong coupling calculation

In the previous calculation of the specific heat, we used the approximation of an inelasstic scatterer. An approximation which is well founded for temperatures much larger than the boson frequency. Calculating the low temperature specific heat down to zero temperature, this range of validity was clearly exceeded. To exclude the possibility of anomalies due to the approximation, the boson mode should be included in a full strong coupling calculation. Following the lines of Bergmann et al. [81] the coupling to the boson field is renormalizing the frequency as

$$\tilde{\omega}(n) = \omega_n + \pi T \sum_m \lambda(\omega_n - \omega_m) \frac{\tilde{\omega}(m)}{[\tilde{\omega}^2(m) + \Delta^2]^{1/2}} \tag{3.24}$$

$$\lambda(\omega_n - \omega_m) = 2 \int_0^\infty \mathrm{d}\omega \frac{\omega \alpha^2 F(\omega)}{\omega^2 + (\omega_n - \omega_m)^2} \,, \tag{3.25}$$

and the free energy including the boson field can be written as

$$\begin{aligned} \frac{\Omega_N - \Omega_S}{N_0} =& 2\pi T \sum_n \omega_n \Big(\frac{\tilde{\omega}(n)}{[\tilde{\omega}^2(n) + \Delta^2]^{1/2}} - \operatorname{sign} \omega_n \Big) \\ &+ \pi^2 T^2 \sum_{n,m} \Big[\Big(\frac{\tilde{\omega}(n)}{[\tilde{\omega}^2(n) + \Delta^2]^{1/2}} \frac{\tilde{\omega}(m)}{[\tilde{\omega}^2(m) + \Delta^2]^{1/2}} - \operatorname{sign}(\omega_n \omega_m) \Big) \lambda(\omega_n - \omega_m) \,. \\ &\quad + \frac{\Delta}{[\tilde{\omega}^2(n) + \Delta^2]^{1/2}} \frac{\Delta}{[\tilde{\omega}^2(m) + \Delta^2]^{1/2}} \lambda(\omega_n - \omega_m) \Big] \end{aligned} \tag{3.26}$$

Here we used the fact, that the boson mode due to the different symmetry does not contribute to the pairing. Therfor the offdiagonal self-energy Δ is not a function of energy as in usual strong coupling calculations. Using the aforementioned stationary conditions and thereby given expressions for the self-energies, the free energy can be expressed by

$$\begin{aligned} \frac{\Omega_N - \Omega_S}{N_0} = 2\pi T \sum_{n>0} \Big(& 2 \big\{ [\tilde{\omega}^2(n) + \Delta^2]^{1/2} - \tilde{\omega}(n) - \frac{1}{2} \frac{\Delta^2}{[\tilde{\omega}^2(n) + \Delta^2]^{1/2}} \big\} \\ & - [\tilde{\omega}(n) - \tilde{\omega}_0(n)] \big\{ \frac{\tilde{\omega}(n)}{[\tilde{\omega}^2(n) + \Delta^2]^{1/2}} - 1 \big\} \Big) \end{aligned} \,. \tag{3.27}$$

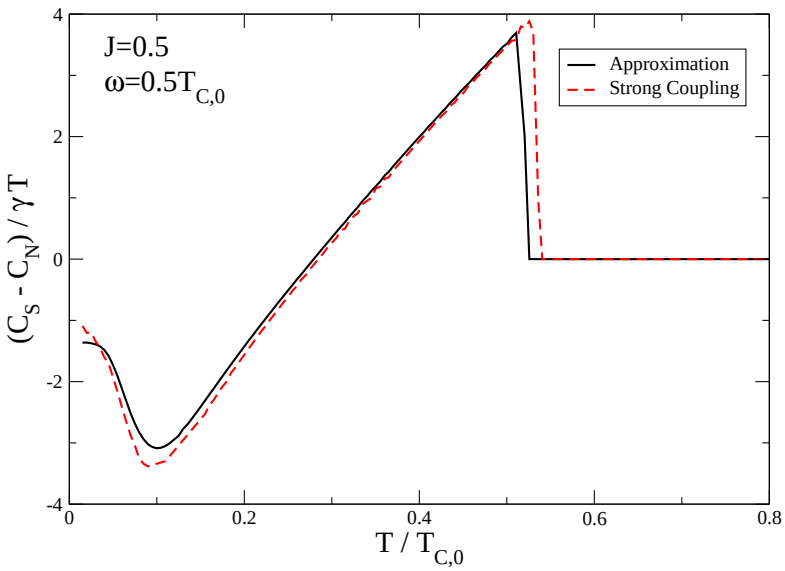

Figure 3.9: Comparison of the specific heat within the inelastic scatter approximation and full strong coupling calculation

This expression is especially well suited for numerical calculations. In Fig. 3.9 results for a fixed coupling and boson frequency are shown. The exact calculation approves the qualitative results of the approximated computation. In the approximation the reduction of the critical temperature is overestimated, while the contributions of the phonon mode to the specific heat are underestimated. In the limit $T \to 0$ the approximation shows little deviations from the analytically expected $(C_S - C_N)/\gamma T = -1$, a deviation which is cured by the strong coupling analysis.

4 Tunneling spectroscopy on cuprate superconductors

The unexpected discovery of superconductivity in the doped Mott insulator $La_{2-x}Ba_xCuO_4$ (LBCO) with an unusually high critical temperature of 35K introduced a whole new class of superconducting compounds, the cuprates. All materials of this class are copper based antiferromagnetic insulators in the undoped state and share a similar crystal structure. Superconductivity is attained by doping, at which one has to distinguish two subclasses: electron-doped and hole-doped alloys. The doping dependence is depicted in the phenomenological phase diagram sketched in Fig. 4.1.

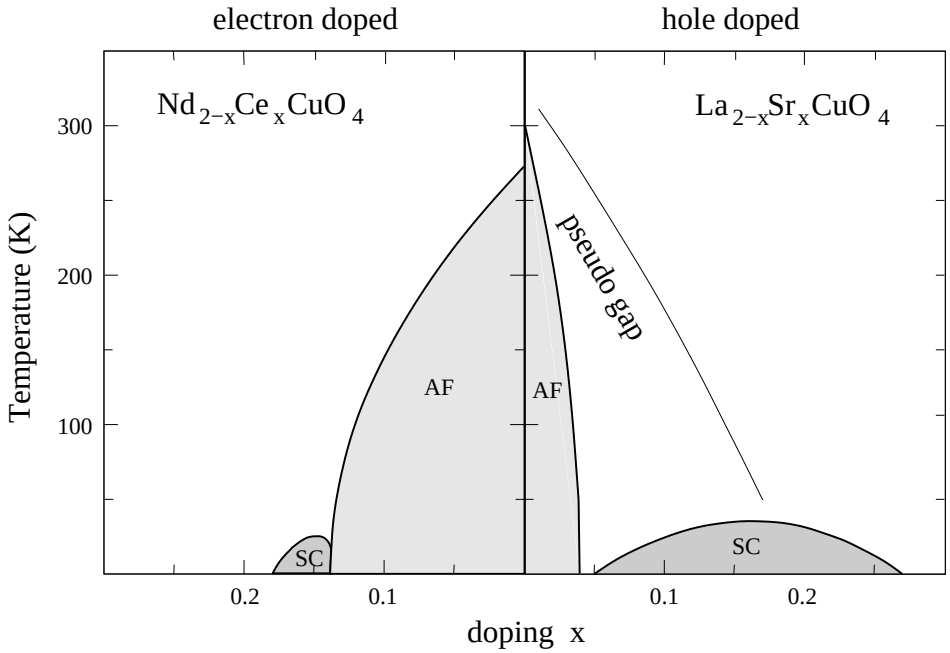

Figure 4.1: Phase diagram of electron- and hole-doped high-temperature superconductors exemplarily shown for $Nd_{2-x}Ce_xCuO_{4-\delta}$ and $La_{2-x}Sr_xCuO_4$ [82]. The antiferromagnetic (AF) and superconducting (SC) phases are drawn.

The original LBCO, as well as the technologically most popular and best known compounds $Bi_2Sr_2Ca_nCu_{n+1}O_{2n+6+\delta}$ and $YBa_2Cu_3O_{7-x}$, are hole-doped. Their insulating

antiferromagnetic phase is restricted close to half filling and superconductivity is observed in a broad range of doping. On the "opposite side" of the phase diagram, for the electron-doped cuprates like $Nd_{2-x}Ce_xCuO_{4-\delta}$ and $Pr_{2-x}Ce_xCuO_{4-\delta}$ the antiferromagnetic phase is dominant and superconductivity is only found in a narrow doping range. A fact not only making sample preparation and studies on doping dependence a challenge, but also pointing to the possibility of subtle differences. A possibility which strongly supported, e.g., by Nernst experiments [83] on the vortex phase in both classes of HTSC.

Before turning to the electron-doped materials and the controversial discussion of the order parameter symmetry there, we will first investigate some properties of the hole-doped class.

4.1 Hole-doped cuprates

After a lot of discussion about the nature of the order parameter in the high-T_c materials, a number of experiments have made it virtually certain that hole-doped cuprates like $YBa_2Cu_3O_{7-x}$ (YBCO) are superconductors whose order parameter has a d-wave symmetry. A fact especially established by phase-sensitive experiments [18, 19] that investigated superconducting quantum interference devices or ring structures containing junctions either between YBCO and ordinary superconductors, or between different domains of YBCO.

4.1.1 Broadening of Andreev bound states

As explained in unconventional superconductors like those with a d-wave symmetry, the order parameter is sensitive to scattering from non-magnetic impurities and surface roughness. The order parameter also has a non-trivial structure close to surfaces and interfaces. Surfaces and interfaces can be pair-breaking, i.e., the order parameter is suppressed on a length scale given by the coherence length as shown, e.g., in Fig. 4.2. Andreev reflection processes of quasi-particle excitations from the spatial profile of the order parameter, combined with conventional (and/or Andreev) reflection from the surface (interface) can result under certain conditions in surface (interface) bound states [84, 85]. In particular, it has been shown [21] that an interface for which the sign of the order parameter changes along a given trajectory will *always* support a bound state at the Fermi energy. A mathematically equivalent situation arises if we consider a specular reflecting wall [84, 86–88] for which the sign of the order parameter is different for incoming and outgoing quasiparticles, i.e., there will also be a bound state.

These bound states lead to a qualitative change of the Josephson current through a tunnel junction as has been found in Refs. [89–91]. It was shown that the temperature dependence of the critical current is dramatically different from the standard Ambegaokar-Baratoff prediction. The critical current may increase substantially at

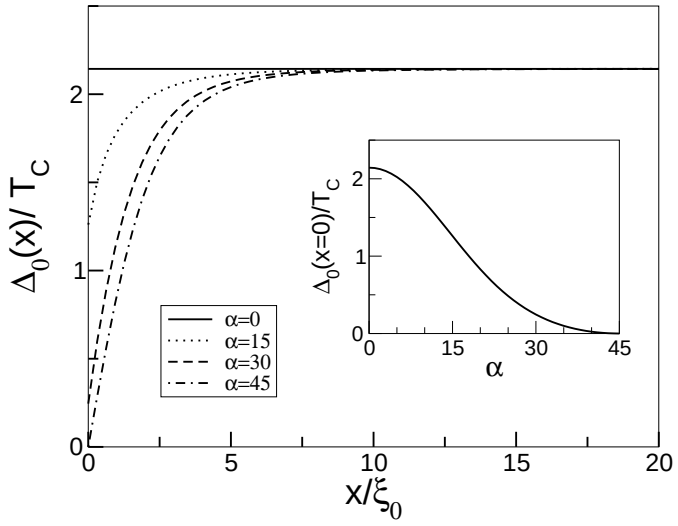

Figure 4.2: Suppression of a d-wave order at a specular reflecting surface. The order parameter profile is given for different surface misorientations.

low temperatures [89] or even change sign, i.e., the junction may change its nature from an ordinary junction to a π-junction characterized by a current-phase relation $I = I_c \sin(\phi + \pi) = -I_c \sin(\phi)$. The authors of Ref. 89 also considered the influence of surface roughness on this phenomenon and showed that it gets weaker because of a broadening of the bound states. In this section, we want to discuss how scattering from bulk impurities changes the bound states and, as a consequence, the Josephson critical current [92].

Using the quasiclassical theory we include bulk impurities in the standard way by using an impurity self-energy. The self-energy is calculated in the selfconsistent t-matrix approximation, and we concentrate on two limits, viz., the limits of Born scattering (weak scattering, scattering phase shift $\delta_0 \ll 1$) and unitary scattering (strong scattering, $\delta_0 \to \pi/2$).

We calculate the angle-resolved density of states and the Josephson critical current in the presence of impurity-broadened bound states. By numerical calculation we find that bulk impurities will cut off the zero-temperature divergences in the critical current predicted for clean systems. We also develop an analytical understanding of these results and give analytical expressions for small scattering rates. Surprisingly, we find that the bound states are more sensitive to Born scatterers than to unitary scatterers at a given scattering rate.

Formalism and model assumptions

In the following we consider the system shown in Fig. 4.3, consisting of a junction between two $d_{x^2-y^2}$ superconductors. The order parameter on side i, $(i = l, r)$ is rotated by an angle α_i with respect to the surface normal. The junction is assumed to be weakly transparent and will be modeled as a tunnel junction. We assume that the superconductors contain a small concentration of impurities, and we would like to study the influence of these impurities on the quasiparticle bound states formed at the junction [21, 89].

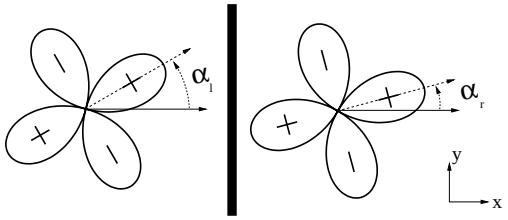

Figure 4.3: Geometry of the model system: a tunnel junction between two misoriented $d_{x^2-y^2}$ superconductors

In unconventional superconductors, the order parameter is spatially inhomogeneous close to obstacles like surfaces or interfaces. The quasiclassical formalism of superconductivity [25, 26, 93] is ideally suited for calculating the structure of the order parameter in a self-consistent way.

The pairing interaction in the $d_{x^2-y^2}$ channel is defined by

$$V(\boldsymbol{p}_F, \boldsymbol{p}_F{}') = \lambda \cos(2\phi - 2\alpha_i) \cos(2\phi' - 2\alpha_i) \,, \tag{4.1}$$

where $i = l, r$, and ϕ is the azimuthal angle between $\boldsymbol{p}_F$ and the surface normal $\hat{\boldsymbol{n}}$. The amplitude of the pairing interaction is denoted by λ which will be eliminated in favor of the critical temperature T_c in our calculations.

The self-energy $\hat{\sigma}$ describes impurity scattering, and we consider two limits, viz., weak scattering (scattering phase shift $\delta_0 \ll 1$), which will be treated in the Born approximation, and unitary scattering ($\delta_0 \to \pi/2$). For an isotropic point-like impurity potential, the off-diagonal components of the self-energy vanish for order parameters transforming according to non-trivial representations of the point symmetry group of the crystal. This is the case for the d-wave order parameter studied here. The self-energy is then characterized by a single scalar function. In the Born limit the self-energy is given by

$$\sigma_{imp}(\boldsymbol{R}; \varepsilon_n) = \frac{\Gamma_b}{\pi} \langle g(\boldsymbol{R}, \boldsymbol{p}_F; \varepsilon_n) \rangle \quad , \qquad \Gamma_b = \frac{1}{2\tau} \,, \tag{4.2}$$

where τ denotes the elastic scattering time in the normal metal, whereas in the unitary limit

$$\sigma_{imp}(\boldsymbol{R};\varepsilon_n) = -\Gamma_u \frac{\pi}{\langle g(\boldsymbol{R},\boldsymbol{p}_F;\varepsilon_n)\rangle} \ , \qquad \Gamma_u = \frac{n_i}{\pi N_F} \ . \tag{4.3}$$

Here, n_i is the concentration of impurities, and N_F is the (normal) density of states at the Fermi energy.

In the framework of the quasiclassical formalism, interfaces are taken into account by Zaitsev's boundary conditions [35]. The properties of the barrier are characterized by the transmission probability $D(\boldsymbol{p}_F)$.

In the limit of zero transparency (illustrated in Fig. 4.4) the boundary conditions reduce to $\hat{g}(\boldsymbol{p}_{F,in}, 0^+) = \hat{g}(\boldsymbol{p}_{F,out}, 0^+)$. We will assume specular reflection.

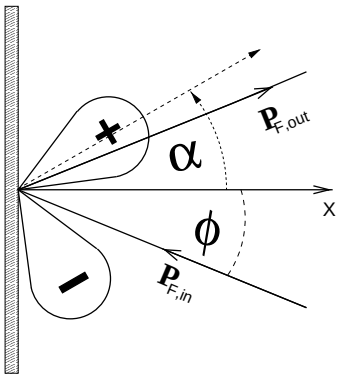

Figure 4.4: Geometry of incoming and outgoing quasiparticle trajectories for a nontransparent interface.

We are interested in the Josephson current through the system shown in Fig. 4.3. In first order in the transparency this can be expressed as

$$j_c = \frac{eN_F^l}{2\pi} T \sum_{\varepsilon_n} \Big\langle v_{F_\perp}^l(\boldsymbol{p}_{F,in}^l) D(\boldsymbol{p}_{F,in}^l) \Big[f^l(\boldsymbol{p}_{F,in}^l;\varepsilon_n) \tilde{f}^r(\boldsymbol{p}_{F,out}^r;\varepsilon_n) - \tilde{f}^l(\boldsymbol{p}_{F,in}^l;\varepsilon_n) f^r(\boldsymbol{p}_{F,out}^r;\varepsilon_n) \Big] \Big\rangle_{\boldsymbol{p}_{F,in}^l} \ , \tag{4.4}$$

where the Green's functions have to be evaluated at the interface for real order parameters, as if they would not have complex phases. In the results, we will eliminate the transparency and express it through the normal-state resistance of the junction which is given by (again in first order of the transparency)

$$R_N^{-1} = e^2 A N_F^l \Big\langle v_{F_\perp}^l(\boldsymbol{p}_{F,in}^l) D(\boldsymbol{p}_{F,in}^l) \Big\rangle_{\boldsymbol{p}_{F,in}^l} \ . \tag{4.5}$$

In the calculation, we will assume the model directional dependence of the transparency for a δ-potential in the tunneling limit: $D(\phi) = D_0 \cos(\phi)^2$.

Results for Born and unitary limit

A surface of an unconventional superconductor may support a bound state at the Fermi energy [21, 84–89, 94, 95]. We reproduce this phenomenon by a self-consistent solution of a real-time version of the Eilenberger equation taking into account bulk impurity scattering. Figure 4.5 shows the angle-resolved local density of states (taken at the surface) obtained in the Born limit for the geometry shown in Fig. 4.4. The bound states present in a clean system can be seen to be broadened by impurity scattering.

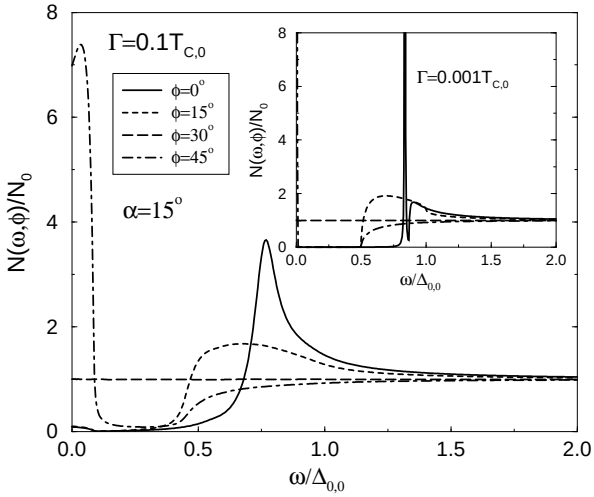

Figure 4.5: Local density of states calculated for a misorientation angle of $\alpha = 15°$ at a scattering rate of $\Gamma_b = 0.1T_{c,0}$ in Born approximation. The temperature is $T = 0.01T_{c,0}$. Inset: The same for a low scattering rate $\Gamma_b = 0.001T_{c,0}$.

In order to estimate the dependence of the height of the zero-energy peak in the density of states on the relaxation time in the Born limit, we proceed analogously to the analytical consideration developed in Ref. [94], based on the Eilenberger equations. In particular, the residue of the Green's function for midgap states were analytically calculated there in the clean limit. Due to the presence of impurities the pole of the retarded Green's function at zero energy moves into the complex plane, although its midgap value at the surface $g(x = 0, \boldsymbol{p}_F; \varepsilon = 0) \equiv g(\boldsymbol{p}_F, 0)$ is still large in the case of a sufficiently large relaxation time. Under this condition we obtain the following integral

equation for $g(\boldsymbol{p}_F, 0)$:

$$2\pi^2|v_x|\tau = -g(\boldsymbol{p}_{F,in}, 0) \times \int_0^\infty \mathrm{d}x \left\langle g(\boldsymbol{p}_F{}', 0) \exp\left[-\int_0^x \mathrm{d}x' \frac{2|\Delta(\boldsymbol{p}_F{}', x')|}{|v_x'|}\right]\right\rangle_{\boldsymbol{p}_F{}'}$$
$$\times \left(\exp\left[-\int_0^x \mathrm{d}x' \frac{2|\Delta(\boldsymbol{p}_{F,in}, x')|}{|v_x|}\right] + \exp\left[-\int_0^x \mathrm{d}x' \frac{2|\Delta(\boldsymbol{p}_{F,out}, x')|}{|v_x|}\right]\right) . \quad (4.6)$$

The order parameter can be factorized in the form $\Delta(\boldsymbol{p}_F, x) = \Delta_0\psi(\boldsymbol{p}_F, x)$. Here $\psi(\boldsymbol{p}_F, x)$ is a dimensionless normalized function of the momentum direction and the distance from the surface ($|\psi(\boldsymbol{p}_F, x)| \leq 1$), while Δ_0 is the maximum value of the bulk order parameter depending upon temperature and impurity concentration. The spatial dependence of $\psi(\boldsymbol{p}_F, x)$ reduces to a dependence upon dimensionless coordinate $X = \Delta_0 x/\boldsymbol{v}_F$. Introducing the dimensionless variables X, X' into Eq. (4.6), we see that the propagator has the form $g(\boldsymbol{p}_F, 0) = -i\sqrt{\tau\Delta_0}\bar{g}(\boldsymbol{p}_F, 0)$, where $\bar{g}(\boldsymbol{p}_F, 0)$ does not contain τ and Δ_0. Hence, the height of the peak in the density of states is proportional to $\sqrt{\tau\Delta_0}$. By considering a generalization of the integral equation (4.6) to nonzero (although sufficiently small) values of the energy, one can show analytically that the shift of the pole position from its zero value is proportional to $\sqrt{\Delta_0/\tau}$. Thus, introducing the dimensionless quantity $\Omega_n = \varepsilon_n\sqrt{\tau/\Delta_0}$, we can represent the contribution of the midgap states to the Green's function as $g(x = 0, \boldsymbol{p}_F; \varepsilon_n) = -i\sqrt{\tau\Delta_0}\bar{g}(\boldsymbol{p}_F, \Omega_n)$.

The relative strength of the influence of impurities on bound states in the Born and in the unitary limits can be understood qualitatively by looking at Eqs. (4.2) and (4.3). In the absence of bound states, the Green's function $g(\boldsymbol{R}, \boldsymbol{p}_F; \varepsilon_n)$ is usually quite small (compared to the normal-state value) for sufficiently small ε_n. In this case, according to Eqs. (4.2) and (4.3), the self-energy function for unitary scatterers can be significantly greater than the one in the Born limit. By contrast, if there are bound states on (or quite close to) the Fermi surface, then the corresponding large pole-like term in the expression for $g(\boldsymbol{R}, \boldsymbol{p}_F; \varepsilon_n)$ essentially rises with decreasing temperature. This leads to the inverse situation, that is to small values of the self-energy for unitary scatterers as compared to the Born limit for the same values of the scattering rates. An analogous conclusion can be drawn for the retarded propagator and the self-energy function taken at energies close to some bound state, even if it is not at the Fermi surface. Since the pole-like term decreases with increasing Γ, the above consideration, in general, does not work for sufficiently large values of Γ_b, Γ_u. Our numerical calculations justify the above conclusion: in the presence of unitary scatterers, for sufficiently small values of Γ_u, the bound states are broadened much more weakly than in the Born limit. In contrast to the Born limit, the dependence of the propagator on the parameter Δ_0/Γ_u does not reduce to a power-law behavior in the unitary limit, so that simple scaling estimates are not fruitful in this limit. However, some rough qualitative estimates can be done in

the unitary limit as well, in particular, by considering the simplest model d-wave order parameter, whose momentum direction dependence reduces to Δ_0 (for $0 < \phi < \pi/2$ and $\pi < \phi < 3\pi/2$) and to $-\Delta_0$ (for $\pi/2 < \phi < \pi$ and $3\pi/2 < \phi < 2\pi$). Then for small enough Γ_u we find the propagator $g(x = 0, \boldsymbol{p}_F; \varepsilon_n = 0)$ to be proportional to $\sqrt{\Gamma_u/\Delta_0}\exp(A\Delta_0/\Gamma_u)$ with some numerical factor A of the order of unity.

We will now concentrate on the temperature and impurity dependencies of the Josephson critical current. Two typical and experimentally relevant geometries will be studied: the "symmetric" junction for which $\alpha_l = \alpha_r$, and the "mirror" junction for which $\alpha_l = -\alpha_r$.

In contrast to surface roughness, bulk impurities not only broaden the bound states but also change the maximum of the bulk pair potential and the critical temperature from their clean-system values $\Delta_{0,0}$ and $T_{c,0}$. This can be seen in the lower panel of Fig. 4.6, where the finite scattering rate leads to a renormalized value of T_c. Figure 4.6 shows the critical current for the symmetric geometry in Born approximation. The anomalous temperature dependence discussed in Ref. 89 is still visible, but bulk impurities cut off the divergence at zero temperature.

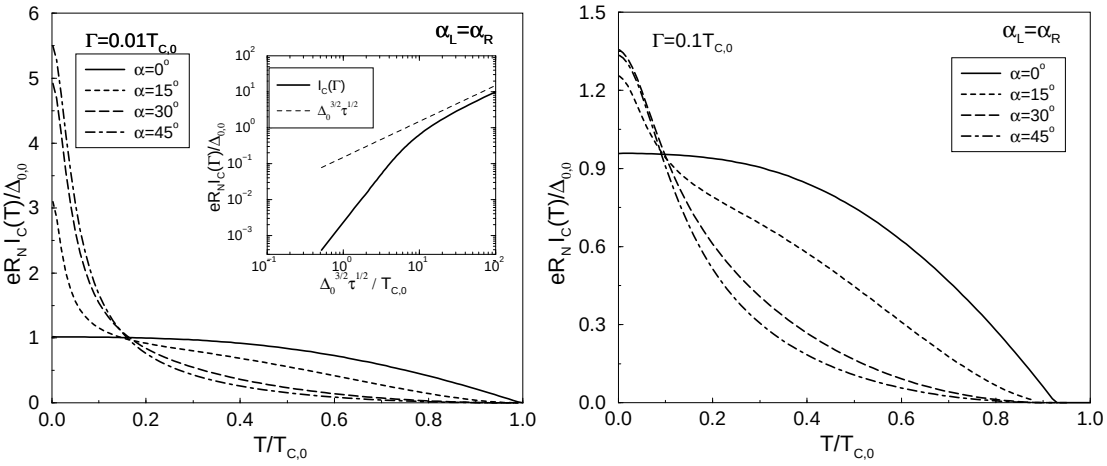

Figure 4.6: Temperature dependence of the critical current for the symmetric junction, i.e., $\alpha_l = \alpha_r$, and different misorientation angles α. Impurity scattering is parametrized by the scattering rate Γ_b using the Born approximation, Eq. (4.2). Inset: Critical current for misorientation $\alpha = 45°$ and fixed temperature $T = 0.005T_{c,0}$ as a function of the scattering rate.

We obtain an analytical estimate of the Josephson critical current in the zero-temperature limit from Eq. (4.4), taking into account the large low-energy values of the quantities $f^{L(R)}$, which are associated with g the same way as in the clean limit [89, 94]: $f(x = 0, \boldsymbol{p}_F; \varepsilon_n) = -\tilde{f}(x = 0, \boldsymbol{p}_F; \varepsilon_n) = -i\mathrm{sign}(v_x\Delta_\infty(\boldsymbol{p}_F))\, g(x = 0, \boldsymbol{p}_F; \varepsilon_n)$. Proceeding

analogously to Ref. 89 for the symmetric (mirror) junction and introducing Ω as a new integration variable, we get

$$j_c = \pm\frac{eN_F^l}{2\pi^2}\Delta_0^{3/2}\tau^{1/2}\int_{-\infty}^{\infty} d\Omega \left\langle D(\boldsymbol{p}_{F,in}^l)v_x^l(\boldsymbol{p}_{F,in}^l)\bar{g}^2(X=0,\boldsymbol{p}_{F,in}^l;\Omega)\right\rangle_{\boldsymbol{p}_{F,in}^l} \quad . \quad (4.7)$$

The plus (minus) sign corresponds here to the symmetric (mirror) junction.

Thus, in the Born limit and under the condition $\Delta_0\tau \gg 1$ the critical current turns out to be proportional to $\Delta_0^{3/2}\tau^{1/2}$.

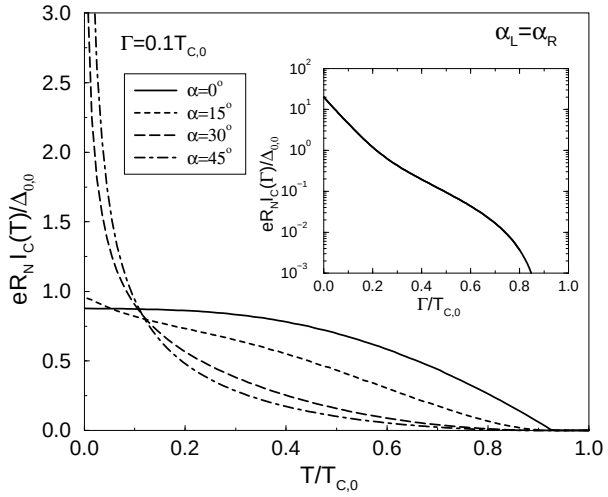

Figure 4.7: Critical current as a function of temperature for the symmetric junction in the unitary limit. Inset: Critical current for misorientation $\alpha = 45^\circ$ and fixed temperature $T = 0.01T_{c,0}$ as a function of the scattering rate.

In the unitary limit, shown in Fig. 4.7, we find that the bound states are remarkably stable to impurity scattering, according to our conclusion made above. For sufficiently large values of Γ_u (when $\Gamma_u/T_{c,0}$ is of the order of unity), however, the influence can be substantial as can be seen in the inset of Fig. 4.7.

Figures 4.8 and 4.9 show the corresponding results for the mirror junction. As in Ref. 89, the critical current changes sign, i.e., the junction changes character (for some misorientation angles) and becomes a π-junction at low temperatures. Bulk impurity scattering weakens this tendency.

At this point, we would like to comment on the range of validity of the Born and unitary approximation. The Born approximation for impurity scattering in superconductors is valid if the characteristic parameter $\tan(\delta_0)\langle g\rangle/\pi \ll 1$. The unitary limit holds

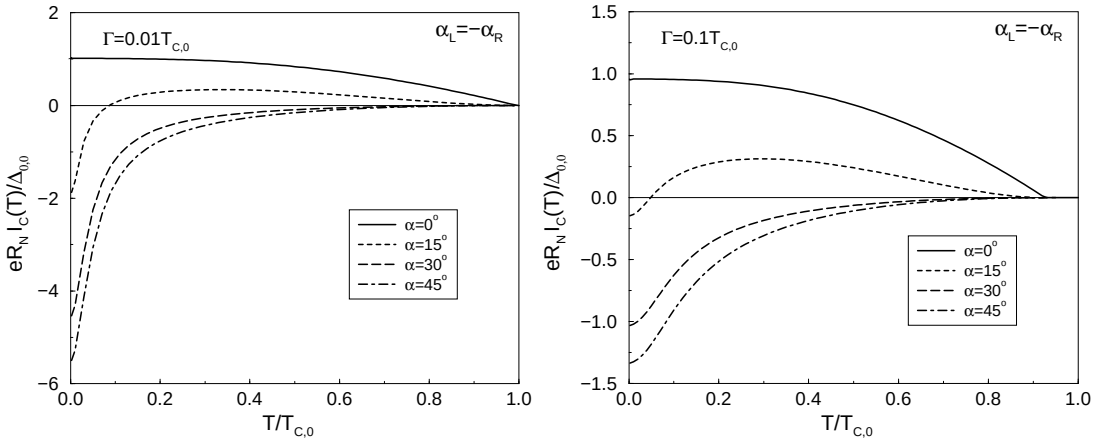

Figure 4.8: Temperature dependence of the critical current for the mirror junction, i.e., $\alpha_l = -\alpha_r$ for two scattering rates Γ_b in Born approximation.

under the opposite condition $\tan(\delta_0)\langle g\rangle/\pi \gg 1$. Even if the impurities in the normal metal are Born impurities ($\delta_0 \ll 1$), the large value of the averaged propagator $\langle g\rangle$ may therefore lead to a situation in which the Born approximation cannot be applied to study Andreev bound states in superconductors. As a result, the region of applicability of the Born approximation is greatly reduced (and the region of applicability of the unitary limit expanded) for the systems studied here. Using the Born approximation beyond that region can lead to overestimating the effect of impurities on Andreev bound states.

The stability of the bound states with respect to impurity scattering in the unitary limit has consequences for one of the models used to describe rough surfaces, viz., the thin dirty layer model [89, 93, 96–98] In this model, a thin dirty layer containing Born impurities near the surface (or around the interface) is used to mimic a rough surface. The degree of roughness is measured by the ratio $\rho_0 = d/l$, where d is the thickness of the layer, and l the mean free path in the layer. For a given scattering rate and impurity concentration the self-energy (that enters the equation for the dirty layer) at the bound-state energy value will be significantly less in the unitary limit than for Born scatterers. Accordingly, the broadening of bound states by roughness can be significantly different in those two limits for the same value of the roughness parameter $\rho_0 \ll 1$ (in the rough limit $\rho_0 \gg 1$ bound states will be wiped out in both cases). As a consequence, a dirty layer with unitary scatterers will influence the bound states and the Josephson critical current less strongly than in the Born limit (for the same value of the scattering rate). This is another example that shows that the choice of the most suitable model for surface and interface roughness for a given experimental situation is still open.

In conclusion, quasiparticle scattering by bulk impurities as well as surface rough-

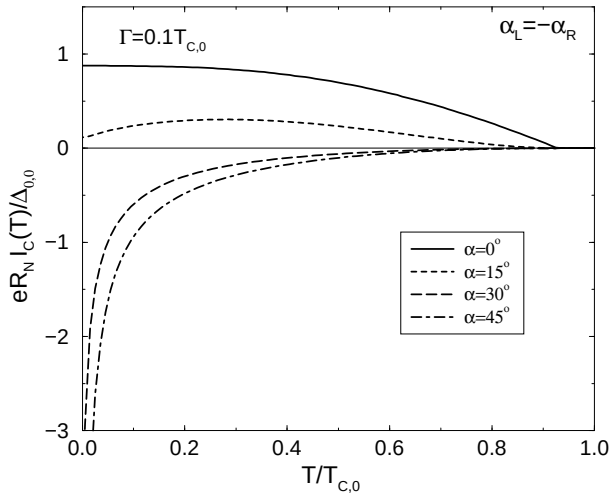

Figure 4.9: Critical current as a function of temperature for the mirror junction and scattering in the unitary limit.

ness results in the broadening of surface (interface) quasiparticle bound states in tunnel junctions of d-wave superconductors. We have studied this broadening due to bulk impurities and shown that scatterers can essentially reduce the height of the peak in the density of states and the low-temperature anomaly in the Josephson critical current. We have shown that bound states are more sensitive to Born scatterers than to unitary scatterers at a given value of the scattering rate. Thus, unitary scatterers would be less detrimental than Born scatterers to the observability of the low-temperature anomalies in the Josephson critical current caused by bound states.

4.1.2 Magnetic field dependence

As explained in the previous section there is a growing consensus that the Zero-Bias Conductance Peak (ZBCP) seen in *ab*-plane tunneling on YBCO is a direct consequence of a $d_{x^2-y^2}$ order parameter [99, 100] (and references therein). Applying an external magnetic field along the crystal $\hat{c}$-axis induces Meissner screening currents in the *ab*-plane. The currents shift the quasiparticle energy, $\epsilon \to \epsilon - \boldsymbol{v}_F \cdot \boldsymbol{p}_s$ along a trajectory $\boldsymbol{v}_F$ by the projection of $\boldsymbol{v}_F$ on the superfluid momentum $\boldsymbol{p}_s = \frac{\hbar}{2}\nabla\chi - \frac{e}{c}\boldsymbol{A}$.

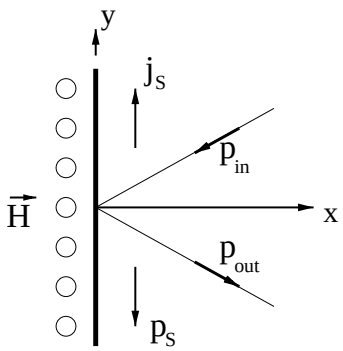

A test for the *d*-wave origin of the ZBCP is that this energy shift $\boldsymbol{v}_F \cdot \boldsymbol{p}_s$ shows up as a field dependent splitting of the ZBCP on a magnetic scale given by the thermodynamical critical field, $H_o = \Phi_o/\pi\xi_o\lambda_L$, which for YBCO is ~ 1 Tesla [101]. This splitting has reproducibly been seen in experiments [99, 102] where others do not reproduce it [100].

In the following we will show, by direct calculation of the low-bias conductance, that experiments not showing a split of the ZBCP vs. field, still are compatible with the *d*-wave origin of the ZBCP when effects of surface disorder is taken into account.

The typical measured ZBCP show a considerable broadening, roughly 25% of the gap Δ, compared to the ideal δ-peak predicted by theory [21]. To account for this broadening one can consider the effect of elastic impurity scattering either as a distribution of bulk impurities [92] like in the last section or as a diffusive surface layer [103]. Both models yield if the impurities are Born scatterers a ZBCP broadening $\sim \sqrt{\Gamma\Delta}$, where $\Gamma = 1/2\tau$ is the pair-breaking parameter. This estimate agrees with measurements of the ZBCP on He^+ ion irradiated thin YBCO films [104]. In addition to the impurity induced broadening there is a split $\sim \sqrt{\Gamma\Delta}$ of the ZBCP away from zero energy [92]. As shown in 4.1.1 in the strong scattering limit only an exponentially small broadening of the zero bias structure occurs [92, 103].

Again using the quasiclassical theory the order parameter profile in the surface region is calculated self consistently together with the superfluid momentum $\boldsymbol{p}_s$. We apply the diffusion layer model to describe the surface region in a *d*-wave superconductor. In short, the diffusion layer model (Fig. 4.10) assumes increased disorder in a narrow region close to the interface. The layer width is typically on the order of $5\xi_o$ and is characterized

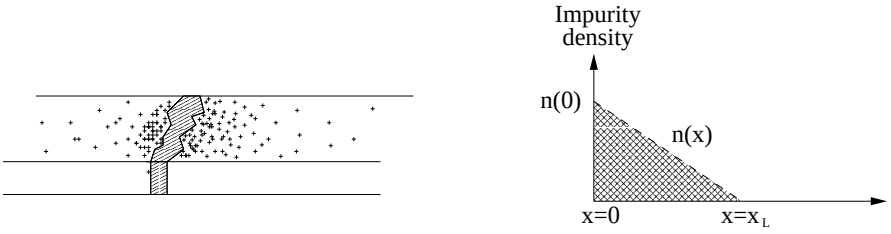

Figure 4.10: The diffusion layer model: Disorder is increased in a narrow region close to the interface

by its minimal mean free path right at the surface. The presence of local impurity scattering gives an energy dependent renormalization of the quasiparticle energy and of the order parameter. The details of the impurity renormalization is in the impurity t-matrix which depends on the (isotropic) impurity potential $\hat{u} = u_p\hat{1} + \boldsymbol{u}_s \cdot \hat{\boldsymbol{\sigma}}$. The two entering impurity potentials u_p and $\boldsymbol{u}_s$ scatter either by potential scattering (u_p) or by spin exchange with randomly oriented classical moments ($\boldsymbol{u}_s$). In the Born limit, on which we will concentrate, the equilibrium impurity self-energy reads

$$\hat{\sigma}_{imp} = \frac{1}{2\tau}\Big(\langle g\rangle\hat{\tau}_3 \pm \frac{1}{2}\langle f + \tilde{f}\rangle i\hat{\tau}_2 \pm \frac{1}{2}\langle f - \tilde{f}\rangle\hat{\tau}_1\Big) \tag{4.8}$$

for either purely potential (+) or purely spin-exchange (−) scattering impurities. For a d-wave order parameter the Fermi-surface averages $\langle\cdots\rangle$ of the anomalous Green's functions f and $\tilde{f}$ vanish by symmetry. This leads to the t-matrices being the same for the potential-scattering model and for the spin-exchange model.

With applied magnetic field the presence of a superfluid momentum breaks the symmetry that made $\langle f\rangle$ and $\langle\tilde{f}\rangle$ zero. In particular, in absence of surface disorder the average $\langle f - \tilde{f}\rangle$ is non-zero in vicinity of the surface as soon as a superfluid momentum is present. $\langle f - \tilde{f}\rangle$ being non-zero is a surface effect and is most pronounced for a crystal cut along the (110) crystal direction. The magnitude of $\langle f - \tilde{f}\rangle$ is comparable to the average $\langle g\rangle$, which in the low-energy range $\epsilon \ll \Delta$ is dominated by the surface bound state and hence $\sim 1/\epsilon$. How $\langle f - \tilde{f}\rangle$ couples back to the surface spectra when surface disorder is introduced depends sensitively on the impurity type and must be studied by a direct calculation of the angle resolved surface density of states $N(\phi, \boldsymbol{R}_s; \epsilon)$.

In Figure 4.11 we display the field evolution of the angle resolved DOS $N(\phi, \boldsymbol{R}_s; \epsilon)$ at an angle of incidence of 45^o to the surface normal both for a potential scattering and a magnetic scattering surface model. The minimal mean free path in Fig. 4.11 characterizing the surface disorder is $5\xi_o$. As seen the details of the two sets of spectra differs considerably. At small applied fields, $H \leq 0.05H_o$, we see a redistribution of spectral weight within impurity broadening of the peak structure that differs significantly between the two impurity types. For the potential scattering model there is a distinct change in the spectra as weight is shifted from negative to positive energy giving a very

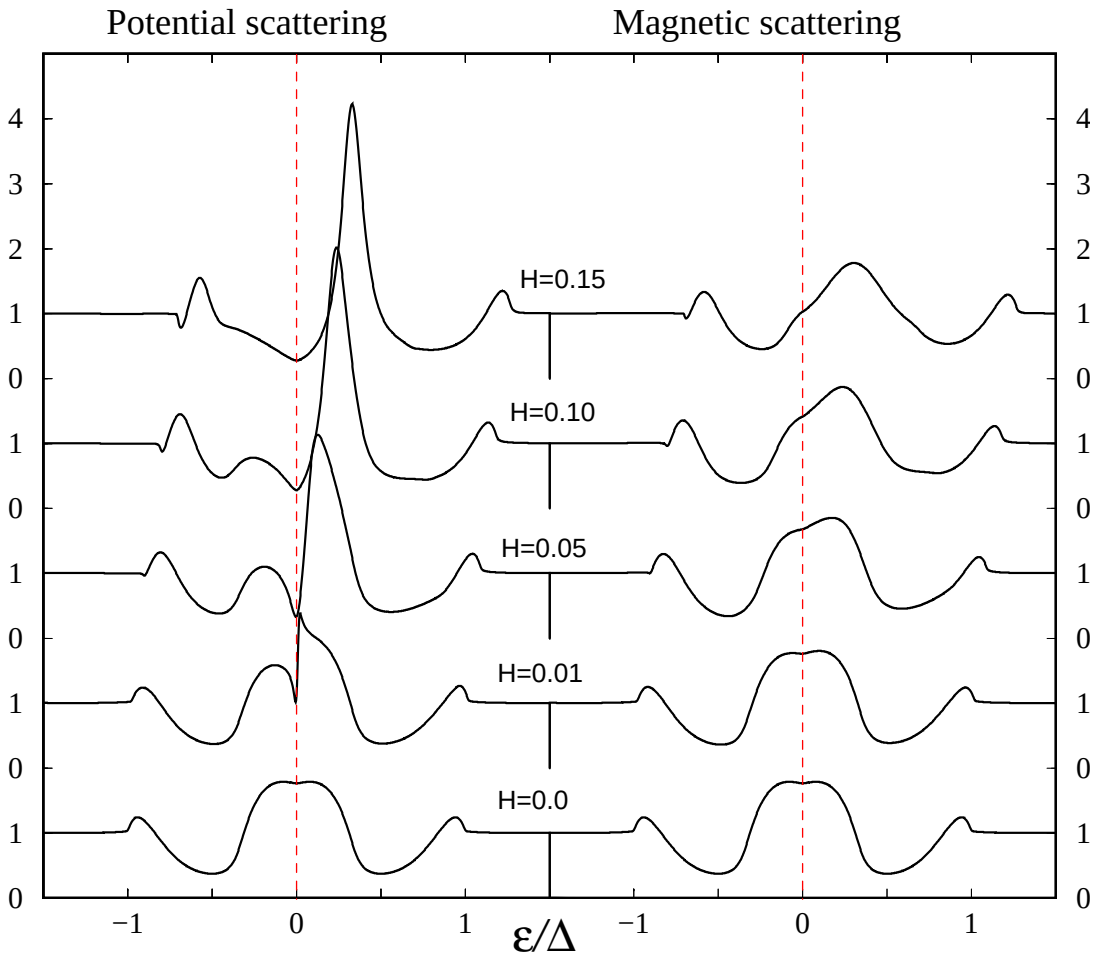

Figure 4.11: Trajectory resolved density of states on a trajectory with $\boldsymbol{v}_F \cdot \boldsymbol{p}_s > 0$ for different magnetic fields. Left graph: Potential scatterers, right graph: magnetic scatterers. The applied magnetic field is normalized to H_o. ($H_o = \Phi_o/\pi\xi_o\lambda_L$, with ξ_o the coherence length and λ_L the penetration depth).

sharp feature just above zero energy. For the magnetic scattering model this shifting of weight is also present but much less pronounced as seen in Fig. 4.11. As the field is increased the Doppler shift exceeds the impurity induced width of the peak, i.e., $|\boldsymbol{v}_F \cdot \boldsymbol{p}_s| > \sqrt{\Gamma\Delta}$, and for both impurity types the peak in the spectra evolves with field as $\boldsymbol{v}_F \cdot \boldsymbol{p}_s$. Nonetheless there is still a difference in the peak broadening. The magnetic impurity model show a very broad peak and also a considerable spectral weight stays put at zero bias for all fields. In case of potential scatterers the peak at $\boldsymbol{v}_F \cdot \boldsymbol{p}_s$ is sharper and show a satellite peak at $-\boldsymbol{v}_F \cdot \boldsymbol{p}_s$. In addition the spectral weight at zero bias is decreased with increasing field.

Turning to conductance data, the different impurity models translate into distinctly different field dependencies of the ZBCPs as shown in Figure 4.12. In the case of potential scatterers the field dependence manifests in clearly split ZBCP which evolves as $H_o(\phi_c) = H_o/\sin\phi_c$, where ϕ_c is the limiting angle of a phenomenological tunneling cone. This is contrasted by an unsplit ZBCP for the magnetic scatterers. Even though the angle resolved DOS show a Doppler shifted peak, the angle averaged DOS, i.e,. the conductance, picks up its main contribution from the spectral weight left at zero bias. This results in a central peak at all fields. The spectral weight "melts"to higher bias as the field is increased.

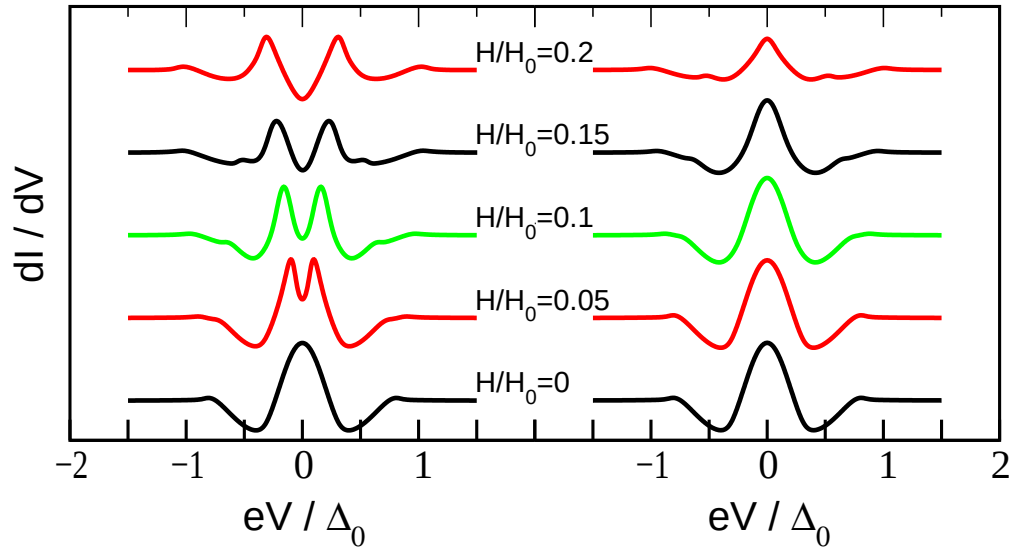

Figure 4.12: Tunneling differential conductance for different magnetic fields. Left graph: Potential scatterers, right graph: magnetic scatterers

Comparing these two sets of calculated conductances with the measured ones [99, 100, 102] there is an agreement between the potential scattering surface layer and NIS-junction realized in Refs. [99, 102] while the magnetic scattering surface layer and the

grain-boundary junctions in Ref. [100] show the same field dependence.

In conclusion, we report a consistent way to understand discrepancies seen in experiments of the field evolution of the ZBCP.

4.2 Electron-doped cuprates

In the case of the hole-doped cuprates a dominant d-wave order parameter is by now well established, and almost all experimental findings can be explained in a consistent way. For the electron-doped compounds the situation is by far less settled. Since the these materials are less on the focus, at first a more extensive review of the contradictory experimental observation will be given.

4.2.1 Experimental backdrop

First investigations by Wu et al. [105] on $Nd_{2-x}Ce_xCuO_{4-\delta}$ (NCCO) thin films and single crystals suggested an s-wave order parameter. The in-plane penetration depth λ and surface resistance R_s were measured on samples with a critical temperature of about $T_c \approx 21 - 22K$ down to 4 K. Both observables displayed a clear activated temperature dependence and could be fitted to exponential laws with $2\Delta/k_B T_c = 4.1$. And not only at low temperatures but up to T_c the behavior could be fitted by a conventional BCS-description. Potential temperature laws as expected for an d-wave order parameter could not be fitted to their data. A result which was confirmed by Andreone et al. [106] and Anlage et al. [107] investigating the same quantities albeit with some quantitative differences in, e.g., the size of the gap. A fact which could be attributed to different sample quality.

However as pointed out by Cooper [108] the measurement of the low-temperature penetration depth could be affected by paramagnetism of the Nd^{3+} ions. Taking into account changes of the magnetic susceptibility due to the magnetic moments of Nd^{3+} a power-law behavior of the corrected penetration depth might still be possible. And indeed Alff et al. observed an increase of the penetration depth with decreasing temperature below 4K in NCCO [109] which is in agreement with Coopers suggestion. In their penetration depth measurements on NCCO and $Pr_{2-x}Ce_xCuO_{4-\delta}$ (PCCO), the anomalous low-temperature dependence of NCCO could be explained by the magnetic moments of the Nd^{3+} ions. And correcting the data, the results of NCCO coincide with the ones on PCCO which does not have magnetic moments and thus no anomaly was observed or expected. But in contrast to the proposal of Cooper they claim that the temperature dependence of the penetration depth is still consistent with an isotropic s-wave order parameter, and their data could be fitted with $\Delta\lambda_{ab}(T) \propto \sqrt{\Delta/T}\exp^{-\Delta/k_B T}$ and $\Delta_0 = 3$meV at least from 2K up to 13K.

Tunneling experiments as powerful tool to gain an insight on the symmetry of the order parameter have been introduced in the last section. As explained, since a sign

change of an unconventional order parameter on the Fermi surface can lead to zero energy bound states (ZEBS), these experiments can also give information on the phase. An observation of a zero bias conductance peak (ZBCP) would be a clear indication of an unconventional order parameter, although, as other mechanism could also lead to a ZBCP [110], the origin in superconductivity has to be carefully etablished.

First Low Temperature Scanning Tunneling Microscopy/Spectroscopy (LTSTM/S) results have been reported by Alff et al. [111,112]. In Ref. 111 the authors report about LTSTS experiments on (110) oriented YBCO thin films and NCCO single crystals at 4.2 K. In the case of YBCO at 51 equidistant points pronounced ZBCP were observed as expected in the case of a *d*-wave order parameter. The data for NCCO in contrary show no sign of a ZBCP, instead a clear gapped structure was observed with a gap of about 4.5 meV, and the structure could be fitted assuming an BCS density of states with a life-time broadening of about half the gap. In the subsequent paper [112] in addition data for (100) are shown. For (100) in YBCO a gap-like structure was observed, at single measurement points also small ZBCPs are observable. This confirms the *d*-wave picture of YBCO, where (on specular reflecting) (100) boundaries no ZBCP is expected. The ZBCPs where seen at points where the surface gets rougher as seen in the topographic image. In NCCO no ZBCP could be observed (as in the (110) and (001) direction), and a gap of about 5meV ($2\Delta_0/\mathrm{k_B}T_c \approx 6.6$) is found. Different points only vary in the strength of the gap-like structure which can be explained by the surface roughness. In conclusion these measurements clearly contradict a *d*-wave symmetry of the order parameter in NCCO. In a later publication by Kashiwaya et al. [113] STM measurements on NCCO confirmed the results while other STM/STS measurements by Hayaashi et al. [114] on NCCO report the existence of ZBCP also in NCCO. Surprisingly there they usually observe the ordinary gap structure in (110) direction and often a ZBCP along the (100) direction. Once they observe a ZBCP it is reproducible irrespective of fixing or shifting the tip position. Unfortunately no temperature or magnetic field dependence of the ZBCP is shown, therefore a different mechanism for the ZBCP can not be ruled out. In retrospect it is interesting to note, that in the early experiments the clear differences of electron- and hole-doped compounds was used to fortify the *d*-wave order parameter in the hole-doped cuprates, because the *s*-wave pairing in NCCO seemed to be established.

Tunneling spectra measurements on bicrystal grain-boundary junctions (GBJs) [100, 109, 115, 116] support this result. In Ref. 116 tunneling spectra of YBCO, BSCCO, LSCO and NCCO are shown. Grain boundary junctions the hole-doped LSCO films with a critical temperature of about 24K show a reduced DOS below the gap voltage and a pronounced ZBCP. The ZBCP reduces with rising temperature and vanishes at T_c as expected for an *d*-wave order parameter. In the other hole-doped materials BSCCO and YBCO (optimal and underdoped) the same can be observed.

The results for NCCO GBJs exhibit a striking different behavior. The DOS is enhanced to about 110% at the gap voltage and reduced to about 40% at zero voltage and no ZBCP is observable. Results which were reproduced in PCCO [117] but quantitatively

attributed to an anisotropic s-wave order parameter $\Delta(\theta) = |\cos(2\theta)|$ in contradiction to the penetration depth results on the same samples.

The circumstances suddenly changed when three publications reported at the same time about strong indications of an d-wave order parameter:

In reinvestigations of the penetration depths of PCCO by Prozorov et al. [118] down to low temperatures of $T \approx 0.5K$ below 1.8 K samples exhibit a quadratic behavior with temperature. One sample shows a linear variation extending from 1.8 to 4.2 K while the other stays quadratic. These results suggest a d-wave order parameter with unitary impurities. As shown by Hirschfeld et al. [119] [120], in case of strong scatterers a crossover from a quadratic to a linear temperature dependence at a temperature $T^\star \approx 6\ln(2)\gamma \approx 0.83(\Gamma\Delta_0)^{1/2}$ is expected. The two different experimental observations can therefore be explained by different scattering rates in the two samples. In the same publication also penetration depth measurements on NCCO are reported. As in the measurements of Alff et al. an upturn of the penetration depth below 4K is observed. But the data can be fitted to a linear dependence, whereas a fit of the low temperature region to an activated behavior was only successful with an unreasonable low gap of $\Delta(0) = 1.3meV$ and clearly deviates at higher temperatures.

In an accompanying paper by Kokales et al. [121] measurements of the penetration depth, as well as the surface resistance on the same samples of NCCO and PCCO are reported. In NCCO the upturn of the penetration depth is observable at about 3.8 K. The PCCO sample shows a quadratic behavior. As the authors remark the data could also be "forced"to fit an activated behavior but with unreasonable high penetration depth and again a too low gap.

Most telling Tsuei et al. performed a phase-sensitive tricrystal experiment [122] on NCCO and PCCO like in the hole-doped superconductors [123]. The observation of a spontaneous half flux quantum in frustrated and no flux in other geometries strongly suggest a dominant d-wave order parameter. It should be noted this experiment is especially remarkable since these kind of investigations in the electron-doped are much more involved than in the hole-doped materials. Here it is difficult to produce grain boundaries with sufficient large critical currents and the spontaneous vortex with a total flux of half a flux quantum cannot be demonstrated as easy (and impressive) as in hole-doped materials: Due to the small critical currents the flux cannot be constrained by a small ring. Instead the total flux through the whole sample has to be measured and integrated.

Assuming an d-wave order parameter the absence of the ZBCP in the tunneling experiments is sometimes attributed to impurity scattering. And indeed in the d-wave superconductor YBCO the reduction and disappearance of the ZBCP with disorder by ion-irradiation could be demonstrated [104]. But analyzing this study carefully, at the same time the ZBCP is suppressed also all gap like features are broadened and vanish. An observation advising to reinvestigate the tunneling results theoretically including impurity scattering, to test the consistence of the experiments with the different suggested

order parameters.

4.2.2 Theoretical investigations

To investigate the possibility of the different order parameter symmetries in the light of the experimental tunneling results, we use the surface model introduced in the last chapter. Local surface disorder is modeled as a layer of magnetic or non-magnetic impurities at the surface with a linear decreasing concentration, and in addition a homogeneous distribution of bulk impurities is included. The surface layer is given by a linear decreasing density and characterized by its depth, the scattering rate at the interface ($x = 0$) and the type and strength of the impurity potentials.

s-wave order parameter

To start with the originally discussed order parameter, the results as expected by our calculations for an *s*-wave symmetry are analyzed. As discussed in the introductory theoretical chapter 2 the superconducting properties in case of an isotropic order parameter are unaffected by potential scattering, Anderson's theorem is valid. Not recapitulating the old well known results on pure conventional superconductors we will immediately turn to the presence of magnetic scatterers. Having a look at the surface density of states shown in Fig. 4.13 for different scattering rates of magnetic impurities in the surface layer, one observes that the original sharp square root divergence at the gap

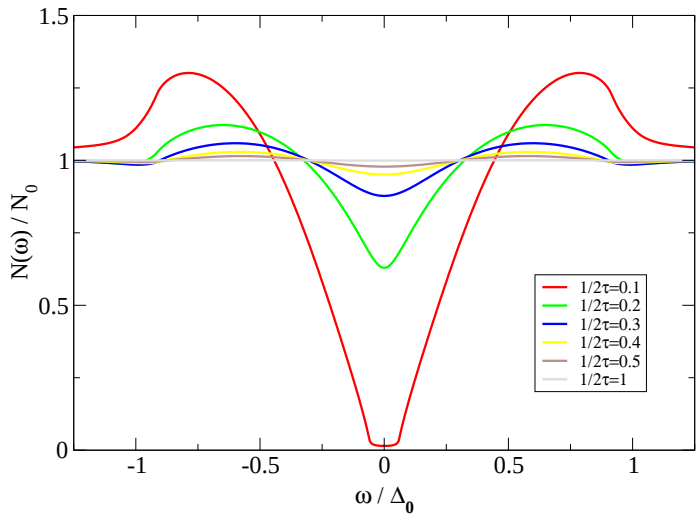

Figure 4.13: Density of states and conductivity for an *s*-wave order parameter for different scattering rates $1/2\tau$ of magnetic impurities. The scattering rates are given in units of $T_{c,0}$.

edge is drastically washed out. At higher scattering rates the gap like features are almost washed out and a finite residual density of states at zero is growing with impurity concentration until no signs of superconductivity are observable any more. A result expected remembering the well known contributions on gapless superconductivity [47]. A subtle difference should not be forgotten. In our case the dominant effects are by the small surface layer. Thus the bulk order parameter and therefore also the position of the gap edge is almost unaffected by scattering. Turning to the tunneling differential conductance as measured in experiment: Our results are given in Fig. 4.14 including the experimental data [117, 124].

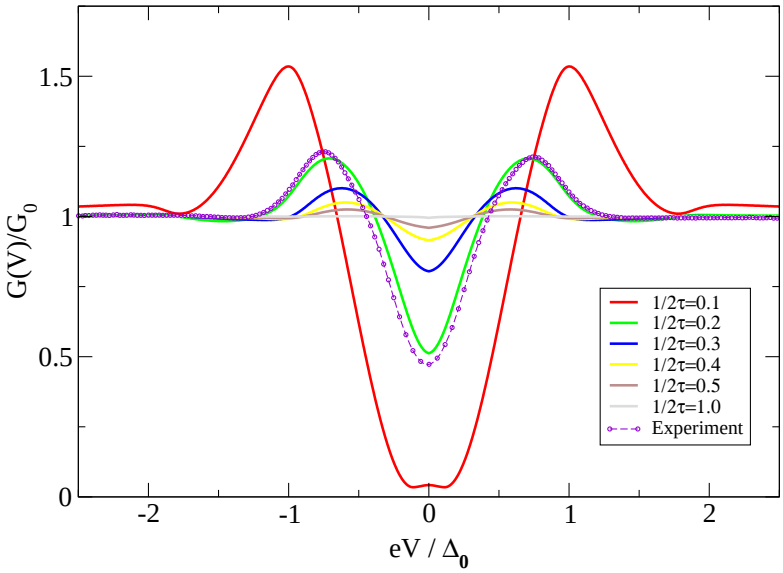

Figure 4.14: Tunneling differential conductance for an s-wave order parameter in the presence of magnetic impurities close to the surface. The scattering rate $1/2\tau$ is given in Units of T_c. For comparison, the experimental data of Ref. [117, 124] are included.

As shown there, the experimental findings are in agreement with an s-wave order parameter, if magnetic surface disorder is assumed. While the qualitative features are almost perfectly reproduced, a caveat should not be hidden. The large value of the (bulk) gap is not in agreement with BCS theory and had to be taken from experiment as fit parameter. The fit requires a fairly strong scattering rate, resulting in a gapless density of states. But the penetration depth measurements on the samples clearly exhibit a activated temperature dependence. Calculations of the penetration depth of Fogelström [125] for the same parameters are given in Fig. 4.15. Since the order parameter is only suppressed in a small vicinity of the surface (as shown in the inset) the penetration depth of these strong class II superconductors are only marginally affected by the presence of

surface disorder. In all cases a clear activated behavior is expected, as observed in the experiment.

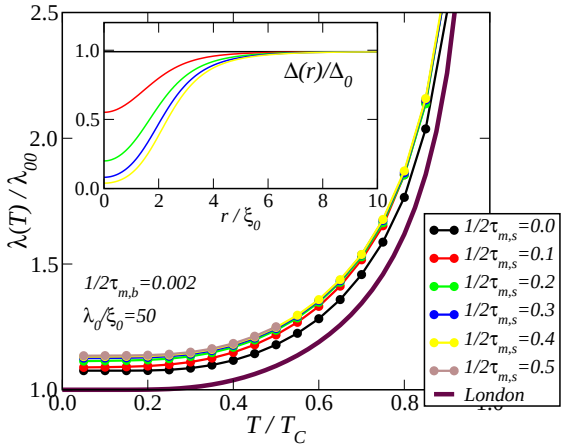

Figure 4.15: Penetration depth for an s-wave order parameter and surface impurities (Fogelstroem [125]). The penetration depth still shows an activated behavior

Anisotropic s-wave

In some publications the tunneling results have been interpreted as signs of an anisotropic s-wave order parameter $\Delta(\boldsymbol{p}_F) = \Delta_0|\cos(2\phi)|$. For such an anisotropic order parameter symmetry both magnetic and potential (isotropic) are affecting the properties but in a quite different way as we show in Fig. 4.16 giving the surface density of states. While potential scattering will reduce the position of the gaplike structures saturating at an averaged value, at the same time a spectral gap is opened at low energies. Magnetic impurities on the other hand are again pairbreaking like in the previously discussed case.

This is well reflected in the tunneling conductance as shown in Fig. 4.17. Potential impurities will open a gap, giving for high concentration almost a dI/dV as expected for conventional BCS superconductors. A result clearly deviating from all experimental findings. The controlled implatation of potential scatterers would offer a way to distinguish d-wave from anisotropic s-wave superconductivity. [120]

In contrast, the result with magnetic surface disorder and an anisotropic s-wave order reproduces the experimental data.

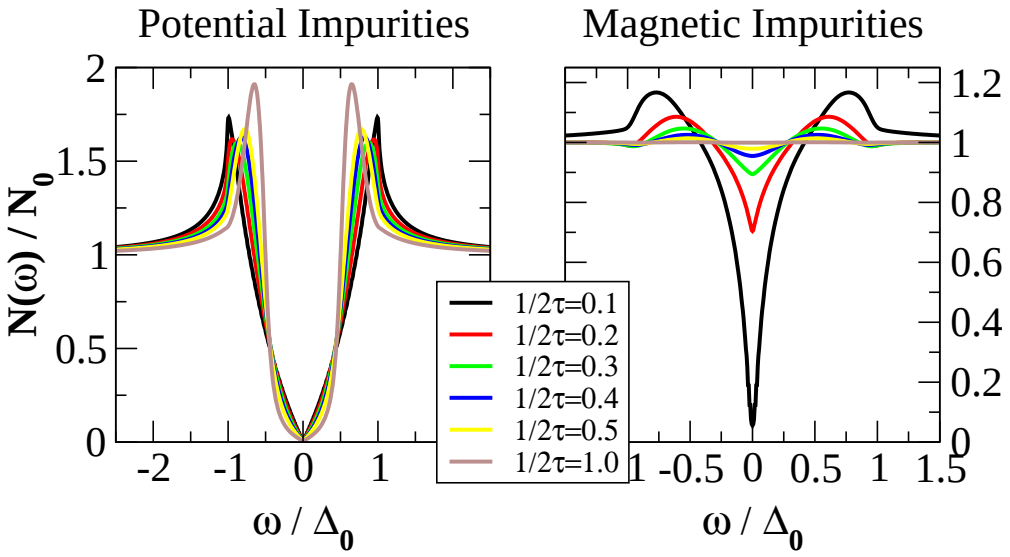

Figure 4.16: Density of states for an anisotropic s-wave order parameter, with magnetic and potential impurities. Potential impurities will open a spectral gap [120]

.

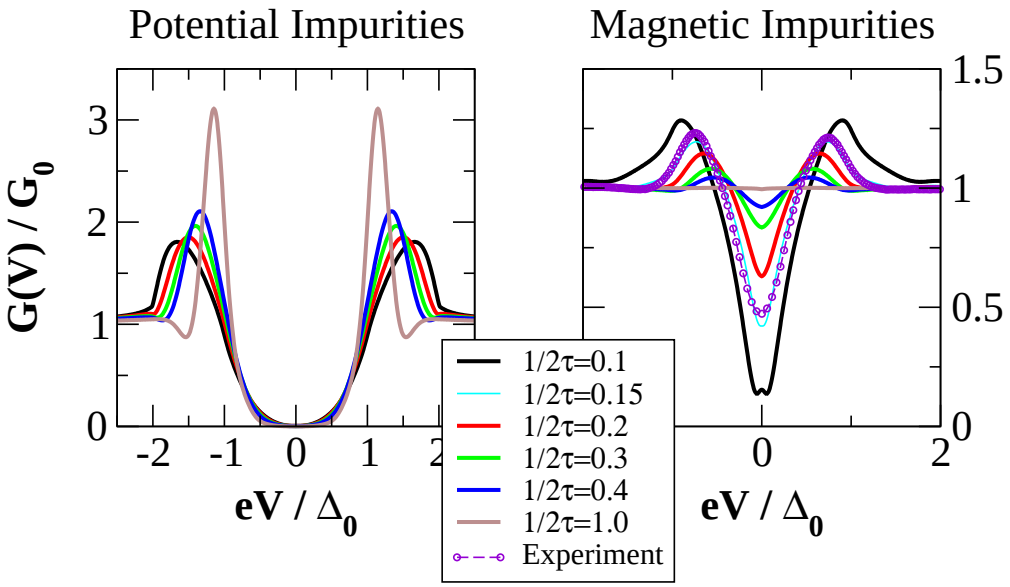

Figure 4.17: Tunneling conductivity for the anisotropic s-wave order parameter. The experimental results of Ref. [117] are in agreement with magnetic surface scatterers.

d-wave

Finally turning to the *d*-wave order parameter as suggested by, e.g., the tricrystal experiment. As discussed before for this unconventional order parameter, potential and magnetic impurities will (in the absence of an external applied magnetic field) have the same influence on the superconducting properties. Therefore, we will not distinguish the impurity types in the following discussion. In Fig. 4.18 the density of states for different misorientations and two impurity configurations is given. For sufficiently large misorien-

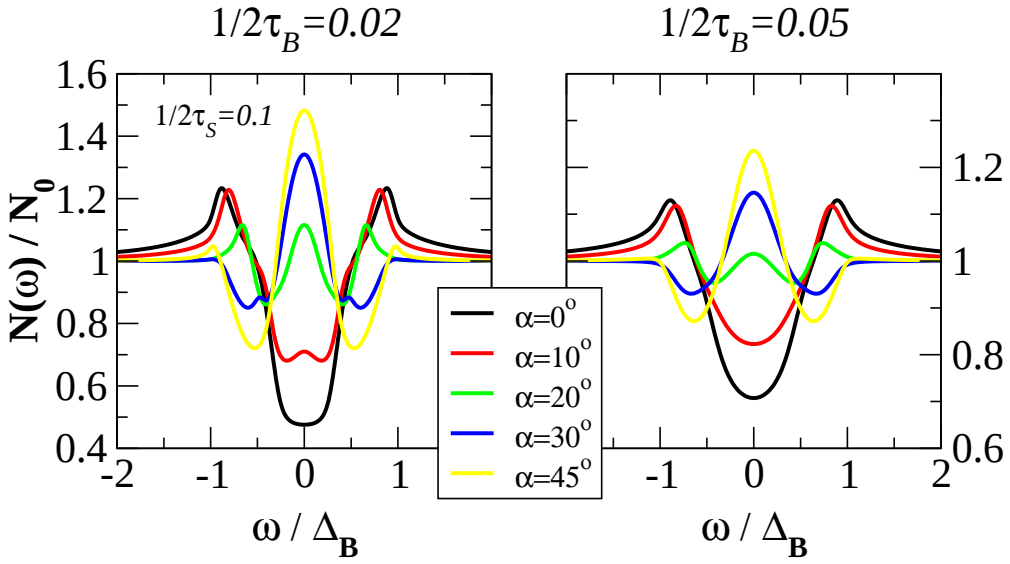

Figure 4.18: Density of states for a *d*-wave order parameter and different misorientation of the order parameter to the surface

tation a well pronounced ZEBS is seen which gets broadened with bulk impurities but is still a distinguishable feature. Exploring the tunneling conductance (Fig. 4.19) including not only the PCCO data but also ones on the hole-doped LSCO [116] the difference is more than obvious. While the LSCO data are fairly well described within our model, there is no way to make the PCCO data agree with theory. They are best described by a $\alpha = 0°$ misoriented junction, which is far from the experimental setup and even then the gap-like features are much more pronounced than expected by theory. Postulating a *d*-wave order parameter and using the misorientation of the experimental setup, there is no way to get agreement. Impurities can annihilate the ZBCP but only in configurations where at the same time all signs of superconductivity are lost.

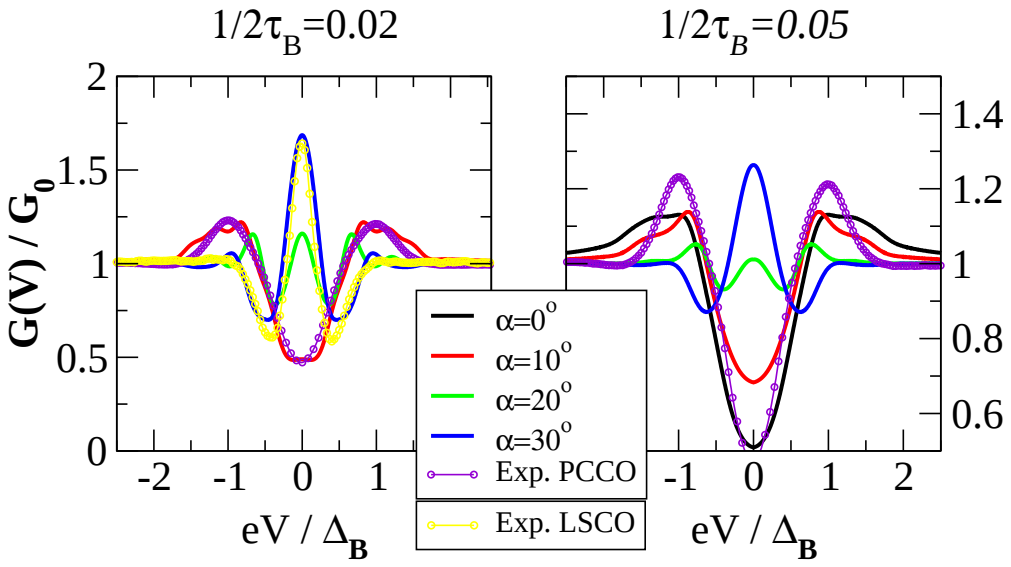

Figure 4.19: Tunneling conductance for a *d*-wave order parameter with different bulk scattering rates. In the left panel experimental data on the hole-doped compound LSCO are included, in the right, the data on PCCO.

4.2.3 Conclusions

As our results show, an isotropic as well as an anisotropic *s*-wave order parameter are in agreement with the experimental tunneling data on grain boundary junctions of electron-doped cuprates, premising magnetic surface disorder. A disorder which was, even with the same parameters, used in the last section to explain the magnetic field dependence of tunneling spectra in hole-doped cuprates.

In contrast the experimental results cannot be explained even qualitatively within a *d*-wave picture, even if impurity scattering is taken into account. A different tunneling mechanism compared to the hole-doped cuprates which might aid seems to be causeless.

A surprising solution to the puzzle of experiments supporting an *s*-wave order parameter and others, like the distinctive tricrystal experiment of Kirtley et al., endorsing *d*-wave symmetry might be given by recent observations:

Point contact spectroscopy data by Biswas et al. [126] and penetration depth measurements of Skinta et al. [127] show strong evidence for a transition of the order parameter symmetry with doping. As they report, underdoped samples show *d*-wave optimally doped and overdoped samples *s*-wave symmetry. The possibility, that different nominally optimally doped samples in fact have a different order parameter would be a natural explanation. Especially noting, that no inconsistencies have been reported between different measurements on the same samples.

A change of the order parameter with doping would of course be interesting in the

context of the question about the pairing mechanism.

5 Sub-harmonic gap structure in d-wave superconductors

In the previous chapter the description of interfaces was restricted to the tunneling limit doing transport calculations in first order in the interface transparency only. A restriction which will be dropped in the following and the method generalized to weak links with arbitrary transparency. As explained below, in the case of high transparency constrictions a novel transport mechanisms becomes important. Andreev reflections give rise to an enhancement of the current in S-c-N junctions , and for S-c-S junctions multiple Andreev reflections (MARs) will manifest in a subharmonic gap structure (SGS).

Early in the discussion about the order parameter symmetry of the cuprates, Devereaux and Fulde suggested that the Andreev scattering in SNS contacts could be used to identify the symmetry of the order parameter [128]. Based on their analysis the SGS revealed in different experiments in YBCO contacts were interpreted as an evidence of the existence of a well-defined nonvanishing gap [129, 130]. After more detailed but non-self-consistent analysis, different authors have concluded that the SGS are weak in d-wave superconductors, since averaging over the anisotropic gap washes out prominent features [131, 132].

However, there are also more recent experimental reports of SGS in YBCO edge Josephson junctions [133, 134], and even in the c-axis tunneling of different cuprate contacts [135]. Auerbach and Altman proposed an alternative interpretation of the appearance of pronounced SGS in Ref. 134, suggesting that this structure is an indication of magnon tunneling that can be explained in the context of the SO(5) theory [136].

Since self-consistency proved to be crucial in the case of tunneling junctions, and certainly will be in the more general case, we reinvestigate the question of SGS in d-wave junctions applying the quasiclassical Green's function technique to weak links of arbitrary transparency. This allows us not only to treat the problem self-consistently including also the effect of impurities, but moreover to study the behavior in an external applied magnetic field.

5.1 Multiple Andreev reflection

In the tunneling limit discussed up to now, the only process transferring charge across a barrier except the Josephson current is tunneling of quasiparticles on one side to

unoccupied quasiparticle states on the other side. Thus currents are expected to start off at voltages exceeding the spectral gaps on both sides.

Allowing for higher order processes in the transparency, a new process described by Andreev [137] in the context of studies of thermal transport will provide transport even at voltages smaller than the superconducting gap. In simple terms as sketched in Fig. 5.1, an incoming quasiparticle with momentum $\boldsymbol{k}$ and spin $\boldsymbol{\sigma}$ can not enter the superconductor as quasiparticle due to the absence of available quasiparticle states. Nevertheless accombined with a quasiparticle of opposite spin and momentum it can enter the condensate leaving an empty quasiparticle state. In this process effectively a quasi-hole with $(-\boldsymbol{k}, -\boldsymbol{\sigma})$ is retro-reflected and a charge of $2e$ transferred. With an applied bias voltage, due to energy conservation, back in the normal conductor the hole effectively has "gained" an additional energy eV, which will become important later.

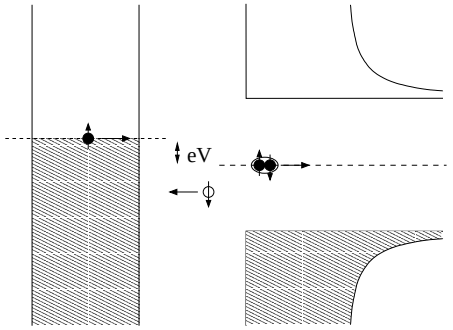

Figure 5.1: Cartoon of an Andreev reflection with applied voltage

In the present context of charge transport, Artemenko et al. [138, 139] observed that the current at high voltages is displaced compared to the normal state by a finite excess current which is dependent on the magnitude of the gap but not the voltage. And as Zaitsev [140] showed for transport through a constriction between normal- and superconductor not only current can flow for subgap voltages, the low voltage conductance is enhanced compared to the normal state. Andreev reflection spectroscopy by itself is a powerful tool for order parameter spectroscopy. Intensely used to study the electronic excitation spectrum, size of the gap and order parameter symmetry in all materials exhibiting unconventional superconducting properties [141].

Blonder, Tinkham and Klapwijk (BTK) extended the description [142] to systems including a finite barrier potential using Bogoliubov equations. Giving a full and intuitive description of the problem. In the same year the same authors (but in different order, usually cited as KBT) attributed the observation of subharmonic gap structures in the current of S-c-S junctions to multiple Andreev reflections [143]. These clear structures at $2\Delta/n$, where $n = 2, 3, \ldots$ were observed early in several experiments [144–146]. The simple explanation is as follows: if both sides of the constriction are superconducting

Andreev reflections are possible at both superconductors. Since at each reflection an energy of eV is gained, with a voltage V at the interface a cascade of $n = 2\Delta/eV$ Andreev reflections will take place until the gap edge is reached and a quasiparticle channel becomes available. Thereby n charges are transferred, as visualized in Fig. 5.2.

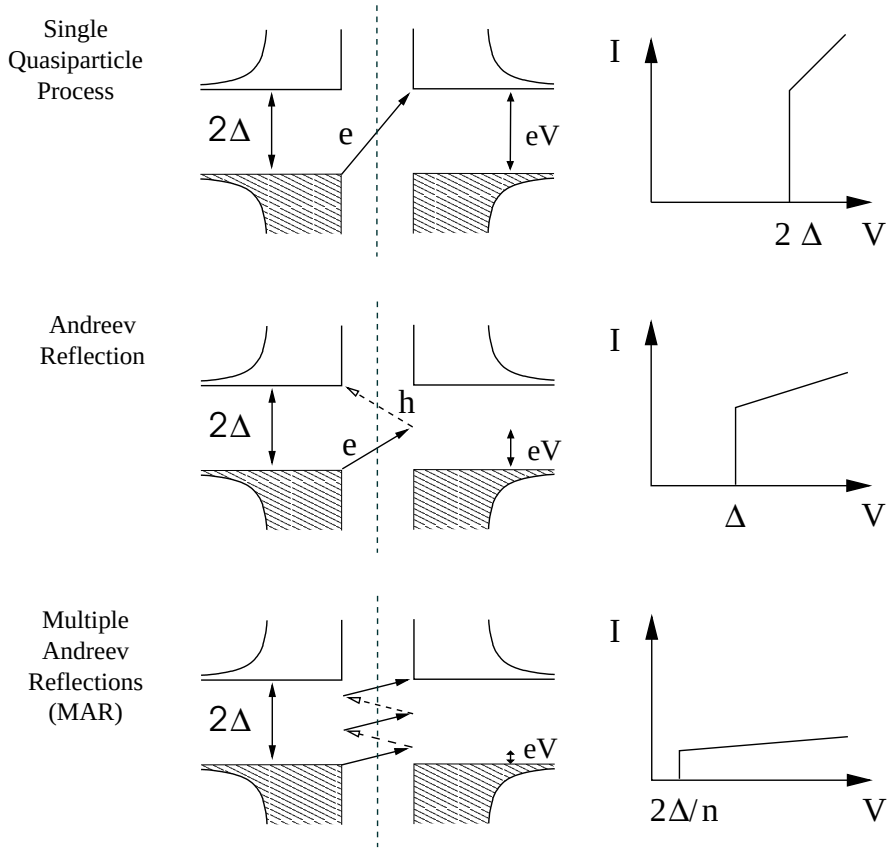

Figure 5.2: Sketch of multiple Andreev reflection in s-wave superconductors. New transport channels open at voltages $2\Delta/n$

Subsequent microscopic calculation by Arnold [147] , investigations in the scattering formalism [148, 149] and Hamiltonian approach [150] completed the understanding.

At first glance the probability of n multiple Andreev reflections is proportional D^n. Therefore, at lower transparency the contribution of higher order processes is reduced. one finds that while the onset of a new channel is dominant, at the same voltages the higher order processes might encounter resonances making them more important than the simple picture suggests. This is best displayed in studies about of the full counting statistics [151, 152] of the system.

On the experimental side, measurements on well controllable break junction contacts

[153–155] complemented the picture confirming the theoretical predictions.

5.2 Subharmonic gap structure

It is obvious that for a d-wave order parameter with varying gaps in momentum space including nodes, the SGS will change significantly in comparison to the s-wave case with just one well defined energy gap. Furthermore the possibility of an ZEBS (or midgap state (MGS) as called in a couple of papers concerning the present subject) will have a drastic impact on the structure, as explained in earlier works [131, 132, 156–158] We consider a voltage biased contact, consisting of two $d_{x^2-y^2}$ superconductors separated by a single interface of arbitrary transparency. The order parameter on side $i, i = l, r$ might be rotated (or misoriented) by an angle α_i with respect to the surface normal, and the junction type will be denoted by the relative crystal orientations as $d_{\alpha_l-\alpha_r}$. There are

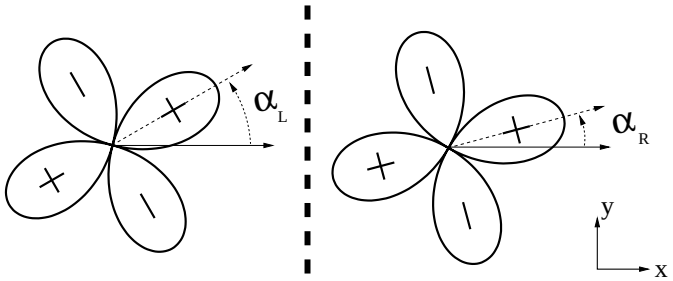

Figure 5.3: Design of the junction. The misorientation of the order parameters is described by the angles α_l and α_r. The transmittance of the interface can vary from tunneling limit to perfect transparency.

several experimental realizations of the misoriented system, among which the bicrystal grain-boundary junctions are ideal examples [100, 116]. The calculations of the current follows the lines of Ref. 39 and the reader is referred to this work for all technical details.

In the case of a constant bias voltage V, one can show that the current oscillates in time with all the harmonics of the Josephson frequency, i.e., $I(t) = \sum_m I_m e^{im\phi(t)}$, where $\phi(t) = \phi_0 + (2eV/\hbar)t$ is the time-dependent superconducting phase difference. Here, we concentrate ourselves on the analysis of the dc current, denoted from now on as I. Furthermore, we assume that the interface conserves the momentum of the quasiclassical trajectories, which allows us to write the current as a sum over independent trajectory contributions: $I = \frac{1}{2}\int_{-\pi/2}^{\pi/2} d\boldsymbol{p}_F \; I(\boldsymbol{p}_F)\cos(\boldsymbol{p}_F)$, where $\boldsymbol{p}_F$ defines the Fermi surface position. For the angular dependence of the transmission coefficient we use the expression $D(\boldsymbol{p}_F) = D\cos^2(\boldsymbol{p}_F)/[1 - D\sin^2(\boldsymbol{p}_F)]$, resulting from a δ-like potential. Here D is the transmission for the trajectory perpendicular to the interface.

At first we will analyze the simple case of a symmetric d_0-d_0 junction in the clean limit.

In this case, the order parameter is constant up to the surface, and there are no bound states for any trajectory. The I-V characteristics of a single trajectory, $I(\boldsymbol{p}_F)$, coincide with those of isotropic s-wave superconductors, and exhibit a pronounced SGS at $eV = 2\Delta(\boldsymbol{p}_F)/n$. Since the different trajectories see different gaps, the relevant question is whether the SGS survives after averaging. The answer is given in Fig. 5.4, where both the current and differential conductance are shown for different transmissions.

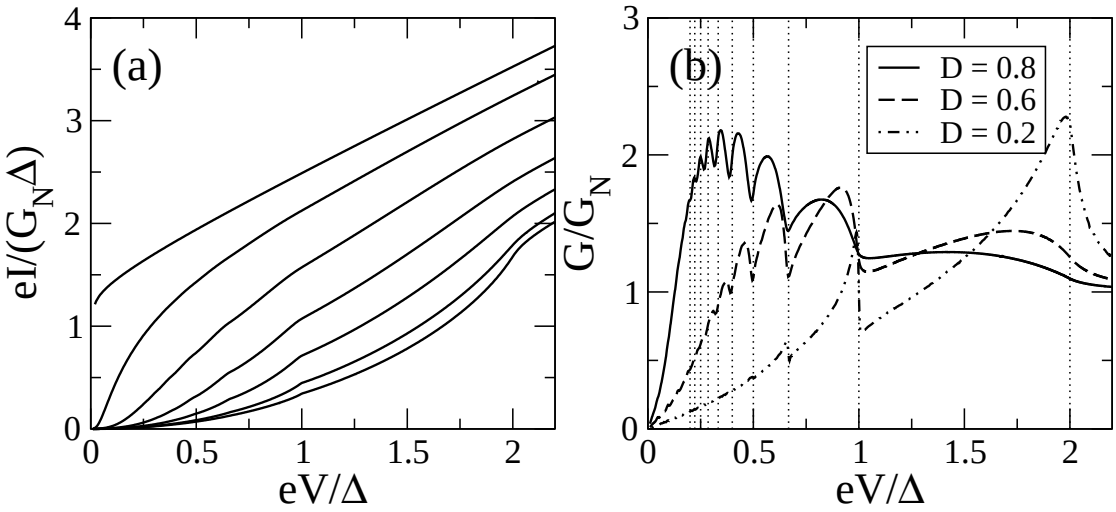

Figure 5.4: d_0-d_0 contact in the clean case: (a) I-V characteristics for different transmissions, from bottom to top $D = 0.1, 0.2, 0.4, 0.6, 0.8, 0.95, 1.0$. (b) Differential conductance normalized by the normal state conductance G_N. The dotted vertical lines indicate $eV = 2\Delta/n$.

Due to fact, that for this misorientation the order parameter stays constant selfconsistency does not affect the result. Consequently the I-V characteristic reproduces the earlier results of Ref. [131] and, as stated there the characteristics are "partially washed out". Approving this point, it is consequentially to investigate the differential conductance. And there one can clearly see a SGS at $eV = 2\Delta/n$, although it is more rounded than in the s-wave case. It should be noticed also that the SGS are better defined as minima in the conductance at the subharmonic voltages, i.e., as maxima in the differential resistance. At this point a natural question arises: why is the maximum gap the energy scale revealed in the SGS? The idea is that the jump of the current at the opening of a new MAR scales with the gap of the corresponding trajectory. Therefore, the trajectories with the largest gaps dominate the contribution to the SGS.

Let us now consider the case of a $d_{\pi/4}$-$d_{-\pi/4}$ junction. In this case, assuming specular quasiparticle scattering at the interface, an Andreev bound state forms at zero energy for every trajectory [21]. This implies that the surface acts as a pair-breaker [86,159] and

the gap is depressed in the vicinity of the interface, vanishing exactly at the barrier. This order-parameter profile induces the appearance of new bound states at the gap edges for some trajectories [160], which are also visible in the momentum averaged density of states, as shown in Fig. 5.5.

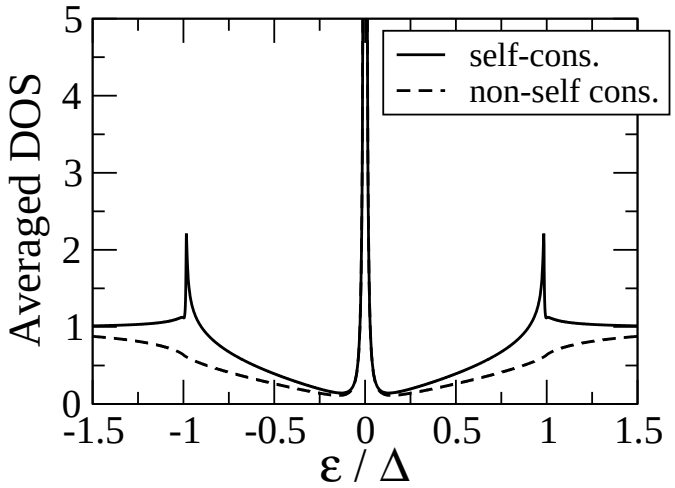

Figure 5.5: Comparison of selfconsistent and non-self-consistent results for the momentum averaged density of states in case of $\alpha = \pi/4$ misorientation.

There it is also shown that these gap singularities are not present in the non-self-consistent calculation. This fact has important consequences in the I-V characteristics. As is shown in Ref. 39 and sketched in Fig. 5.6, assuming an constant order parameter the most prominent feature of the I-Vs is the appearance of SGS at $eV = \Delta/n$, instead of $eV = 2\Delta/n$ as in conventional superconductors.

Its origin can be understood as follows. Inside the gap the current is dominated by multiple Andreev reflections (MAR). In this case there are two types of MAR processes: (a) those which connect the bound states with the gap edges and (b) the usual ones connecting the gap edges. The first ones give rise to the SGS at $eV = \Delta/n$, while the second type could give rise to the series $eV = 2\Delta/n$. However, for the non-self-consistent calculation the DOS at the gap edges is rather small (see Fig. 5.5), and thus, at the opening of this second type of processes their probability is small.

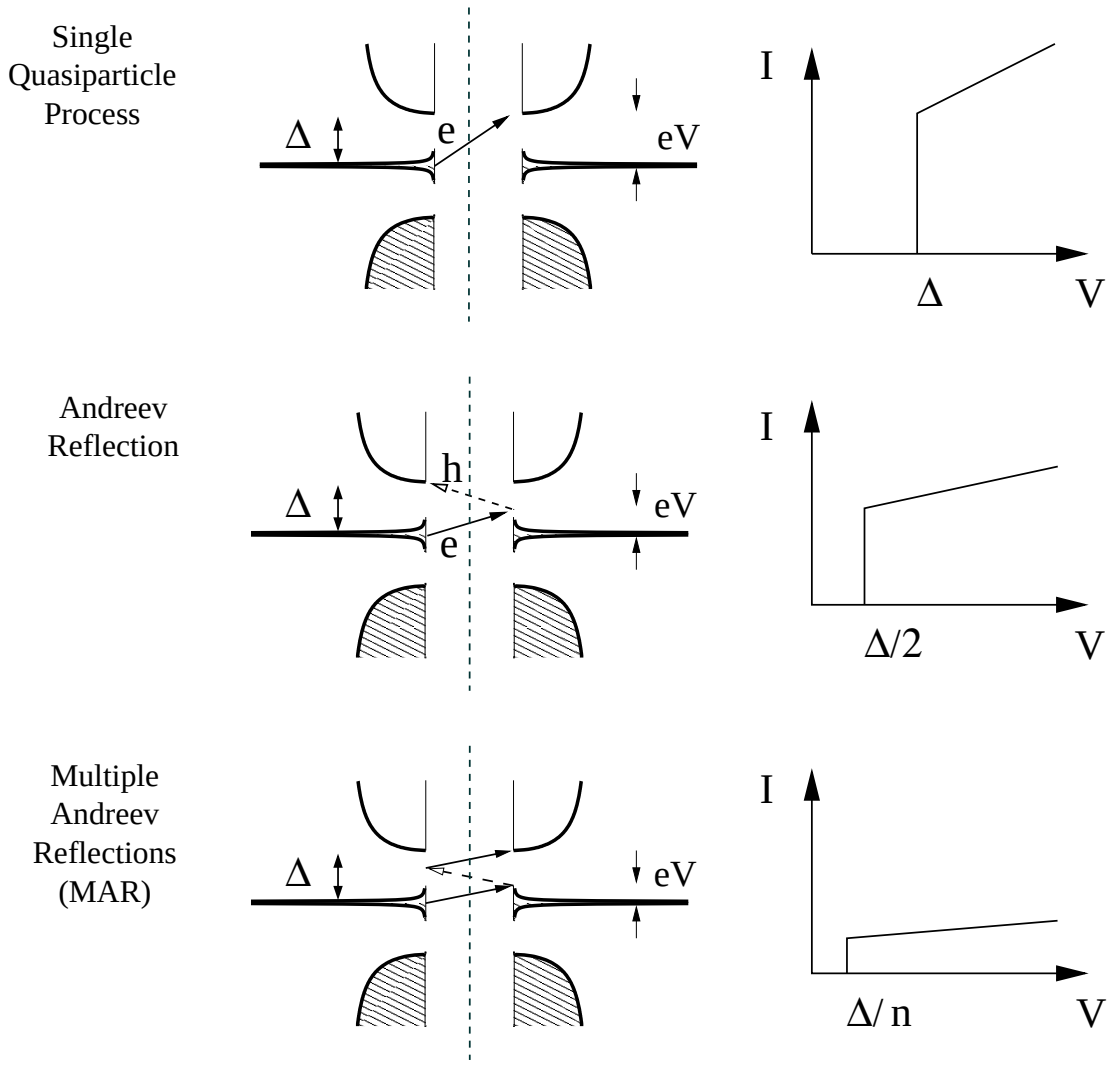

Figure 5.6: Multiple Andreev reflections in d-wave superconductor with a zero energy bound state (non-self-consistent). New transport channels open at voltages Δ/n

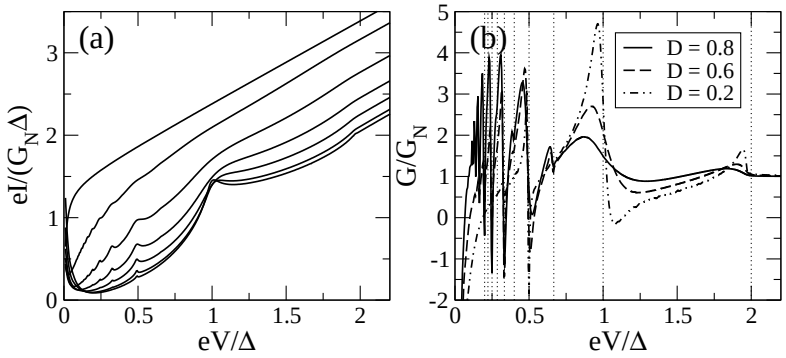

Figure 5.7: $d_{\pi/4}$-$d_{-\pi/4}$ contact in the clean case: (a) I-V characteristics for the same transmissions as in Fig. 5.4a. (b) Differential conductance.

In the self-consistent case the main consequence of the presence of the gap singularities is the recovery of the odd terms in the SGS series $eV = 2\Delta/n$. The odd terms appear now due to the enhancement of the probability of the MARs connecting the gap edges. However, the bound states at the gap edges do not appear for every trajectory, which weakens the SGS due to these processes. In this sense, in Fig. 5.7 one can clearly see a difference between the even and odd maxima of the conductance. This even-odd effect was reported in Ref. 134. This result show clearly the relevance of the self-consistency, even in the ideal clean case.

In d-wave superconductors the order parameter is very sensitive to scattering from nonmagnetic impurities and surface roughness. In particular, it is known that these elastic scattering mechanisms provide an intrinsic broadening for the zero-energy bound states (ZEBS) [92, 161]. For the case of Born scatterers this broadening is $\propto \sqrt{\Gamma\Delta}$, where $\Gamma = 1/2\tau$ is the effective pair-breaking parameter locally at the surface. This is illustrated in Fig. 5.8 for the case of bulk impurities.

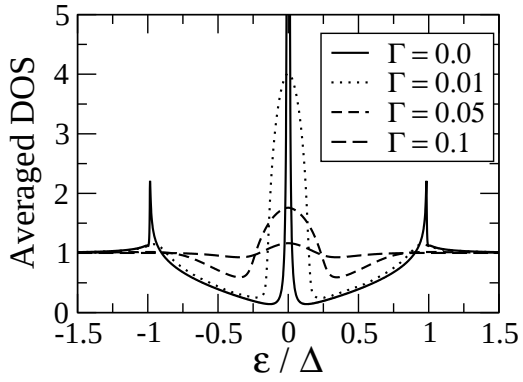

Figure 5.8: Broadening of the Andreev bound states and the gap like structure

The natural question now is: what is the influence of the broadening of the ZEBS on the SGS? In Fig. 5.9 we show the differential conductance of a $d_{\pi/4}$-$d_{-\pi/4}$ junction for different values of the bulk-impurity scattering rate. Notice that as the elastic scattering rate increases the SGS disappears, which can be understood as follows: the increase of density of states in the gap region enhances the probability of single-quasiparticle processes, producing the subsequent reduction of the probability of the Andreev processes, which in turn leads to the suppression of the SGS.

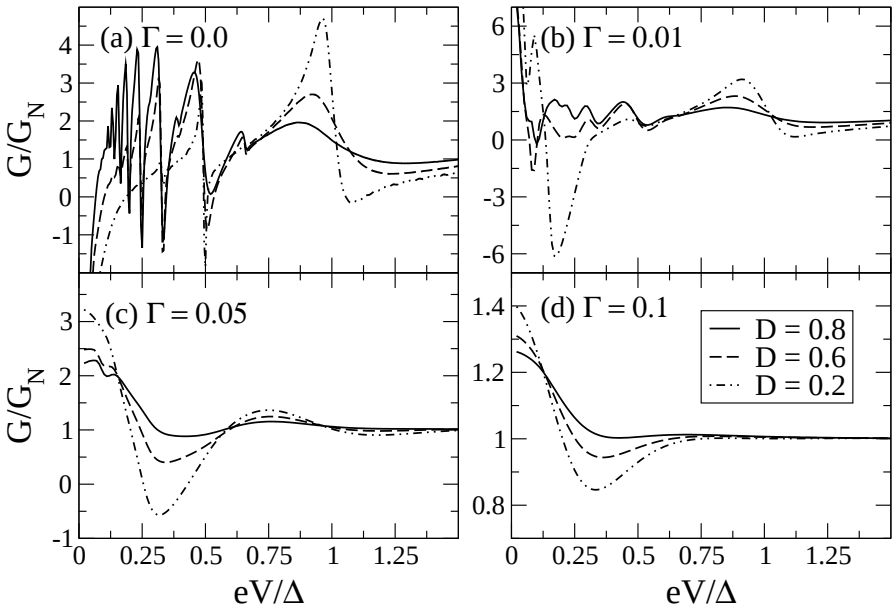

Figure 5.9: Differential conductance for a $d_{\pi/4}$-$d_{-\pi/4}$ contact for different values of the bulk-impurity scattering rate Γ. Transmission rates are given in (d)

Probably the clearest signature of d-wave superconductivity in the SGS is its evolution with magnetic field. It is known that a magnetic field perpendicular to the ab-plane, $\boldsymbol{H} = H\hat{\boldsymbol{z}}$, leads to a Doppler shift in the continuum excitations given by $\boldsymbol{v}_f \cdot \boldsymbol{p}_s$, where the condensate momentum is $\boldsymbol{p}_s = -(e/c)A(x)\hat{\boldsymbol{y}}$, with A the self-consistently determined vector potential [101]. As shown in Fig. 5.10, this means that the Andreev bound states are shifted to an energy which, in the limit of a large ratio λ/ξ_0, can be estimated to be $\epsilon_b(\boldsymbol{p}_F) = (e/c)\boldsymbol{v}_F H\lambda \sin \boldsymbol{p}_F$, λ being the ab-plane penetration depth. We shall use a natural field scale set by a screening current of the order the bulk critical current, $H_0 = c\Delta/e\boldsymbol{v}_F\lambda$, which is of the order of a Tesla [101]. As can be seen in Fig. 5.11, the screening currents flow parallel to the interface and in opposite directions in both electrodes, which means that the trajectory resolved DOS of the left and right superconductors are shifted by $2\epsilon_b(\boldsymbol{p}_F)$ relative to each other.

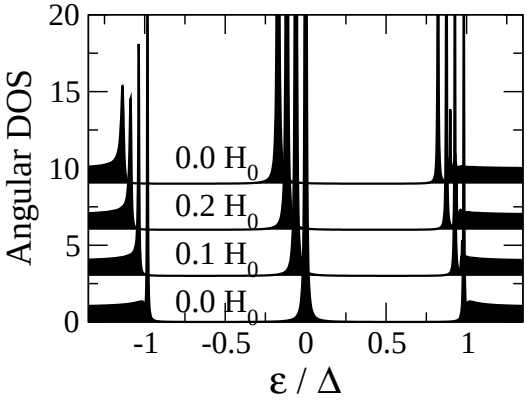

Figure 5.10: Angular resolved for trajectory $\boldsymbol{p}_F = 45°$ for different magenetic fields.

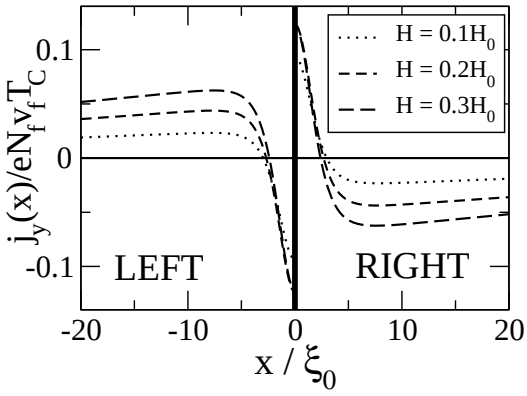

Figure 5.11: Current density, j_y, parallel to the interface at different applied fields for a $d_\pi/4 - d_\pi/4$ contact.

This shift modifies the threshold voltages of MARs starting and ending in different electrodes, leading to the splitting of the peaks with an odd order n in the SGS. On the contrary, since the magnetic field produces a rigid shift of the spectrum, the threshold voltages of those MARs starting and ending in the same electrode are not modified. This means that the positions of the peaks with an even order n in the SGS remain unchanged. This fact gives rise to a rich SGS in the trajectory resolved current, which consists in conductance peaks at the following voltage positions: (a) $[2\Delta(\boldsymbol{p}_F) \pm 2\epsilon_b(\boldsymbol{p}_F)]/n$, with n odd, due to MARs connecting the gap edges of the left and right electrodes (the signs $\pm$ correspond to electron and hole processes), (b) $[\Delta(\boldsymbol{p}_F) \pm 2\epsilon_b(\boldsymbol{p}_F)]/n$, with n odd, due to MARs connecting the bound states and the gap edges of different electrodes, (c) $2\Delta(\boldsymbol{p}_F)/n$, with n even, due to MARs connecting the gap edges of the same electrode, (d) $\Delta(\boldsymbol{p}_F)/n$, with n even, due to MARs connecting the bound states and the gap edges of the same electrode. Finally, there is also structure at $eV = 2\epsilon_b(\boldsymbol{p}_F)/n$, with n odd, due to MARs connecting the bound states.

After doing the angle average most of these features are still clearly visible. This is illustrated in Fig. 5.12 where we show the differential conductance of a $d_{\pi/4}$-$d_{-\pi/4}$ junction with transmission $D = 0.4$ for different values of the magnetic field. Starting at large voltages, the weak structure seen at 2Δ splits with applied field. Around $eV = \Delta$ there are both type (b) and type (c) processes leading to a maximum at $eV = \Delta$, unaffected by the applied field, as well as a field-shift of the dip just above Δ. The field dependence of the differential conductance is most clearly resolved at larger biases, $eV \geq \Delta/2$, as the marks of the various processes begin to overlap at small bias. What is important to note is that it is still the bulk maximum gap that gives the characteristic energy scale for the SGS. The effect of the Doppler shift on the SGS or the differential conductance is only prominent in junctions with a sizable misorientation. For junctions

close to the d_0-d_0 case, the main contribution to the SGS comes from trajectories close to perpendicular incidence, i.e., with $\sin \boldsymbol{p}_F \sim 0$ and thus having a vanishing Doppler shift.

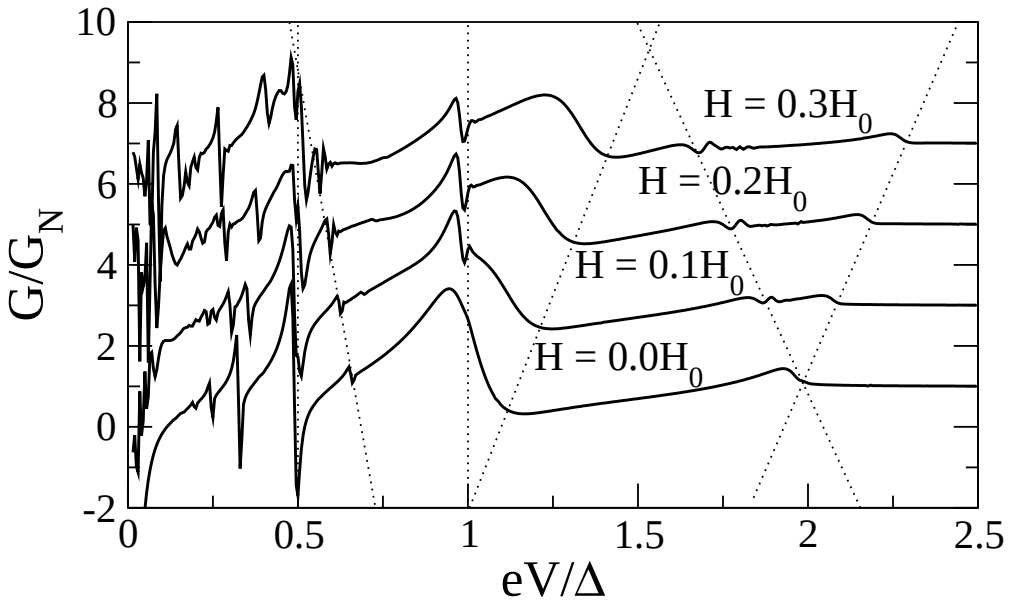

Figure 5.12: Differential conductance of a clean $d_{\pi/4}$-$d_{-\pi/4}$ junction with $D = 0.4$ and different values of the magnetic field. The curves has been vertically displaced for clarity and dotted lines have been added to guide the eye.

In summary, we have presented a self-consistent analysis of the I-V characteristics of d-wave/d-wave contacts at high transparencies. We have shown that it is possible to observe SGS for all crystal misorientations. We predict that the presence of bound states inside the gap gives rise to two new qualitative effects in the SGS: (a) an even-odd effect, and (b) a very peculiar splitting in an external magnetic field. These features are unique hallmarks of the d-wave scenario, and we hope that our analysis will trigger off a more detailed experimental study of the SGS in cuprate Josephson junctions.

6 S-matrix

In the previous chapters, unconventional superconductivity was generated by pairing interactions with unconventional symmetry. But unconventional pairing correlations can also become crucial in systems involving only conventional s-wave superconductors. In heterostructures with ferromagnetic layers, superconductivity and long-range Josephson effects at first sight seem to be an antagonism. Singlet correlations are decaying fast in the superconductor on a short length scale $\sqrt{T_C/h}$ given by the exchange field h. Nevertheless, even in a half-metal pairing correlations with equal-spin pairing are possible. But equal-spin and thus triplet pairing usually involves pairing with an unconventional symmetry in momentum space. As shown in chapter 2 this kind of pairing is very sensitive to any kind of disorder. A long-range proximity effect in impure samples seems to be unlikely. A new non-trivial possibility of triplet pairing, which was originally proposed in the discussion of ^{3}He, is odd-frequency superconductivity. Triplet correlation functions even in momentum, but odd in frequency would also comply with the Pauli principle. These correlations with s-wave symmetry are unaffected by potential impurities and would survive in magnetic systems. A long range proximity effect and Josephson current in S/F/S heterostructures can be mediated. Superconductor-ferromagnet heterostructures and effects like odd frequency triplet superconductivity have been subject of many theoretical and experimental investigations, discussed, e.g., in a review by Bergeret et al. [22].

The group of Klapwijk reported the observation of a Josephson current through the strong ferromagnet CrO_2 [162]. A theoretical description of such a system, involving a half-metal, has been given earlier by Eschrig et al. [163]. In this work, the boundary between superconductor and half-metal has been described by a phenomenological S-matrix. Some processes described by this S-Matrix, e.g., spin-flips, are crucial for the appearance of triplet correlations in the half metal. In this chapter we will give a simple microscopic model of an interface including magnetic impurities and derive an S-matrix, motivating the original ansatz.

6.1 Spin mixing

A Josephson effect in S/F/S heterostructures requires two independent processes at the interface: spin-mixing (or spin rotation) and spin-flip scattering, necessary to induce an equal-spin pairing component in the half-metal. As shown by Tokuyasu et al. [164], spin mixing is a robust feature of any interface to a strong ferromagnet. The spin mixing

angle θ defines a phase difference between waves of opposite spin, reflected at a spin-active interface. E.g., a wave $|\uparrow\rangle_k$, is reflected as $|\uparrow\rangle_{-k} = e^{i\theta/2}|\uparrow\rangle_k$ and $|\downarrow\rangle_k$ as $|\downarrow\rangle_{-k} = e^{-i\theta/2}|\downarrow\rangle_k$. In case of a singlet superconductor, the pair amplitude

$$f \propto |\uparrow\rangle_k|\downarrow\rangle_{-k} - |\downarrow\rangle_k|\uparrow\rangle_{-k} \tag{6.1}$$

by reflection transforms to

$$f \propto e^{i\theta}|\uparrow\rangle_k|\downarrow\rangle_{-k} - \epsilon^{-i\theta}|\downarrow\rangle_k|\uparrow\rangle_{-k}, \tag{6.2}$$

which is a spin singlet-triplet mixture and the first step to equal-spin pairing.

The spin-mixing process can be understood as electrons virtually entering the classical forbidden half-metal, experiencing a spin rotation by the field in the boundary region. A process which is easily understood by a simple calculation: Assuming a barrier $u = V_0\delta(x)$ between a normal conductor and a half-metal the wave functions in the normal conductor are given by

$$\psi_{N,\uparrow}(x) = A_\uparrow e^{ikx} + B_\uparrow e^{-ikx} \qquad \psi_{N,\downarrow}(x) = A_\downarrow e^{ikx} + B_\downarrow e^{-ikx} \tag{6.3}$$

while in the half-metal one component (spin down) is classical forbidden and exponentially decaying

$$\psi_{HM,\uparrow}(x) = C_\uparrow e^{iq_\uparrow x} + D_\uparrow e^{-iq_\uparrow x} \qquad \psi_{HM,\downarrow}(x) = C_\downarrow e^{-q_\downarrow x}\ . \tag{6.4}$$

Matching the wave functions it is straightforward to extract the S-matrix

$$\begin{pmatrix} \psi_{N,\uparrow,out} \\ \psi_{N,\downarrow,out} \\ \psi_{HM,\uparrow,out} \end{pmatrix} = \left(\begin{array}{cc|c} \frac{2\kappa+i(k-q_\uparrow)}{-2\kappa+i(k+q_\uparrow)} & 0 & \frac{2i\sqrt{kq_\uparrow}}{-2\kappa+i(k+q_\uparrow)} \\ 0 & \frac{2\kappa+q_\downarrow+ik}{-2\kappa-q_\downarrow+ik} & 0 \\ \hline \frac{i2\sqrt{kq_\uparrow}}{-2\kappa+i(k+q_\uparrow)} & 0 & \frac{2\kappa+i(q_\uparrow-k)}{-2\kappa+i(k+q_\uparrow)} \end{array}\right) \begin{pmatrix} \psi_{N,\uparrow,in} \\ \psi_{N,\downarrow,in} \\ \psi_{HM,\uparrow,in} \end{pmatrix} \tag{6.5}$$

with $\kappa = \frac{mV_0}{\hbar^2 k}$.

6.2 CrO_2

In the Delft experiments by Keizer et al., CrO_2 was used as strong ferromagnet. The half-metal ferromagnet, due to band splitting, is metallic for one spin component (spin-up), but insulating for the other one (spin-down). The spin polarization has been demonstrated to be close to 100%. CrO_2 is well known and used in industry for decades, e.g., for magnetic tapes. But it should be stressed, that in the experiment, epitaxially grown thin single crystal films were used. While in macroscopic samples the magnetization of CrO_2 is well understood and has a uniaxial magnetic anisotropy, the situation for films

is not yet resolved. In their samples, Keizer et al. demonstrated a biaxial magnetic anisotropy by measurements of the critical Josephson current [162] and the planar Hall effect [165]. The directions of the two easy-axes for the film were identified as 30°, 150°, 210° and 330° to the crystal $\hat{c}$-axis. A fact which might turn out to be crucial. With a magnetization along one easy-axis, the presence of a second non-orthogonal easy-axis is breaking the spin-rotation symmetry. A fact which might be the reason for the occurrence of the unusual triplet correlations in this material [166]. On the same lines, the broken symmetry will be crucial in our model.

6.3 Interface model

Modeling the contact region, we assume magnetic impurities in the superconductor close to the interface. Due to the magnetic asymmetry we assume that the magnetic moments are preferably oriented in direction of an easy-axis of the CrO_2. Thereby the orientation of mis-aligned magnetic moments is most probable in the direction of the second easy-axis, close to the direction of magnetization of the bulk ferromagnet. The impurity is modeled as classical spin with an impurity potential $\hat{u} = J\boldsymbol{S}\boldsymbol{\sigma}$, as before using the Shiba scheme of sending the spin S to infinity while keeping JS constant. Calculating the scattering on a single impurity in t-matrix approximation, it is possible to obtain the according S-matrix. The S-matrix is connected with the on-shell t-matrix by

$$S_{\boldsymbol{k}\boldsymbol{k}'} = \delta(\boldsymbol{k} - \boldsymbol{k}') - 2\pi i\delta(E(\boldsymbol{k}) - E(\boldsymbol{k}'))t_{\boldsymbol{k}\boldsymbol{k}'} \ . \tag{6.6}$$

Solving the t-matrix equation, the S-matrix for a single impurity is given by

$$\hat{S} = \frac{1 - J^2|\boldsymbol{S}|^2G_0^2 - 2\pi iJ^2|\boldsymbol{S}|^2G_0^2 - 2\pi J\boldsymbol{S}\boldsymbol{\sigma}}{1 - J^2S^2G_0^2} \ . \tag{6.7}$$

6.4 S-matrix average

Averaging over impurity configurations turns out to be non-trivial. Usual averaging schemes like using a density matrix and tracing out the impurity degree of freedom are resulting in non-unitary, and thus non-physical S-matrices. Furthermore, in doing spatial averaging one is missing multiple scattering effects, again resulting in a non-unitary S-matrix. For simplicity we will assume a homogeneously "smeared" distribution of impurities by doing a 1-D calculation. The averaging of impurity orientations is done in a more sophisticated way, guaranteeing, by construction, the unitarity of the final S-matrix. As depicted in Fig. 6.1 we are introducing a "beam-splitter" distributing incoming waves according to a weight on subsequent S-matrices.

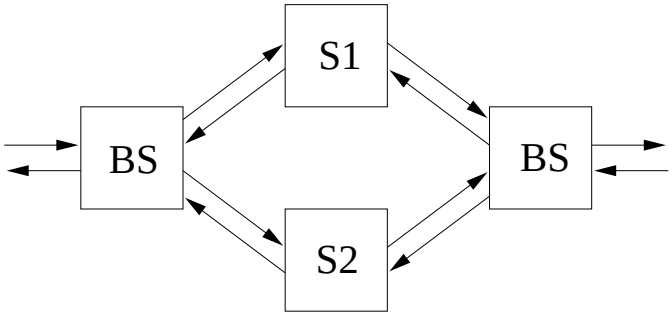

Figure 6.1: Sketch of the averaging scheme. The two S-matrices S1 and S2 are coupled by weighting beam-splitters (BS).

The S-matrix for the beam-splitter is chosen to be neutral (no additional phase shifts) and has the form

$$\hat{S} = \begin{pmatrix} 0 & \hat{\alpha}^T \\ \hat{\alpha} & \hat{\alpha}\hat{\alpha}^T - \hat{1} \end{pmatrix} . \tag{6.8}$$

In the simple case of two S-matrices, it is given by

$$\hat{S} = \begin{pmatrix} 0 & \sqrt{\rho} & \sqrt{1-\rho} \\ \sqrt{\rho} & -(1-\rho) & \sqrt{\rho}\sqrt{1-\rho} \\ \sqrt{1-\rho} & \sqrt{\rho}\sqrt{1-\rho} & -\rho \end{pmatrix} , \tag{6.9}$$

but the scheme can easily be extended to an arbitrary or even number continuous S-matrices. The scheme does not only guarantee unitarity of the averaged S-matrix, it accounts for all multiple reflection processes between the different scatterers.

In case of only two S-matrices, the total averaged S-matrix is given by

$$S = \rho S_1[1+\rho S_2+(1-\rho)S_1]^{-1}(1+S_2)+(1-\rho)S_2[1+\rho S_2+(1-\rho)S_1]^{-1}(1+S_1) . \tag{6.10}$$

6.4.1 The interface S-matrix

To model the whole interface, the general S-matrix for a spin-active interface parameterized by

$$\hat{S} = \left(\begin{array}{ccc|c} & r_{\uparrow\uparrow}e^{i(\phi+\frac{\theta}{2})} & 0 & d_{\uparrow\uparrow}e^{i(\theta_{\uparrow\uparrow}+\frac{\theta}{4}+\frac{\alpha+\phi}{2})} \\ & 0 & e^{i(\phi-\frac{\theta}{2})} & 0 \\ \hline d_{\uparrow\uparrow}e^{i(-\theta_{\uparrow\uparrow}+\frac{\theta}{4}+\frac{\alpha+\phi}{2})} & 0 & & -r_{\uparrow\uparrow}e^{i\alpha} \end{array} \right) \tag{6.11}$$

is put into series with the impurity S-matrices as depicted in Fig. 6.2.

Averaging scattering on magnetic moments, mis-aligned by an angle α, with an S-matrix given by Eq. (6.7) and absence of any scattering on impurities, the final S-matrix

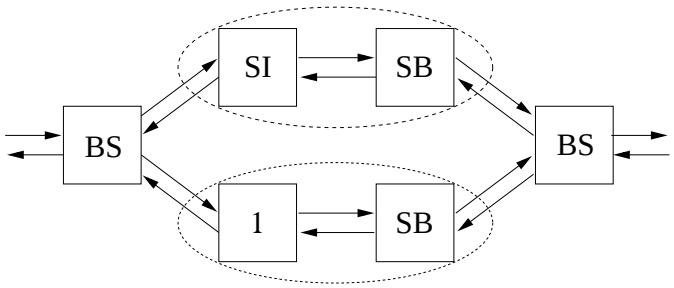

Figure 6.2: Sketch of the averaged boundary S-matrix. The impurity S-matrix (SI) and the purely transmitting S-matrix (1) are in parallel, each one is in series with a boundary S-matrix (SB).

is obtained as

$$
\begin{aligned}
S_{11} &= -\frac{\gamma^2\rho^2[e^{i\theta}(4-t^2)+8e^{i\frac{\theta}{2}}+(4+t^2)]+2i\gamma\rho\sin(\frac{\alpha}{2})[e^{i\theta}(t^2-4)-4e^{i\frac{\theta}{2}}]+e^{i\theta}(t^2-4)}{\gamma^2\rho^2[e^{i\theta}(4-t^2)+8e^{i\frac{\theta}{2}}+(4+t^2)]+i\gamma\rho\sin(\frac{\alpha}{2})[e^{i\theta}(t^2-4)+(4+t^2)]+e^{i\frac{\theta}{2}}(4+t^2)} \\
S_{12} &= \frac{\gamma\rho\cos(\frac{\alpha}{2})(1+e^{i\frac{\theta}{2}})[e^{i\frac{\theta}{2}}(4-t^2)+(4+t^2)]}{\gamma^2\rho^2[e^{i\theta}(4-t^2)+8e^{i\frac{\theta}{2}}+(4+t^2)]+i\gamma\rho\sin(\frac{\alpha}{2})[e^{i\theta}(t^2-4)+(4+t^2)]+e^{i\frac{\theta}{2}}(4+t^2)} \\
S_{13} &= \frac{-4te^{\frac{i}{4}(\theta+4\theta_{\uparrow\uparrow})}[\gamma\rho\sin(\frac{\alpha}{2})(e^{i\frac{\theta}{2}}+1)-ie^{i\frac{\theta}{2}}]}{\gamma^2\rho^2[e^{i\theta}(4-t^2)+8e^{i\frac{\theta}{2}}+(4+t^2)]+i\gamma\rho\sin(\frac{\alpha}{2})[e^{i\theta}(t^2-4)+(4+t^2)]+e^{i\frac{\theta}{2}}(4+t^2)} \\
S_{21} &= -S_{12} \\
S_{22} &= \frac{-4\gamma^2\rho^2[e^{i\theta}+2e^{i\frac{\theta}{2}}-t^2(e^{i\theta}-1)]-2i\gamma\rho\sin(\frac{\alpha}{2})[4e^{i\frac{\theta}{2}}+(4+t^2)]-t^2}{\gamma^2\rho^2[e^{i\theta}(4-t^2)+8e^{i\frac{\theta}{2}}+(4+t^2)]+i\gamma\rho\sin(\frac{\alpha}{2})[e^{i\theta}(t^2-4)+(4+t^2)]+e^{i\frac{\theta}{2}}(4+t^2)} \\
S_{23} &= \frac{-4\gamma\rho\cos(\frac{\alpha}{2})te^{\frac{i}{4}(4\alpha+\theta)}(1+e^{i\frac{\theta}{2}})}{\gamma^2\rho^2[e^{i\theta}(4-t^2)+8e^{i\frac{\theta}{2}}+(4+t^2)]+i\gamma\rho\sin(\frac{\alpha}{2})[e^{i\theta}(t^2-4)+(4+t^2)]+e^{i\frac{\theta}{2}}(4+t^2)} \\
S_{31} &= e^{2i\alpha}S_{13} \\
S_{32} &= -e^{2i\alpha}S_{23} \\
S_{33} &= -\frac{\gamma^2\rho^2[e^{i\theta}(4+t^2)+8e^{i\frac{\theta}{2}}+(4+t^2)]-i\gamma\rho\sin(\frac{\alpha}{2})[e^{i\theta}(4+t^2)+(t^2-4)]+e^{i\frac{\theta}{2}}(4-t^2)}{\gamma^2\rho^2[e^{i\theta}(4-t^2)+8e^{i\frac{\theta}{2}}+(4+t^2)]+i\gamma\rho\sin(\frac{\alpha}{2})[e^{i\theta}(t^2-4)+(4+t^2)]+e^{i\frac{\theta}{2}}(4+t^2)}\,.
\end{aligned}
\tag{6.12}
$$

Obviously the found S-matrix has all the necessary components for a singlet - triplet conversion: Spin mixing and spin-flip terms.

Using the S-matrix for boundary conditions in the quasiclassical Green's function technique, it is convenient to choose a parametrization which extracts the spin-independent phases. Having a look at the boundary conditions of Millis et al. [36] channel-independent

phases only enter in the evaluation of the *drone* amplitudes but drop out of the boundary conditions of the quasiclassical Green's functions. Thus extracting these phases without physical relevance makes it easier to identify the $n^2 - 4$ relevant parameters.

In the discussion of the of half-metal/superconductor heterostructures, Eschrig et al. [167] used the parametrization

$$\hat{S} = \left(\begin{array}{c|c} r^S & t^{SF} \\ \hline t^{FS} & -r^F \end{array}\right) = \left(\begin{array}{cc|c} r_{\uparrow\uparrow} e^{\frac{i}{2}\vartheta} & r_{\uparrow\downarrow} e^{i(\vartheta_{\uparrow\uparrow}-\vartheta_{\downarrow\uparrow})} & d_{\uparrow\uparrow} e^{i(\vartheta_{\uparrow\uparrow}+\frac{\vartheta}{4})} \\ r_{\downarrow\uparrow} e^{i(\vartheta_{\uparrow\uparrow}-\vartheta_{\downarrow\uparrow})} & r_{\downarrow\downarrow} e^{-\frac{i}{2}\vartheta} & d_{\downarrow\uparrow} e^{i(\vartheta_{\downarrow\uparrow}-\frac{\vartheta}{4})} \\ \hline d_{\uparrow\uparrow} e^{-i(\vartheta_{\uparrow\uparrow}-\frac{\vartheta}{4})} & d_{\downarrow\uparrow} e^{-i(\vartheta_{\downarrow\uparrow}+\frac{\vartheta}{4})} & -\underline{r}_{\uparrow\uparrow} \end{array}\right) \tag{6.13}$$

which can be connected with the transmission amplitudes by

$$r_{\uparrow\uparrow} = 1 - t_{\uparrow\uparrow}^2/2W \tag{6.14}$$

$$r_{\downarrow\downarrow} = 1 - t_{\downarrow,\uparrow}^2/2W \tag{6.15}$$

$$r_{\uparrow\downarrow} = r_{\downarrow\uparrow} = -t_{\uparrow\uparrow} t_{\downarrow\uparrow}/2W \tag{6.16}$$

$$\underline{r}_{\uparrow\uparrow} = 1 - (t_{\uparrow\uparrow}^2 + t_{\downarrow\uparrow}^2)/2W \tag{6.17}$$

$$d_{\uparrow\uparrow} = t_{\uparrow\uparrow}/W \tag{6.18}$$

$$d_{\downarrow\uparrow} = t_{\downarrow\uparrow}/W \tag{6.19}$$

$$W = 1 + (t_{\uparrow\uparrow}^2 + t_{\downarrow\uparrow}^2)/4 \tag{6.20}$$

The five real parameters characterizing the S-matrix are $t_{\uparrow\uparrow}, t_{\downarrow\uparrow}, \vartheta, \vartheta_{\uparrow\uparrow}, \vartheta_{\downarrow\uparrow}$. Here, ϑ is the spin rotation angle.

For un-coupled systems one has the freedom to choose the spin quantization axis in each system separately. While for the half-metal the direction of the magnetization is a natural choice, in the superconductor no distinguished orientation exists. It is therefore possible to choose the quantization axis in a way, that the boundary condition and expressions for observables like the supercurrent simplify. In comparison with microscopically derived S matrices one has to be aware of the fact that the quantization axis on both sides of the boundary might be (and usually are) chosen differently and apply the necessary transformations to adjust them accordingly. A tedious task which is usually beyond analytic computation. A numerical transformation and the extraction of relevant parameters of the S-matrix derived in this chapter is given in the diploma thesis of Gero Bergner [168].

7 Conclusions

This thesis was devoted to unconventional superconductors and in particular to the influence of inhomogeneities on the properties of these compounds. Using the quasiclassical theory of superconductivity we investigated a broad range of properties and materials. After a brief introduction to the quasiclassical theory and the basic results at first we addressed Sr_2RuO_4.

Strontium ruthenate attracted a lot of attention in recent years not only because of the structural similarity to the high-temperature superconductors. An unconventional triplet order parameter was proposed and many experiments support this suggestion. Nevertheless, the exact symmetry is still subject of discussions. Thermodynamic properties like the specific heat show (in clean samples) a linear temperature dependence. Pointing towards an order parameter with line nodes. This contradicts the original proposal of a p-wave order parameter $k_x + ik_y$. In-plane measurements do not show traces of vertical gap nodes leading to a proposal of Zhitomirsky and Rice [14] of an interband proximity effect giving rise to an order parameter with horizontal line nodes. The band structure of Sr_2RuO_4 provides three conduction bands, making multi-band superconductivity like in MgB_2 [169, 170] an attractive idea. Early experiments of, e.g., the specific heat suggested a high residual density of states, interpreted as normal conductivity in a part of the bands. Later in samples of improved quality the specific heat vanishes linearly with temperature $T \to 0$, pointing towards superconductivity in all bands. In their model, Zhitomirsky and Rice assumed one active band with an attractive pairing interaction coupled to the other bands. Due to this coupling also in these bands superconductivity is induced, and the form of the coupling will yield an order parameter with horizontal line nodes varying as $\cos(k_z/2)$. In the first part of chapter 3 we adopted this model including inhomogeneities in the form of potential impurities. In a fully self-consistent calculation solving the impurity problem in t-matrix approximation we investigated basic thermodynamic properties. Measurements of the nuclear spin relaxation rate in samples with a reduced transition temperature provide information about the impurity scattering rate and the residual density of states. Calculating this property for different interband coupling parameters and impurity strengths as function of the scattering rate and by comparison with the experimental results it is possible to extract estimates of the coupling parameter and the scattering phase shift. As we showed, to agree with experiment the scattering has to be in an intermediate range and neither in unitary nor in Born limit. After this we calculated the specific heat as function of the temperature for different coupling parameters in the clean case. A expected the qualita-

tive low temperature behaviour is strongly connected to the coupling: For low coupling the specific heat seems to saturate before dropping again being zero at $T \to 0$ and also strong coupling results in a crossover from linear to exponential growth at intermediate temperatures. But taking the coupling parameter extracted from the NQR experiment, a linear dependence is found and the experimental results can be fitted in a broad temperature range only showing deviations in the behavior close to the critical temperature. Using the same parameters we calculated the spin relaxation rate. For impurity scattering rates as given by the measured critical temperature T_c, the experimental observed crossover from linear to a T^3 law in the spin relaxation rate was reproduced.

Measurements of the excess current in point contacts by Laube et al. [16] exhibited an unusual temperature dependence. A temperature dependence which is also not expected in case of an unconventional order parameter. A possible explanation, a low lying boson mode effectively acting as scattering centers with a temperature dependent scattering rate, was proposed by the authors and could fit the data. In the second part of chapter 3.4 we studied the specific heat for this new model. We assumed a single band p-wave order parameter (as originally proposed) including the boson mode. At first we were using the simplified effective model, as derived by Millis et al. [80]. This description is well suited for temperatures larger than the boson mode. The obtained specific heat shows an activated low temperature behavior due to the spectral gap, and an additional dip at the boson frequency. Since the property calculated is the difference of specific heat in the superconducting and the normal state, this dip is most likely a rise in the normal state, absent in the superconducting state. To exclude anomalies caused by the approximation in the effective model, we extended the calculations to a strong coupling calculation taking into account the exact frequency dependence of the electron-phonon self-energies. The Eliashberg like calculation is non-local in energy but, in contrast to the usual strong coupling formalism, the order parameter is still energy independent. The s-wave phonon coupling does not contribute to the p-wave pairing. The results of the full calculation deviate surprisingly little from the ones obtained before. Concluding this section, the model used to explain the excess current cannot attribute for the experimentally obtained specific heat. It would be valuable to re-investigate the problem to find a consistent explanation.

The next chapter 4 was devoted to new materials and new kind of inhomogeneities. The symmetry of the order parameter in the high-temperature superconductors is a central question. At first it should be noted, that this family of superconductors in fact consists of two different classes, electron- and hole-doped compounds. Being similar but, as already the phase diagram exhibits, also distinct. In the hole-doped cuprates a $d_{x^2-y^2}$ order parameter is now well established by countless and partially even phase sensitive experiments, giving a consistent answer. The order parameter is not only sensitive to scattering on impurities, scattering on walls and junctions can also be pair-breaking. This suppression and the resulting spatially varying order parameter leads to Andreev bound states at the surfaces. These are formed by normal reflection at the interface

and Andreev reflection at the order parameter profile. It is known that a change in the sign of the order parameter along such a trajectory will result in a bound state strictly at zero energy. In Sec. 4.1.1 we studied the influence of bulk impurities on these Andreev bound states and the implications on transport properties like the Josephson critical current. We could show that quasiparticle scattering by impurities results in the broadening of these surface quasiparticle bound states. Scatterers can essentially reduce the height of the peak in the density of states. A reduction which will also depress the low-temperature anomaly in the Josephson critical current expected in tunnel junctions of d-wave superconductors. We have shown that bound states are more sensitive to weak (Born) scatterers, than to strong (unitary) impurities at a given value of the scattering rate. While Born scatterers yield a broadening $\propto \sqrt{\Gamma\Delta}$, where $\Gamma = 1/2\tau$ is the effective pair breaking parameter, in the unitary limit the bound states are remarkably stable to impurity scattering.

In the next section 4.1.2, we investigated the magnetic field dependence of the Andreev bound states (ABS). Tunneling spectroscopy experiments on grain boundary junction did not show a splitting of the ABS as expected by theory and observed in other tunneling experiments. Nevertheless, spectral weight was shifted to higher energies. To explain this discrepancy we studied the local density of states with an applied magnetic field, again including (surface) impurities. Without magnetic field, for an unconventional order parameter, magnetic and potential scatterers behave identical. This is no longer true in case of an applied magnetic field. With the broken symmetry potential impurities become less effective, while magnetic scatterers will still significantly broaden the bound states. Turning to the differential conductance, we could show that in case of potential impurities the splitting will be present, while in case of magnetic scatterers it is not observable. This is a reasonable explanation for the different observations in the tunneling experiments, especially accounting for the fact that the nature of the tunneling barriers in the conflicting experiments was substantially different.

The final section 4.2 of chapter 4 focused on the electron-doped cuprates. While in the hole-doped compounds a d-wave order parameter is well established by now, in the electron-doped cuprates the order parameter symmetry is still under debate. Early experiments convincingly concluded that in these materials the superconducting state is of conventional s-wave pairing. A more recent phase-sensitive experiment [122] observed d-wave symmetry and was followed by several supporting investigations. Within the discussion the absence of the expected zero bias anomaly due to Andreev bound states is often attributed to impurity scattering. We performed fully self-consistent calculations of the surface density of states and the tunneling conductance. Including the effects of impurity scattering, we compared our results for several discussed order parameter symmetries with the experimental findings. As our results show, an isotropic as well as an anisotropic s-wave order parameter are in agreement with the experimental tunneling data on grain boundary junctions. The necessary assumption is surface disorder with magnetic impurities. This assumption and the parameters used are the same as used in

the previous section to explain the magnetic field dependence observed in grain-boundary junctions of hole-doped cuprates. In contrast, our results contradict the d-wave picture. Albeit taking impurities into account, our results for a d-wave order parameter can not even qualitatively explain the experimentally observed conductance spectra. The contradiction to the phase sensitive experiments is puzzling, but might be explained by recent experiments [126, 127] indicating a doping dependence of the order parameter symmetry.

In chapter 5 we addressed the question of the observability of subharmonic gap structure in d-wave superconductors. We presented a self-consistent theory of the current-voltage characteristics of d-wave/d-wave contacts at arbitrary transparency. In particular, we addressed the open problem of the observation of subharmonic gap structure (SGS) in cuprate junctions. Our analysis showed that SGS is possible in d-wave superconductors. The existence of bound states within the gap results in a peculiar even-odd effect in the SGS. In the maxima of the conductance at $eV = 2\Delta/n$ one can clearly see a difference between even and odd n. Elastic scattering mechanisms, like impurities or surface roughness, may suppress the SGS. As could be demonstrated, in the presence of a magnetic field the Doppler shift of the Andreev bound states leads to a splitting of the SGS, which would be an unambiguous fingerprint of d-wave superconductivity.

Subject of the last chapter 6 were heterostructures incorporating only conventional BCS superconductors. Also in superconductor-ferromagnet heterostructures pairing correlations with an unconventional symmetry are expected. While singlet correlations decay in the ferromagnet on a short length scale, triplet correlations can give rise to a long range proximity effect and Josephson critical currents. A necessity for the occurrence of such triplet correlations are spin-flip processes in the boundary. In combination with spin-rotation, they make a conversion of the singlet pairing functions in the BCS superconductor to triplet correlations in the ferromagnet possible. In this chapter we motivated the occurrence of such spin-flip terms. Within a simple model of magnetic scatterers close to the surface, we calculated the boundary S-matrix. A crucial point of the model is the breaking of rotational symmetry. It is motivated by the fact that in experiment the used CrO_2 films exhibited two non-orthogonal easy axes of magnetization. We accounted for this fact assuming a preferred orientations of the misaligned magnetic moments. We could show that in our model the resulting boundary S-matrix contains the necessary spin-flip terms.

In conclusion in this thesis we covered a number of different systems and physical properties. The conjoint question was the impact of inhomogeneities on systems with unconventional superconducting correlations.

A Notation

The non-commutative product $\otimes$ is defined as

$$\hat{A} \otimes \hat{B}(\varepsilon, t) = \exp\left[\frac{i\hbar}{2}\left(\partial_\varepsilon^A \partial_t^B - \partial_t^A \partial_\varepsilon^B\right)\right] \hat{A}(\varepsilon, t)\hat{B}(\varepsilon, t) \tag{A.1}$$

$$\hat{A} \otimes \hat{B}(\varepsilon, \omega) = \int_{-\infty}^{\infty} \frac{\mathrm{d}\omega'}{2\pi}\frac{\mathrm{d}\omega''}{2\pi}\delta(\omega' + w'' - \omega)\hat{A}\left(\varepsilon + \frac{\hbar\omega'}{2}, \omega''\right)\hat{B}\left(\varepsilon - \frac{\hbar\omega''}{2}, \omega'\right) \tag{A.2}$$

which in equilibrium reduce to simple matrix products. The commutator

$$\left[\hat{A}, \hat{B}\right]_\otimes = \hat{A} \otimes \hat{B} - \hat{B} \otimes \hat{A} \tag{A.3}$$

is accordingly determined with the non-commutative product.

The Fermi surface average $\langle \ldots \rangle_{\boldsymbol{p}_F}$ is defined

$$\langle \ldots \rangle_{\boldsymbol{p}_F} = \frac{1}{N_F} \int \frac{\mathrm{d}^2 \boldsymbol{p}_F}{(2\pi\hbar)^3 |\boldsymbol{v}_F(\boldsymbol{p}_F)|} \ldots , \tag{A.4}$$

N_F is the total density of states at the Fermi surface in the normal state

$$N_F = \int \frac{\mathrm{d}^2 \boldsymbol{p}_F}{(2\pi\hbar)^3 |\boldsymbol{v}_F(\boldsymbol{p}_F)|} \tag{A.5}$$

and $\boldsymbol{v}_F(\boldsymbol{p}_F)$ the normal state Fermi velocity on the Fermi surface at $\boldsymbol{p}_F$

$$\boldsymbol{v}_F(\boldsymbol{p}_F) = \frac{\partial \xi(\boldsymbol{p})}{\partial \boldsymbol{p}}\Big|_{\boldsymbol{p}=\boldsymbol{p}_F}. \tag{A.6}$$

Obviously in general the Fermi velocity $\boldsymbol{v}_F(\boldsymbol{p}_F)$ needn't be directed in the same direction as $\boldsymbol{p}_F$. But in the case of cylindrical or spherical Fermi surfaces this is the case and the Fermi surface average simplifies to an angular average. E.g., in (quasi) 2d it is simply given by

$$\langle \ldots \rangle_{\boldsymbol{p}_F} = \int \frac{\mathrm{d}\phi}{2\pi} \ldots . \tag{A.7}$$

B Propagators

Since in the literature different definitions and conventions are used, the exact definitions used in this thesis should be given. Full Green's functions and self-energies will be denoted by capital $\hat{G}, \hat{\Sigma}$, the quasiclassical counterparts with lowercase $\hat{g}, \hat{\sigma}$. The hat $\hat{}$ denotes 4x4 matrices in Nambu and spin space.

B.1 Definitions

In the following l, l' denote the 4 dimensional Nambu indices in spin and particle-hole space. The full propagators are defined by

$$\hat{G}^R(x,t;x',t')_{ll'} = -i\theta(t-t')\left\langle\left\{\psi_l(x,t),\psi_{l'}^\dagger(x',t')\right\}\right\rangle \tag{B.1}$$

$$\hat{G}^A(x,t;x',t')_{ll'} = \ \ i\theta(t'-t)\left\langle\left\{\psi_l(x,t),\psi_{l'}^\dagger(x',t')\right\}\right\rangle \tag{B.2}$$

$$\hat{G}^K(x,t;x',t')_{ll'} = -i\left\langle\left[\psi_l(x,t),\psi_{l'}^\dagger(x',t')\right]\right\rangle \tag{B.3}$$

$$\hat{G}^M(x,x';\tau)_{ll'} = -\left\langle T_\tau\left(\psi_l(x,-i\tau)\psi_{l'}^\dagger(x',0)\right)\right\rangle \tag{B.4}$$

with creation ($\psi^\dagger$) and destruction (ψ) operators defined in Nambu space as

$$\psi_1 = \psi_\uparrow, \qquad \psi_2 = \psi_\downarrow, \qquad \psi_3 = \psi_\uparrow^\dagger, \qquad \psi_4 = \psi_\downarrow^\dagger\,. \tag{B.5}$$

In the unperturbed homogeneous case, assuming an unitary order parameter, the equilibrium propagators of the superconducting state are given by:

$$\hat{G}^M(\boldsymbol{p};\varepsilon_n) = \frac{-\xi_{\boldsymbol{p}}\hat{\tau}_3 - i\varepsilon_n + \hat{\Delta}(\boldsymbol{p})}{\xi_{\boldsymbol{p}}^2 + {\varepsilon_n}^2 + |\hat{\Delta}(\boldsymbol{p})|^2} \tag{B.6}$$

$$\hat{G}^{R,A}(\boldsymbol{p};\varepsilon) = \frac{\xi_{\boldsymbol{p}}\hat{\tau}_3 + \varepsilon + \hat{\Delta}(\boldsymbol{p})}{(\varepsilon \pm i\delta)^2 - \xi_{\boldsymbol{p}}^2 - |\hat{\Delta}(\boldsymbol{p})|^2} \tag{B.7}$$

$$\hat{G}^K(\boldsymbol{p};\varepsilon) = \left[\hat{G}^R(\boldsymbol{p};\varepsilon) - \hat{G}^A(\boldsymbol{p};\varepsilon)\right]\tanh\left(\frac{\varepsilon}{2\mathrm{k_B}T}\right)\,. \tag{B.8}$$

The undressed phonon propagator is

$$D_0(\boldsymbol{k},\omega_n) = -\frac{\omega_0^2(\boldsymbol{k})}{{\omega_n}^2 + \omega_0^2(\boldsymbol{k})}, \qquad \omega_n = 2n\pi T\,. \tag{B.9}$$

Again assuming a homogeneous system in equilibrium and an unitary order parameter the unperturbed quasiclassical propagators are given by:

$$\hat{g}_0^{R,A}(\boldsymbol{p}_F, \boldsymbol{R}; \varepsilon, t) = -\pi \frac{\varepsilon\hat{\tau}_3 - \hat{\Delta}_0(\boldsymbol{p}_F)}{\sqrt{|\hat{\Delta}_0(\boldsymbol{p}_F)_0|^2 - (\varepsilon \pm i\delta)^2}} \tag{B.10}$$

$$\hat{g}_0^{K}(\boldsymbol{p}_F, \boldsymbol{R}; \varepsilon, t) = -2\pi i \tanh\left(\frac{\varepsilon}{2T}\right) \mathrm{Im}\left[\frac{1}{\sqrt{|\hat{\Delta}_0(\boldsymbol{p}_F)|^2 - (\varepsilon + i\delta)^2}}\right] (\varepsilon\hat{\tau}_3 - \hat{\Delta}_0(\boldsymbol{p}_F)) \tag{B.11}$$

$$\hat{g}_0^{M}(\boldsymbol{p}_F, \boldsymbol{R}; \varepsilon_n, t) = -\pi \frac{i\varepsilon_n\hat{\tau}_3 - \hat{\Delta}_0(\boldsymbol{p}_F)}{\sqrt{|\hat{\Delta}_0(\boldsymbol{p}_F)|^2 + {\varepsilon_n}^2}} \tag{B.12}$$

In equilibrium the quasiclassical normal state propagators are given by the simple expressions

$$\hat{g}_0^{M}(\boldsymbol{p}_F, \boldsymbol{R}; \varepsilon_n) = -i\pi\,\mathrm{sign}(\varepsilon_n)\hat{\tau}_3 \tag{B.13}$$

$$\hat{g}_0^{R,A}(\boldsymbol{p}_F, \boldsymbol{R}; \varepsilon, t) = \mp i\pi\hat{\tau}_3 \tag{B.14}$$

$$\hat{g}_0^{K}(\boldsymbol{p}_F, \boldsymbol{R}; \varepsilon, t) = -2\pi i \tanh(\varepsilon/2T)\hat{\tau}_3\ . \tag{B.15}$$

B.2 Symmetries

The introduced notation in Nambu space incloses redundant information. This redunancy is reflected in additional symmetries of the Nambu matrices:

$$\hat{X}^{M}(\boldsymbol{p}_F, \boldsymbol{R}; \varepsilon_n)^{\dagger} = \hat{\tau}_3\hat{X}^{M}(\boldsymbol{p}_F, \boldsymbol{R}; -\varepsilon_n)\hat{\tau}_3 \tag{B.16}$$

$$\hat{X}^{R}(\boldsymbol{p}_F, \boldsymbol{R}; \varepsilon, t)^{\dagger} = \hat{\tau}_3\hat{X}^{A}(\boldsymbol{p}_F, \boldsymbol{R}; \varepsilon, t)\hat{\tau}_3 \tag{B.17}$$

$$\hat{X}^{K}(\boldsymbol{p}_F, \boldsymbol{R}; \varepsilon, t)^{\dagger} = -\hat{\tau}_3\hat{X}^{K}(\boldsymbol{p}_F, \boldsymbol{R}; \varepsilon, t)\hat{\tau}_3 \tag{B.18}$$

and

$$\hat{X}^{M}(\boldsymbol{p}_F, \boldsymbol{R}; \varepsilon_n)^{tr} = \hat{\tau}_2\hat{X}^{M}(-\boldsymbol{p}_F, \boldsymbol{R}; -\varepsilon_n)\hat{\tau}_2 \tag{B.19}$$

$$\hat{X}^{R}(\boldsymbol{p}_F, \boldsymbol{R}; \varepsilon, t)^{tr} = \hat{\tau}_2\hat{X}^{A}(-\boldsymbol{p}_F, \boldsymbol{R}; -\varepsilon, t)\hat{\tau}_2 \tag{B.20}$$

$$\hat{X}^{K}(\boldsymbol{p}_F, \boldsymbol{R}; \varepsilon, t)^{tr} = \hat{\tau}_2\hat{X}^{K}(-\boldsymbol{p}_F, \boldsymbol{R}; -\varepsilon, t)\hat{\tau}_2 \tag{B.21}$$

Sometimes it is useful to parametrize the 4x4 Nambu matrices in a form which explicitly exhibits the structure in spin space. In terms of scalars a, b and vectors $\boldsymbol{a}, \boldsymbol{b}$ with $\boldsymbol{\sigma}$ being a vector of Pauli matrices all[1] Nambu matrices can be written in the form

$$\hat{X} = \begin{pmatrix} a + \boldsymbol{a}\boldsymbol{\sigma} & (b + \boldsymbol{b}\boldsymbol{\sigma}) i\hat{\sigma}_2 \\ i\hat{\sigma}_2 \, (\widetilde{b} + \tilde{\boldsymbol{b}}\boldsymbol{\sigma}) & \tilde{a} - \hat{\sigma}_2 \, \tilde{\boldsymbol{a}}\boldsymbol{\sigma}\hat{\sigma}_2 \end{pmatrix} . \tag{B.22}$$

The conjugation ($\widetilde{\ }$) of the form

$$\tilde{x}(\boldsymbol{p}_F, \boldsymbol{R}; \varepsilon, t) = x(-\boldsymbol{p}_F, \boldsymbol{R}; -\varepsilon, t)^* \tag{B.23}$$

is assuring that the matrix fulfills the symmetry condition given above.

[1] Exluding Keldysh matrices which, to allow a consistent definition of the "conjugation", have to be parameterized with different signs as: $\hat{X}^K = \begin{pmatrix} a + \boldsymbol{a}\boldsymbol{\sigma} & (b + \boldsymbol{b}\boldsymbol{\sigma}) i\hat{\sigma}_2 \\ -i\hat{\sigma}_2 \, (\widetilde{b} + \tilde{\boldsymbol{b}}\boldsymbol{\sigma}) & -(\tilde{a} - \hat{\sigma}_2 \, \tilde{\boldsymbol{a}}\boldsymbol{\sigma}\hat{\sigma}_2 \,) \end{pmatrix}$.

C Riccati parameterization

The numerical solution of the Eilenberger equation (2.3) proves to be in many cases non-trivial. The transport equation is unstable to spurious unphysical solutions.

Using a special parameterization of the Green's functions, as in the most general case given by Eschrig [37], the numerical effort is significantly reduced. The Green's functions can be parameterized by 2x2 spin matrix coherence functions $\gamma, \tilde{\gamma}$ and distribution functions $x^K, \tilde{x}^K$ in the form

$$\hat{g}^{R,A} = \mp i\pi \hat{N}^{R,A} \otimes \begin{pmatrix} (1+\gamma^{R,A}\otimes\tilde{\gamma}^{R,A}) & 2\gamma^{R,A} \\ -2\tilde{\gamma}^{R,A} & -(1+\tilde{\gamma}^{R,A}\otimes\gamma^{R,A}) \end{pmatrix} \tag{C.1}$$

$$\hat{g}^{K} = -2\pi i \hat{N}^{R} \otimes \begin{pmatrix} (x^K - \gamma^R\otimes\tilde{x}^K\otimes\tilde{\gamma}^A) & -(\gamma^R\otimes\tilde{x}^K - x^K\otimes\gamma^A) \\ -(\tilde{\gamma}^R\otimes x^K - \tilde{x}^K\otimes\tilde{\gamma}^A) & (\tilde{x}^K - \tilde{\gamma}^R\otimes x^K\otimes\gamma^A) \end{pmatrix} \otimes \hat{N}^{A} \tag{C.2}$$

$$\hat{N}^{R,A} = \begin{pmatrix} (1-\gamma^{R,A}\otimes\tilde{\gamma}^{R,A})^{-1} & 0 \\ 0 & (1-\tilde{\gamma}^{R,A}\otimes\gamma^{R,A})^{-1} \end{pmatrix} , \tag{C.3}$$

and the transport equation for the 2x2 matrix functions are

$$i\hbar \boldsymbol{v}_F \boldsymbol{\nabla}\gamma^{R,A} = \gamma^{R,A}\otimes\tilde{\Delta}^{R,A}\otimes\gamma^{R,A} + \Sigma^{R,A}\otimes\gamma^{R,A} - \gamma^{R,A}\otimes\tilde{\Sigma}^{R,A} + 2\varepsilon\gamma^{R,A} - \Delta^{R,A} \tag{C.4}$$

$$i\hbar \boldsymbol{v}_F \boldsymbol{\nabla}\tilde{\gamma}^{R,A} = \tilde{\gamma}^{R,A}\otimes\Delta^{R,A}\otimes\tilde{\gamma}^{R,A} + \tilde{\Sigma}^{R,A}\otimes\tilde{\gamma}^{R,A} - \gamma\tilde{}^{R,A}\otimes\Sigma^{R,A} - 2\varepsilon\tilde{\gamma}^{R,A} - \tilde{\Delta}^{R,A} \tag{C.5}$$

$$\begin{aligned} i\hbar(\boldsymbol{v}_F\boldsymbol{\nabla}+\partial_t)x^K =& (\gamma^R\otimes\tilde{\Delta}^R + \Sigma^R)\otimes x^K + x^K\otimes(\Delta^A\otimes\tilde{\gamma}^A - \Sigma^A) - \gamma^R\otimes\tilde{\Sigma}^K\otimes\tilde{\gamma}^A \\ &+ \Delta^K\otimes\tilde{\gamma}^A + \gamma^R\otimes\tilde{\Delta}^K - \Sigma^K \end{aligned} \tag{C.6}$$

$$\begin{aligned} i\hbar(\boldsymbol{v}_F\boldsymbol{\nabla}+\partial_t)\tilde{x}^K =& (\tilde{\gamma^R}\otimes\Delta^R + \tilde{\Sigma}^R)\otimes\tilde{x}^K + \tilde{x}^K\otimes(\tilde{\Delta}^A\otimes\gamma^A - \tilde{\Sigma}^A) - \tilde{\gamma}^R\otimes\Sigma^K\otimes\gamma^A \\ &+ \tilde{\Delta}^K\otimes\gamma^A + \tilde{\gamma}^R\otimes\Delta^K - \tilde{\Sigma}^K \end{aligned} . \tag{C.7}$$

These Riccati-type differential equations are numerical stable [1] and provide an efficient

[1] In fact these are stiff differential equations, but stable using the correct quadrature scheme, i.e., to integrate along the quasiclassical trajectories in the right directions.

way to treat inhomogeneous and non-equilibrium systems.

In equilibrium the distribution function is given by

$$\hat{x}_{eq} = (1 - \gamma^R \tilde{\gamma}^A) \tanh \frac{\varepsilon}{2T} \,, \tag{C.8}$$

and, in the simple case of a homogeneous superconductor in equilibrium, the coherence functions are given by [2]

$$\gamma^{R,A}_{hom} = \frac{-\Delta^{R,A}}{\varepsilon^{R,A} \pm \sqrt{(\varepsilon^{R,A})^2 + \Delta^{R,A}\tilde{\Delta}^{R,A}}} \tag{C.9}$$

$$\tilde{\gamma}^{R,A}_{hom} = \frac{\tilde{\Delta}^{R,A}}{\varepsilon^{R,A} \pm \sqrt{(\varepsilon^{R,A})^2 + \tilde{\Delta}^{R,A}\Delta^{R,A}}} \tag{C.10}$$

($\varepsilon^{R,A} = \varepsilon \pm i0^+$). In the presence of homogeneous perturbations, like scattering on a homogeneous distribution of impurities, the expression is still valid, but ε, Δ and $\tilde{\Delta}$ are renormalized by the corresponding self-energies.

[2] The general notation might be misleading. In case of an unitary order parameter $\Delta\tilde{\Delta}$ is proportional to the unit matrix in spin space, and $\Delta\tilde{\Delta} = -|\Delta|^2$

Bibliography

[1] D. D. Osheroff, R. C. Richardson, and D. M. Lee, Phys. Rev. Lett. **28**, 885 (1972).

[2] J. C. Wheatley, Rev. Mod. Phys. **47**, 415 (1975).

[3] D. D. Osheroff, Rev. Mod. Phys. **69**, 667 (1997).

[4] D. Vollhard and P. Wölfle, *The Superfluid Phases of* ^3He (Taylor & Francis, London, 1990).

[5] A. J. Leggett, Rev. Mod. Phys. **47**, 331 (1975).

[6] A. J. Leggett, Rev. Mod. Phys. **71**, S318 (1999).

[7] A. J. Leggett, Rev. Mod. Phys. **76**, 999 (2004).

[8] G. E. Volovik, *The Universe in a Helium Droplet* (Oxford University Press, New York, 2003).

[9] G. R. Stewart, Rev. Mod. Phys. **56**, 755 (1984).

[10] M. Sigrist and K. Ueda, Rev. Mod. Phys. **63**, 239 (1991).

[11] J. G. Bednorz and K. A. Müller, Z. Phys. B **64**, 189 (1986).

[12] A. P. Mackenzie and Y. Maeno, Rev. Mod. Phys. **75**, 657 (2003).

[13] T. M. Rice and M. Sigrist, J. Phys. Condens. Matter **7**, L643 (1995).

[14] M. Zhitomirsky and T. Rice, Phys. Rev. Lett. **87**, 057001 (2001).

[15] F. Laube *et al.*, Phys. Rev. Lett. **84**, 1595 (2000).

[16] F. Laube *et al.*, Phys. Rev. B **69**, 014516 (2004).

[17] D. J. Van Harlingen, Rev. Mod. Phys. **67**, 515 (1995).

[18] D. A. Wollman *et al.*, Phys. Rev. Lett. **71**, 2134 (1993).

[19] C. C. Tsuei *et al.*, Phys. Rev. Lett. **73**, 593 (1994).

[20] J. R. Kirtley *et al.*, Nature **373**, 225 (1995).

[21] C.-R. Hu, Phys. Rev. Lett. **72**, 1526 (1994).

[22] F. S. Bergeret, A. F. Volkov, and K. B. Efetov, Rev. Mod. Phys. **77**, 1321 (2005).

[23] A. A. Abrikosov, L. P. Gorkov, and I. E. Dzyaloshinski, *Methods of Quantum Field Theory in Statistical Physics* (Prentice-Hall, Englewood Cliffs, NJ, 1963).

[24] J. R. Schrieffer, *Theory of Superconductivity* (Addison-Wesley, Reading, MA, 1964).

[25] G. Eilenberger, Z. Phys. **214**, 195 (1968).

[26] A. I. Larkin and Y. N. Ovchinnikov, Sov. Phys. JETP **28**, 1200 (1969), [Zh. Eksp. Teor. Fiz (1968)].

[27] G. Eliashberg, Sov. Phys. JETP **28**, 668 (1972).

[28] A. I. Larkin and Y. N. Ovchinnikov, Sov. Phys. JETP **41**, 960 (1975).

[29] A. Larkin and Y. Ovchinnikov, Sov. Phys. JETP **46**, 155 (1977).

[30] J. Serene and D. Rainer, Physics Reports **101**, 221 (1983).

[31] J. Rammer and H. Smith, Rev. Mod. Phys. **58**, 323 (1986).

[32] W. Belzig *et al.*, Superlattices and Microstructures **25**, 1251 (1999).

[33] A. I. Shelankov, J. Low Temp. Phys. **60**, 29 (1985).

[34] L. Buchholtz and D. Rainer., Zeitschrift für Physik B **35**, 151 (1979).

[35] A. V. Zaitsev, Sov. Phys. JETP **59**, 1015 (1984).

[36] A. Millis, D. Rainer, and J. A. Sauls, Phys. Rev. B **38**, 4504 (1988).

[37] M. Eschrig, Phys. Rev. B **61**, 9061 (2000).

[38] M. Fogelström, Phys. Rev. B **62**, 11812 (2000).

[39] J. C. Cuevas and M. Fogelström, Phys. Rev. B **64**, 104502 (2001).

[40] M. Eschrig *et al.*, Adv. in Sol. State Phys. **44**, 533 (2004).

[41] H. Won and K. Maki, Phys. Rev. B **49**, 1397 (1994).

[42] I. S. Gradshteyn and I. M. Ryzhik, *Table of integrals, series, and products* (Academic Press, New York, 1980).

[43] J. Luttinger and J. C. Ward, Phys. Rev. **118**, 1417 (1960).

[44] C. D. Dominicis and P. C. Martin, J. Math. Phys. **5**, 14 (1964).

[45] C. D. Dominicis and P. C. Martin, J. Math. Phys. **5**, 31 (1964).

[46] H. Shiba, Progress of Theoretical Physics **40**, 435 (1968).

[47] K. Maki, in *Superconductivity*, edited by R. D. Parks (Marcel Dekker, New York, 1969), Vol. 2.

[48] P. Hirschfeld, D. Vollhardt, and P. Wölfle, Solid State Comm. **59**, 111 (1986).

[49] S. Schmitt-Rink, K. Miyake, and C. M. Varma, Phys. Rev. Lett. **57**, 2575 (1986).

[50] P. J. Hirschfeld, P. Wölfle, and D. Einzel, Phys. Rev. B **37**, 83 (1988).

[51] H. R. Ott, E. Felder, C. Bruder, and T. M. Rice, Europhysics Letters (EPL) **3**, 1123 (1987).

[52] R. Balian and N. R. Werthamer, Phys. Rev. **131**, 1553 (1963).

[53] Y. Maeno *et al.*, Nature (London) **372**, 532 (1994).

[54] C. Bergemann *et al.*, Adv. Phys. **52**, 639 (2003).

[55] A. P. Mackenzie *et al.*, Phys. Rev. Lett. **76**, 3786 (1996).

[56] T. Oguchi, Phys. Rev. B **51**, 1385 (1995).

[57] I. Mazin and D. J. Singh, Phys. Rev. Lett. **79**, 733 (1997).

[58] I. I. Mazin, D. A. Papaconstantopoulos, and D. J. Singh, Phys. Rev. B **61**, 5223 (2000).

[59] A. Damascelli *et al.*, Phys. Rev. Lett. **85**, 5194 (2000).

[60] D. K. Morr, P. F. Trautman, and M. J. Graf, Phys. Rev. Lett. **86**, 5978 (2001).

[61] A. P. Mackenzie *et al.*, J. Phys. Soc. Jpn. **67**, 385 (1998).

[62] F. Lichtenberg, A. Catana, J. Mannhart, and D. G. Schlom, Appl. Phys. Lett. **60**, 1138 (1992).

[63] Y. Maeno, Physica C **282**, 206 (1997).

[64] A. W. Tyler, A. P. Mackenzie, S. NishiZaki, and Y. Maeno, Phys. Rev. B **58**, R10107 (1998).

[65] E. Ohmichi *et al.*, Phys. Rev. B **61**, 7101 (2000).

[66] K. Ishida *et al.*, Nature **396**, 658 (1998).

[67] J. A. Duffy *et al.*, Phys. Rev. Lett. **85**, 5412 (2000).

[68] G. M. Luke *et al.*, Nature **394**, 558 (1998).

[69] A. P. Mackenzie *et al.*, Phys. Rev. Lett. **80**, 161 (1998).

[70] A. P. Mackenzie *et al.*, Phys. Rev. Lett. **80**, 3890 (1998), (Erratum).

[71] S. Nishizaki *et al.*, J. Phys. Soc. Jpn. **67**, 560 (1998).

[72] S. NishiZaki, Y. Maeno, and Z. Mao, J. Low Temp. Phys. **117**, 1581 (1999).

[73] K. Ishida *et al.*, Phys. Rev. Lett. **84**, 5387 (2000).

[74] I. Bonalde *et al.*, Phys. Rev. Lett. **85**, 4775 (2000).

[75] M. A. Tanatar *et al.*, Phys. Rev. Lett. **86**, 2649 (2001).

[76] C. Lupien *et al.*, Phys. Rev. Lett. **86**, 5986 (2001).

[77] M. A. Tanatar *et al.*, Phys. Rev. B **63**, 064505 (2001).

[78] K. Izawa *et al.*, Phys. Rev. Lett. **86**, 2653 (2001).

[79] S. NishiZaki, Y. Maeno, and Z. Mao, J. Phys. Soc. Jpn. **69**, 572 (2000).

[80] A. J. Millis, S. Sachdev, and C. M. Varma, Phys. Rev. B **37**, 4975 (1988).

[81] D. Rainer and G. Bergmann, J. Low Temp. Phys. **14**, 501 (1974).

[82] A. Damascelli, Z. Hussain, and Z.-X. Shen, Rev. Mod. Phys. **75**, 473 (2003).

[83] Y. Wang, L. Li, and N. P. Ong, Physical Review B (Condensed Matter and Materials Physics) **73**, 024510 (2006).

[84] L. J. Buchholtz and G. Zwicknagl, Phys. Rev. B **23**, 5788 (1981).

[85] W. Zhang, Phys. Lett. A **130**, 314 (1988).

[86] L. J. Buchholtz, M. Palumbo, D. Rainer, and J. A. Sauls, J. Low Temp. Phys. **101**, 1099 (1995).

[87] M. Matsumoto and H. Shiba, **65**, 2194 (1996).

[88] M. Palumbo, L. J. Buchholtz, D. Rainer, and J. A. Sauls, Czech. J. Phys. **46**, 1065 (1996).

[89] Y. S. Barash, H. Burkhardt, and D. Rainer, Phys. Rev. Lett. **77**, 4070 (1996).

[90] M. Fogelström, S. Yip, and J. Kurkijärvi, Physica C **294**, 289 (1998).

[91] Y. Tanaka and S. Kashiwaya, Phys. Rev. B **53**, R11957 (1996).

[92] A. Poenicke, Y. S. Barash, C. Bruder, and V. Istyukov, Phys. Rev. B **59**, 7102 (1999).

[93] in *Proceedings of the 1st International Conference on Quasiclassical Methods in Superconductivity*, edited by D. Rainer and J. A. Sauls (Universität Bayreuth, Bayreuth, 1998).

[94] Y. S. Barash and A. A. Svidzinski, Sov. Phys. JETP **84**, 619 (1997).

[95] M. Fogelström and S.-K. Yip, Phys. Rev. B **57**, R14060 (1998).

[96] Y. N. Ovchinnikov, Sov. Phys. JETP **84**, 853 (1969).

[97] F. J. Culetto, G. Kieselmann, and D. Rainer, in *Proccedings of the 17th International Conference on Low Temperature Physics*, edited by U. Eckern, A. Schmid, W. Weber, and H. Wühl (North Holland, Amsterdam, 1984), p. 1027.

[98] J. Kurkijärvi, D. Rainer, and J. A. Sauls, Can. J. Phys. **65**, 1440 (1987).

[99] M. Covington *et al.*, Phys. Rev. Lett. **79**, 277 (1997).

[100] L. Alff *et al.*, The European Physical Journal B **5**, 423 (1998).

[101] M. Fogelström, D. Rainer, and J. A. Sauls, Phys. Rev. Lett. **79**, 281 (1997).

[102] M. Aprili, E. Badica, and L. H. Greene, Phys. Rev. Lett. **83**, 4630 (1999).

[103] M. Fogelström and J. Sauls, preprint (unpublished).

[104] M. Aprili *et al.*, Phys. Rev. B **57**, R8139 (1998).

[105] D. H. Wu *et al.*, Phys. Rev. Lett. **70**, 85 (1993).

[106] A. Andreone *et al.*, Phys. Rev. B **49**, 6392 (1994).

[107] S. M. Anlage *et al.*, Phys. Rev. B **50**, 523 (1994).

[108] J. R. Cooper, Phys. Rev. B **54**, R3753 (1996).

[109] L. Alff *et al.*, Phys. Rev. Lett. **83**, 2644 (1999).

[110] J. Appelbaum, Phys. Rev. Lett. **17**, 91 (1966).

[111] L. Alff *et al.*, Physica C **282-287**, 1485 (1997).

[112] L. Alff *et al.*, in *Advances in Superconductivity IX*, edited by M. M. S. Nakajima (Springer-Verlag, Tokyo, 1997), p. 49.

[113] S. Kashiwaya *et al.*, Phys. Rev. B **57**, 8680 (1998).

[114] F. Hayashi *et al.*, J. Phys. Soc. Jap. **67**, 3234 (1998).

[115] S. Kleefisch *et al.*, Appl. Phys. Lett. **72**, 2888 (1998).

[116] L. Alff *et al.*, Phys. Rev. B **58**, 11197 (1998).

[117] L. Alff *et al.*, Physica B **284**, 591 (2000).

[118] R. Prozorov, R. W. Giannetta, P. Fournier, and R. L. Greene, Phys. Rev. Lett. **85**, 3700 (2000).

[119] P. J. Hirschfeld and N. Goldenfeld, Phys. Rev. B **48**, 4219 (1993).

[120] L. S. Borkowski and P. J. Hirschfeld, Phys. Rev. B **49**, R15404 (1994).

[121] J. D. Kokales *et al.*, Phys. Rev. Lett. **85**, 3696 (2000).

[122] C. C. Tsuei and J. R. Kirtley, Phys. Rev. Lett. **85**, 182 (2000).

[123] C. C. Tsuei and J. R. Kirtley, Rev. Mod. Phys. **72**, 969 (2000).

[124] L. Alff and S. Kleefisch, private communication.

[125] M. Fogelström (unpublished).

[126] A. Biswas *et al.*, Phys. Rev. Lett. **88**, 207004 (2002).

[127] J. A. Skinta, M.-S. Kim, and T. R. Lemberger, Phys. Rev. Lett. **88**, 207005 (2002).

[128] T. P. Devereaux and P. Fulde, Phys. Rev. B **47**, 14638 (1993).

[129] E. Polturak, G. Koren, D. Cohen, and E. Aharoni, Phys. Rev. B **47**, 5270 (1993).

[130] Y. G. Ponomarev *et al.*, Phys. Rev. B **52**, 1352 (1995).

[131] M. Hurd, Phys. Rev. B **55**, R11993 (1997).

[132] T. Löfwander, V. S. Shumeiko, and G. Wendin, Superconduct. Sci. and Technol. **14**, R53 (2001).

[133] A. Engelhardt, R. Dittmann, and A. I. Braginski, Phys. Rev. B **59**, 3815 (1999).

[134] O. Nesher and G. Koren, Phys. Rev. B **60**, 9287 (1999).

[135] Y. G. Ponomarev *et al.*, cond-mat/0111342.

[136] A. Auerbach and E. Altman, Phys. Rev. Lett. **85**, 3480 (2000).

[137] A. Andreev, Sov. Phys. JETP **19**, 1228 (1964).

[138] S. N. A. amd A.F. Volkov and A. Zaitsev, JETP Lett. **28**, 589 (1979).

[139] S. N. Artemenko, A. F. Volkov, and A. V. Zaitsev, Solid State Commun. **30**, 771 (1979).

[140] A. V. Zaitsev, Sov. Phys. JETP **51**, 111 (1980).

[141] G. Deutscher, Reviews of Modern Physics **77**, 109 (2005).

[142] G. E. Blonder, M. Tinkham, and T. M. Klapwijk, Phys. Rev. B **25**, 4515 (1982).

[143] T. M. Klapwijk, G. E. Blonder, and M. Tinkham, Physica B+C **109–110**, 1657 (1982).

[144] J. M. Rowell and W. L. Feldmann, Phys. Rev. **172**, 393 (1968).

[145] A. A. Bright and J. R. Merrill, Phys. Rev. **184**, 446 (1969).

[146] I. Giaever and H. R. Zeller, Phys. Rev. B **1**, 4278 (1970).

[147] G. Arnold, J. Low Temp. Phys. **68**, 1 (1987).

[148] E. N. Bratus', V. S. Shumeiko, and G. Wendin, Phys. Rev. Lett. **74**, 2110 (1995).

[149] D. Averin and A. Bardas, Phys. Rev. Lett. **75**, 1831 (1995).

[150] J. C. Cuevas, A. Martín-Rodero, and A. L. Yeyati, Phys. Rev. B **54**, 7366 (1996).

[151] J. C. Cuevas and W. Belzig, Phys. Rev. Lett. **91**, 187001 (2003).

[152] G. Johansson, P. Samuelsson, and A. Ingerman, Phys. Rev. Lett. **91**, 187002 (2003).

[153] N. van der Post, E. T. Peters, I. K. Yanson, and J. M. van Ruitenbeek, Phys. Rev. Lett. **73**, 2611 (1994).

[154] E. Scheer *et al.*, Phys. Rev. Lett. **78**, 3535 (1997).

[155] E. Scheer *et al.*, Nature **394**, 154 (1998).

[156] M. Hurd, T. Löfwander, G. Johansson, and G. Wendin, Phys. Rev. B **59**, 4412 (1999).

[157] T. Löfwander *et al.*, Superlattices and Microstructures **25**, 1115 (1999).

[158] T. Löfwander, G. Johansson, and G. Wendin, J. Low Temp. Phys. **117**, 593 (1999).

[159] L. J. Buchholtz, M. Palumbo, D. Rainer, and J. A. Sauls, J. Low Temp. Phys. **101**, 1079 (1995).

[160] Y. S. Barash, A. A. Svidzinsky, and H. Burkhardt, Phys. Rev. B **55**, 15282 (1997).

[161] A. Poenicke, M. Fogelström, and J. Sauls, Physica B **284-288**, 589 (2000).

[162] R. S. Keizer *et al.*, Nature **439**, 825 (2006).

[163] M. Eschrig, J. Kopu, J. C. Cuevas, and G. Schön, Phys. Rev. Lett. **90**, 137003 (2003).

[164] T. Tokuyasu, J. A. Sauls, and D. Rainer, Phys. Rev. B **38**, 8823 (1988).

[165] S. T. B. Goennenwein *et al.*, Appl. Phys. Lett. **90**, 142509 (2007).

[166] M. Eschrig and T. Löfwander, *Nature* advance online publication, 13 January 2008 (DOI 10.1038/nphys831).

[167] M. Eschrig *et al.*, J. Low Temp. Phys. **147**, 457 (2007).

[168] G. Bergner, diploma thesis, Universität Karlsruhe, 2007.

[169] J. Nagamatsu *et al.*, Nature **410**, 63 (2001).

[170] H. J. Choi *et al.*, Nature **418**, 758 (2002).